BNWL-481 1

[redacted]

PACIFIC NORTHWEST LABORATORY ANNUAL REPORT FOR 1966 TO THE USAEC DIVISION OF BIOLOGY AND MEDICINE

VOLUME II: PHYSICAL SCIENCES

PART I. ATMOSPHERIC SCIENCES

OCTOBER, 1967

[redacted]

AEC RESEARCH & DEVELOPMENT REPORT

BATTELLE NORTHWEST
BATTELLE MEMORIAL INSTITUTE PACIFIC NORTHWEST LABORATORY
3000 STEVENS DRIVE, P. O. BOX 999, RICHLAND, WASHINGTON 99352

BNWL-481 1

LEGAL NOTICE

PACIFIC NORTHWEST LABORATORY
RICHLAND, WASHINGTON
operated by
BATTELLE MEMORIAL INSTITUTE
for the
UNITED STATES ATOMIC ENERGY COMMISSION UNDER CONTRACT AT(45-1)-1830

PRINTED BY/FOR THE U. S. ATOMIC ENERGY COMMISSION

DISCLAIMER

BNWL-481 1
UC-48
Biology and Medicine

PACIFIC NORTHWEST LABORATORY
ANNUAL REPORT FOR 1966
to the
USAEC Division of Biology and Medicine
VOLUME II: PHYSICAL SCIENCES
Part 1. Atmospheric Sciences

By

Staff Members of
Atmospheric Sciences Section
Environmental and Radiological Sciences

Edited by
D. W. Pearce and M. R. Compton

October 1967

PACIFIC NORTHWEST LABORATORY
RICHLAND, WASHINGTON

Volume I of this report to the USAEC Division of Biology and Medicine covers work in the biological sciences and is issued as BNWL-480. Volume II of this report covers work in the physical sciences and is issued in four parts: (1) Atmospheric Sciences, BNWL-481 1; (2) Radiological Sciences, BNWL-481 2; (3) Earth Sciences, BNWL-481 3; (4) Instrumentation, BNWL-481 4.

Printed in the United States of America
Available from
Clearinghouse for Federal Scientific and Technical Information
National Bureau of Standards, U.S. Department of Commerce
Springfield, Virginia 22151
Price: Printed Copy $3.00; Microfiche $0.65

TABLE OF CONTENTS

These reports are drawn principally from personnel of the Atmospheric Physics Section of the Environmental and Radiological Sciences Department. Contributions and coauthors from other organizations may also be included and occasional related activities not sponsored by the Division of Biology and Medicine may be included. Such facts are acknowledged by footnotes.

PACIFIC NORTHWEST LABORATORY
ANNUAL REPORT FOR 1966
to the
USAEC Division of Biology and Medicine
VOLUME II: PHYSICAL SCIENCES
Part 1. Atmospheric Sciences

A BASIS FOR COMPARING EXPERIMENTAL MEASUREMENTS OF LATERAL PLUME GROWTH

C. L. Simpson

In the past several years we have investigated the dependence of the lateral growth of a diffusing plume on various meteorological parameters. In the Hanford experimental data a relationship between σ_y^2, the cross-wind exposure variance, and $\sigma_\theta \bar{u}$, the product of the standard deviation of the wind direction and the mean wind speed has been found. This equation made possible the rapid prediction of plume growth from meteorological data taken directly from strip charts. Independent verification of this relation was successful for release times ranging from ten minutes to several hours. Recently we have organized data from other sites to test the Hanford concept and to generalize it further.

The assumption involved is that the correlation coefficient $R(\xi)$ between the velocity experienced by a particle at times t and $t + \xi$ is an exponential of the form

$$R(\xi) = \exp(-\xi/\beta)$$

This assumption is restrictive and perhaps rarely realized. However, this does not detract from its usefulness in specifying the lateral growth if the area below the curve from $t = 0$ to a large value of t approximates that of the "true" correlation function for a given set of meteorological conditions. The success of independent verification of Hanford data has confirmed the attractiveness of this concept. The cross wind variance, then, is

$$\sigma_y^2 = \overline{2v'^2} \int_o^t dt \int_o^t R(\xi)\,d\xi = \overline{2v'^2} \int_o^t dt \int_o^t \exp(-\xi/\beta)\,d\xi \quad . \tag{1}$$

The cross-wind variance of the plume distribution thus depends on the magnitude of the eddy fluctuation and on the way in which motion is correlated. Performing the integration and letting $A = 2\overline{v'^2}\,\beta$ yields an equation in which the unknown variables can be related

to known meteorological quantities. This relation is

$$\sigma_y^2 = A\left\{t - \beta\,[1 - e^{-t/\beta}]\right\} \quad . \qquad (2)$$

Evaluation of the unknown quantities requires two manipulations. First, β can be expressed in terms of A and $(\sigma_\theta \bar{u})$ by approximating the La Grangian parameter, $\overline{v'^2}$, by $\overline{v'^2} \sim (\sigma_\theta \bar{u})^2$; then

$$\beta = A/2(\sigma_\theta \bar{u})^2 \quad .$$

Substitution for β in Equation (2) yields an expression for determining the variance in which the only unknown parameter, A, can be evaluated from experimental results. The second step then was that of determining A independently from crosswind variance calculations of diffusion data obtained at the Hanford site. By choosing travel times sufficiently large, it is permissible to neglect the latter two terms in Equation (2) so that $\sigma_y^2 = At$ without significant error. Values for A were calculated for Hanford diffusion tests from the ratio of the calculated variance and the derived travel time, care being taken that travel times were sufficiently large to assure that the slope of σ_y^2 versus t curve had reached 0.5.

Determinations of A were made from the Hanford Green Glow and 30 Series diffusion tests in which meteorological data were obtained concurrently to evaluate $\sigma_\theta \bar{u}$. The release period for the tracer, zinc sulfide, was usually one-half hour. σ_θ and $\bar{u}$ were derived from strip chart recordings for the release period.

Using many paired values of A and $\sigma_\theta \bar{u}$, regression analysis yielded the linear dependence, $A = K\sigma_\theta \bar{u}$. For these Hanford data the value for K was determined to be 240. This means that β, the factor which governs the rate of decay of correlation, is not constant, but also depends on the variability of the wind, for $\beta = 120/\sigma_\theta \bar{u}$. The larger the value of $\sigma_\theta \bar{u}$, the smaller is β, and the decay of the correlation is rapid. Substitution into Equation (2) yields an equation of the form

$$Y = \Phi + e^{-\Phi} \quad ,$$

$$\left[1 + \frac{\sigma_y^2}{K_s^2/2}\right] = \frac{\sigma_\theta \bar{u} t}{K_s/2} + e^{-\left[\frac{\sigma_\theta \bar{u} t}{K_s/2}\right]} \qquad (3)$$

The subscript s denotes that the value of K may vary from site to site. Diffusion and meteorological data from other sites were examined to test the generality of the model. Earlier comparisons of some of these data indicated that K must be a site variable.

Sites chosen for the study were those in which the diffusion and meteorological measurements were similar to the design used at Hanford. These included O'Neill, Nebraska (Prairie Grass); Cape Kennedy, Florida (Ocean Breeze); Vandenberg, California (Dry Gulch); and Arco, Idaho (NRTS). Although there were some variations in meteorological and sampling equipment and in the way in which the data were summarized all test designs were oriented toward defining the diffusion near the ground. Therefore, diffusion

and wind measurements were obtained within a meter or two from the surface, providing a basis for this comparison. A few of the field tests were excluded, following a screening for completeness and reliability.

Values for the constant, K_s, were determined for each site following the procedure outlined. These values are given in Table I.

TABLE I. Values of K_s

Site	K_s
O'Neill, Nebraska (night)	10
O'Neill, Nebraska (day)	120
Cape Kennedy, Florida	120
Vandenberg, California	120
Hanford, Washington	240
Arco, Idaho	360

Only at O'Neill was it necessary to account for effects of stability on lateral plume growth. At the other locations the effect of varying stability appeared to be negligible. Because the tracer releases at O'Neill were of ten minutes duration, the validity of the small K value found in the nighttime stable condition is questioned. There must be some lower limit on the duration of the release, at present undefined, in which this approach is not valid.

Data from all tests are summarized in Figure 1, showing variations about the theoretical value predicted by Equation (3). Data points are derived for each site using the K_s values listed in Table 1. When we assumed that the correlation function can be approximated by an exponential, i.e., the rate of decay depending on the variability of the wind, a means of comparing σ_y^2 data for sites was evolved. The comparison is reduced to considering variations in K_s, a derived constant. The physical significance of the constant K_s requires further investigation. From the few data that were examined it appears that the larger values of K_s are associated with mountain-generated winds. More data from other sites will, however, be required to provide evidence for any conclusion. However, many data exist that can be used to test the hypothesis that the decay of autocorrelation is dependent upon the magnitude of the wind variability, $\sigma_\theta \bar{u}$.

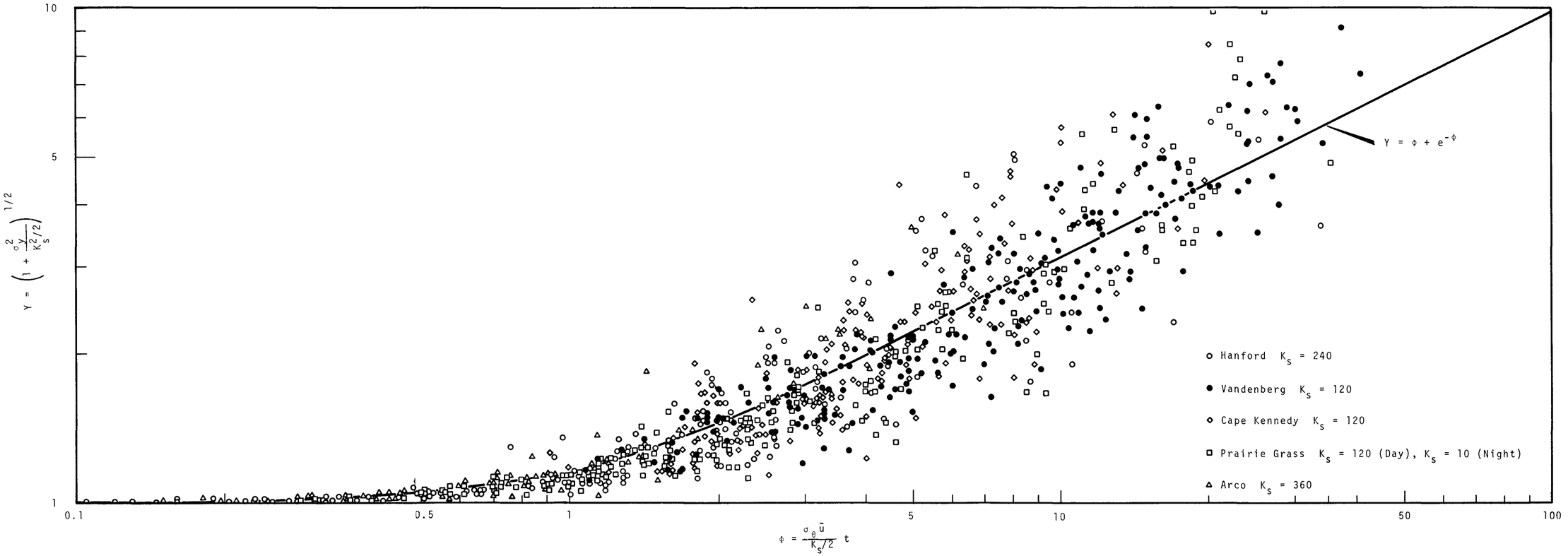

FIGURE 1. Intersite Comparisons of Lateral Growth of a Diffusing Plume Assuming Exponential Decay of Auto-correlation Function

ELEVATED SOURCE DIFFUSION STUDIES

C. E. Elderkin, W. T. Hinds
and J. W. Sloot

Diffusion from an elevated source continued to be a subject of experimental investigation during the last year, eight releases were made from 25.9 m with sampling out to 1600 m from the source over the Hanford sampling grid. During the fall season, routine use was made of the dual tracer procedure developed before at Hanford;[1] six tests were dual tracer studies with simultaneous release at ground and elevated source points. Assay of all dual tracer tests is not yet complete, but analysis has begun on the four tests for which data reduction is complete.

Two of the dual tracer tests were conducted in unstable conditions, and one each in neutral and slightly stable conditions. The results of the former are shown in Figure 1, which present the normalized exposure plotted against distance from the source. The merging of the elevated source data into those from the ground source is obvious and accords well with theoretical expectations; the merger should be exact if the bivariate normal model were accurate. The distance to the maximum exposure from the elevated source is a function of atmospheric stability, and further work will define the dependence on the stability of distance to the maximum.

The results from the test under neutral conditions and from the test under slightly stable conditions are shown in Figure 2. It is important to note that the exposures from the ground

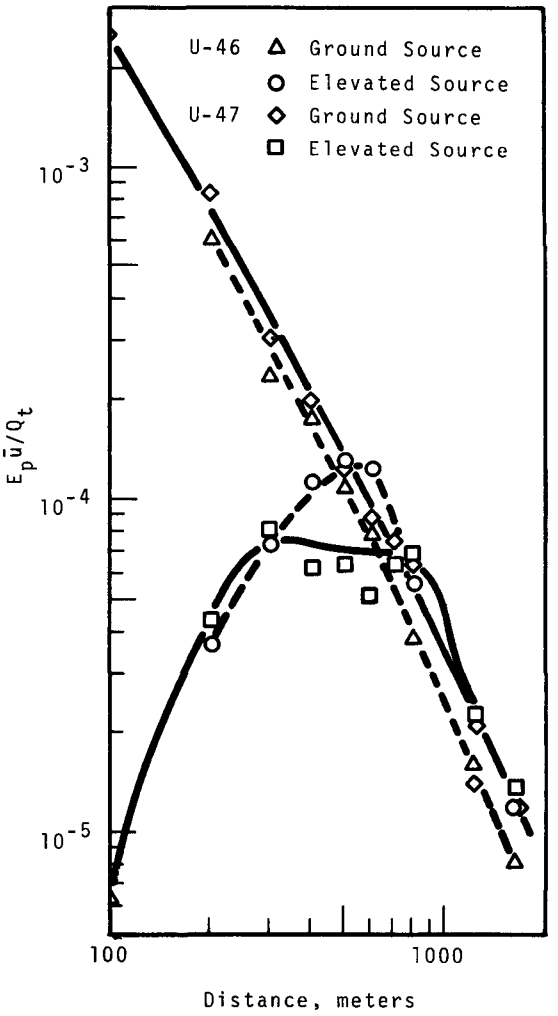

FIGURE 1. Comparison of Ground and Elevated Source Results in Unstable Conditions

source are nearly identical, even though the atmosphere was stable during one test. This is due to the dominant part played by mechanical turbulence in the lower portion of the atmosphere, even in slightly stable conditions. However, as the source height increases, the region dominated by mechanical turbulence is soon surmounted and diffusion

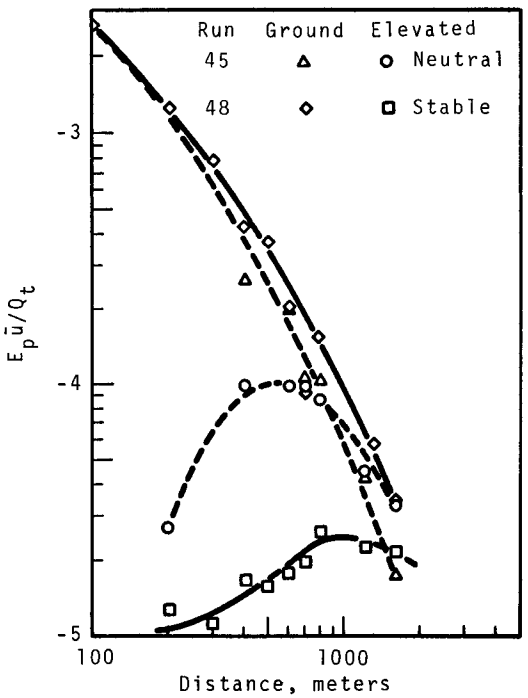

FIGURE 2. Comparison of Ground and Elevated Source Data in Neutral and Stable Conditions

takes place in a region dominated by convective turbulence which is quite sensitive to the dampening effect of atmospheric stability. Thus, the elevated source in the slightly stable atmosphere gives results which are much reduced in exposure compared to those in the neutral test, and the distance to the maximum is considerably greater.

It is apparent in both the figures that exposures from the elevated source can exceed those from the ground source. The same behavior is noted in the crosswind integrated values, so relative rates of plume spread near to and remote from the surface is not a principal cause. It may be that deposition, which acts continually on the ground source plume, reduces the exposures relative to those from the elevated source which are not affected by deposition in the early stages of diffusion.

Since the past work with elevated sources at Hanford has used a height of 56.4 m (185 ft), and the 1966 tests were conducted from 25.9 m (85 ft), source height effects can now be integrated into the diffusion observations. It was shown previously that a normalization procedure can be used to reduce the apparent variation between tests from a single height when the variation is due to differences in turbulence characteristics.[2] The source height was one parameter used in the normalization procedure, so one of the basic steps was similarly to normalize the data from the 25.9 m releases to check the range of source heights for which a single normalized curve is applicable. The results of the comparison between source heights is shown in Figure 3. Although only a few data are available from the lower height, it is apparent that the normalization procedure is applicable at least to heights in the range from 25 to 60 m. Testing will continue with releases from a number of heights and with a larger range of prevailing meteorological conditions including more stable situations.

Further confidence in the use of a single normalized curve resulted from the crosswind integrated data. Tests from both source heights yielded a maximum value of crosswind integrated exposure which is near the value resulting from a bivariate normal model of diffusion; this is shown in Table I.

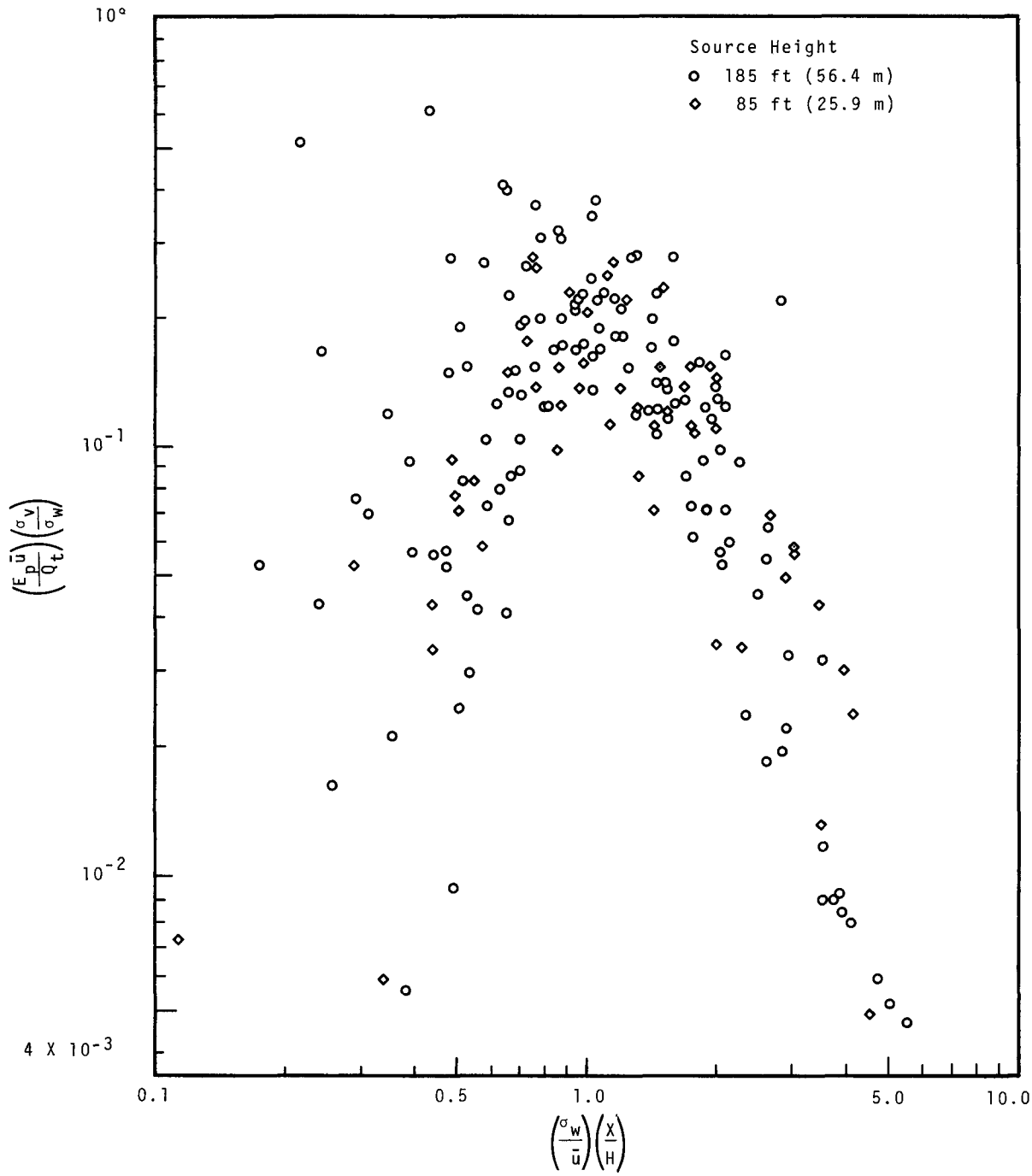

FIGURE 3. Normalized Plot of Exposure Versus Distance

Thus, the observed dependence on source height is nearly that postulated by the bivariate normal model. A full discussion of this point is given in the Annual Reports for 1964 and 1965.

TABLE I. Comparison of Observed and Theoretical Maximum Crosswind Integrated Exposures

Source Height	Observed CIE_{max}	Theoretical CIE_{max}
85 ft	1.44×10^{-2}	1.87×10^{-2}
185 ft	8.0×10^{-3}	8.6×10^{-3}

REFERENCES

1. *P. W. Nickola. "Field Testing of a Fluorescein-Zinc Sulfide Dual Atmospheric Tracer Technique," Hanford Radiological Sciences Research and Development Annual Report for 1964, BNWL-36. Pacific Northwest Laboratory, Richland, Washington, 1965.*
2. *C. E. Elderkin and W. T. Hinds. "Prediction of Exposures from an Elevated Source," Pacific Northwest Laboratory Annual Report for 1965 in the Physical Sciences, Volume 1: Atmospheric Sciences, BNWL-235 1, Pacific Northwest Laboratory, Richland, Washington, May 1966.*

TURBULENCE INVESTIGATIONS

C. E. Elderkin

Studies of the fundamentals of turbulence were initiated at Hanford with a series of measurements made during 1964 and 1965. Analysis was begun and spectral distributions for the longitudinal and vertical wind component fluctuations were discussed in the annual report for 1965.(1) The measurements, made with a fast-response heated thermocouple wire wind sensor termed the wind component meter (WCM), were conducted during a variety of wind speeds and atmospheric stabilities and at a number of heights. The conditions of the tests are listed in Table I. The analysis of the tape recorded WCM signals was performed on an Ease 1132 analog computer. In addition to the power spectra for the longitudinal (u') and the vertical (w') components previously discussed, analog computer analysis has been completed during the past year on the spectral distributions for the lateral (v') component and the cospectral distributions between each of the components. The Reynolds stresses were also calculated with an analog computer program and will be reported here.

COSPECTRA

Cospectral distributions of the $\overline{u'w'}$ covariance for neutral, unstable, and stable cases below 12 m and for all cases above 12 m are shown in Figures 1, 2, 3, and 4, respectively. For the cases below 12 m a distinct similarity is observed in the distributions of cospectral density, $C_{uw}(n)$, normalized with frequency, n, and total covariance $\overline{u'w'}$ (or, equivalently, the square of the friction velocity u^{*2}) when plotted as a function of $nz/\bar{U}$. Here, frequency

TABLE I. Test Conditions

Test	Date	Time	Measurement Height, m	Tower $\overline{U}$, m/sec	WCM $\overline{U}$, m/sec	Ri
2-1	6-26-64	0359 - 0430	3.0	5.29	5.16	+0.01
2-2	6-26-64	0512 - 0550	6.1	3.88	3.90	+0.18
2-3	7-8-64	0355 - 0430	3.0	4.10	3.77	+0.05
4-1	7-16-64	1930 - 1952	3.0		2.18	(a)
5-1	7-17-64	1647 - 1802	3.0	5.3	5.50	-0.02
5-2	7-17-64	1802 - 1824	3.0	6.3	6.54	0.00
5-3	7-17-64	1840 - 1922	3.0	6.9	7.17	0.00
6-1	7-17-64	2005 - 2018	3.0	5.4	5.23	-0.02
6-2	7-17-64	2018 - 2036	3.0	6.6	6.12	-0.01
6-3	7-17-64	2105 - 2207	6.1	8.1	7.40	0.00
7-1	7-18-64	1410 - 1521	6.1	8.5	8.15	-0.09
7-2	7-18-64	1553 - 1655	3.0	9.0	8.59	-0.04
9-1	8-11-64	0140 - 0354	12.2	4.6	3.70	+0.04
11-1	4-9-65	1523 - 1629	6.1	3.6	5.27	-0.03
11-2	4-19-65	1134 - 1219	6.1	3.5	4.86	-0.16
12-1	4-19-65	1415 - 1520	12.2	2.1	3.20	-0.10
12-2	4-28-65	1507 - 1554	12.2	7.8	10.5	-0.08
13-1	5-12-65	1314 - 1414	87.0	7.8	11.1	-0.07

(a) *Mean wind and temperature data were not available during Test 4-1, but conditions were estimated to be slightly stable.*

divided by wind speed, $n/\overline{U}$, serves as an estimate of wave numbers and is normalized with height, z. The slight shift to higher frequency with increasing stability is to be noted in Figure 4. It is also shown in Figure 4 that above 12 m the convective turbulent energy dominates the mechanical turbulence and the similarity in the $\overline{u'w'}$ cospectra is destroyed.

The $\overline{v'w'}$ cospectra, while demonstrating a preponderance of negative spectral density estimates at the higher wave numbers for neutral and unstable cases below 12 m, are seen in Figures 5 through 8 to lack any organized similarity relation. The cospectra for the $\overline{u'v'}$ covariance, shown in Figures 9 through 13, are even less organized, demonstrating only an increased variability with decreasing wave number.

However, the cospectra for all pairs of components show that the requirement for locally isotropic conditions (that the correlation between all pairs of components must be zero) generally holds only at greater wave numbers than $nz/\overline{U}$ = 1.0 to 4.0. It was reported last year that Kolmogoroff's[2] inertial subrange, requiring local isotropy, was anticipated to extend to considerably lower wave numbers than this, based only on the additional requirement for a minus 5/3 law dependence of power spectral density as a function of wave number. The minus 5/3 law extended as

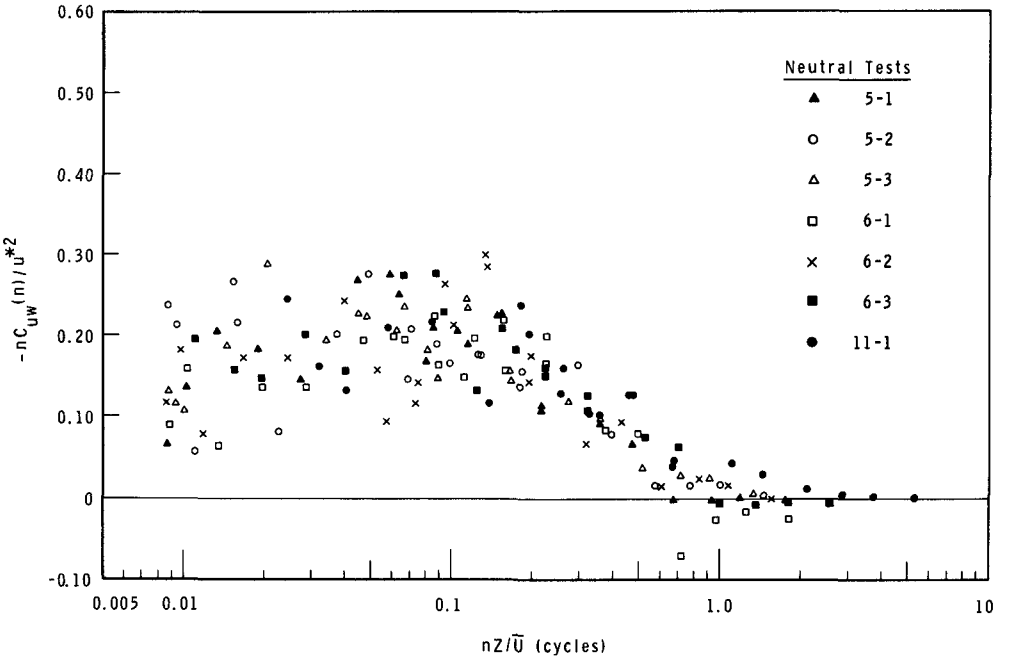

Neg 0660515-4

FIGURE 1. Cospectra Between Longitudinal and Vertical Velocity - Neutral Tests

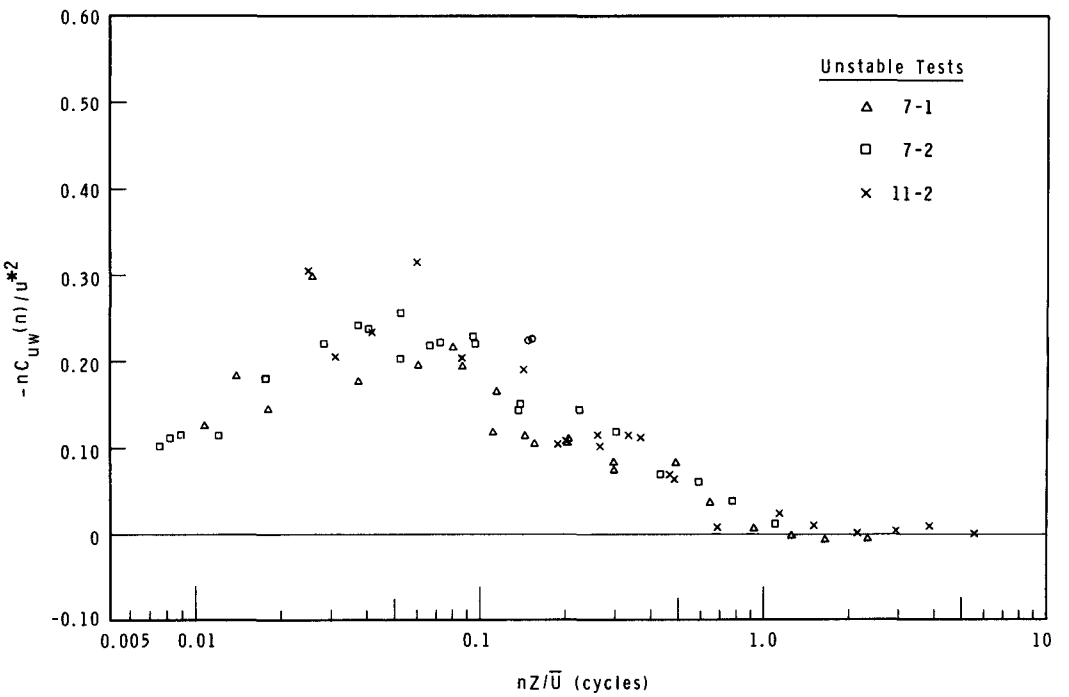

Neg 0661348-4

FIGURE 2. Cospectra Between Longitudinal and Vertical Velocity - Unstable Tests

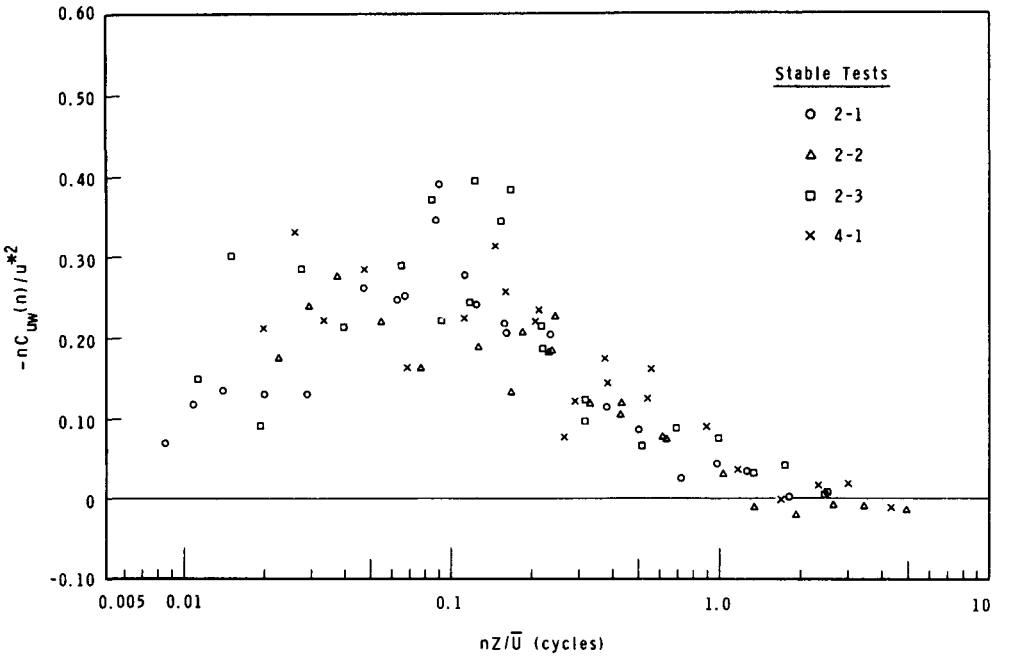

Neg 0660515-2

FIGURE 3. Cospectra Between Longitudinal and Vertical Velocity - Stable Tests

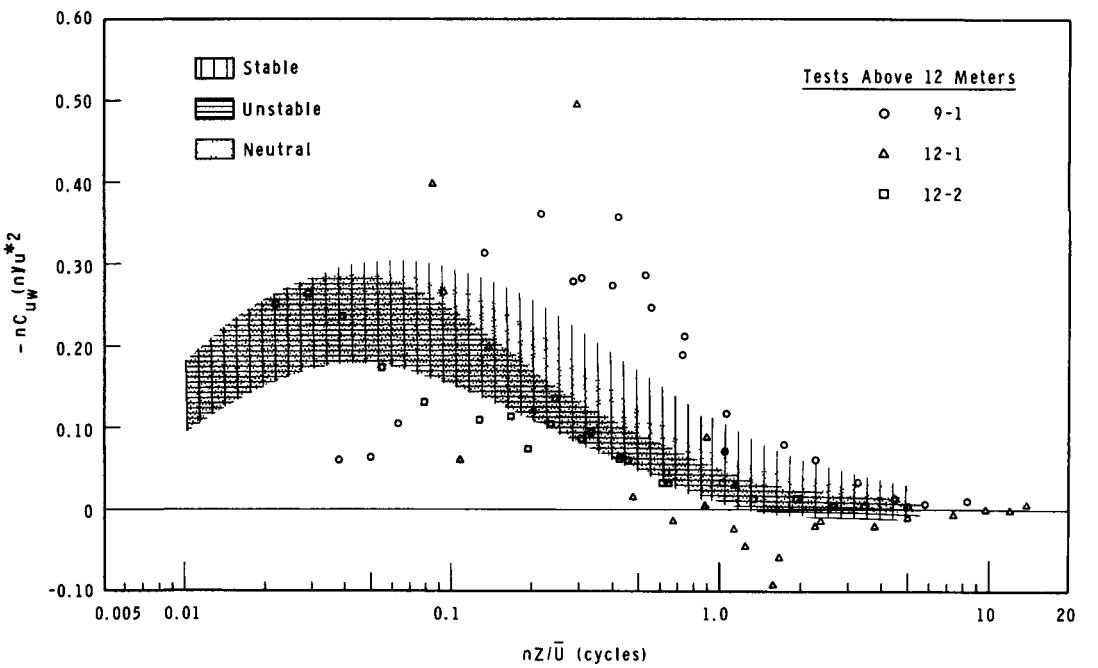

Neg 0660515-1

FIGURE 4. Cospectra Between Longitudinal and Vertical Velocity - Tests Above 12 Meters

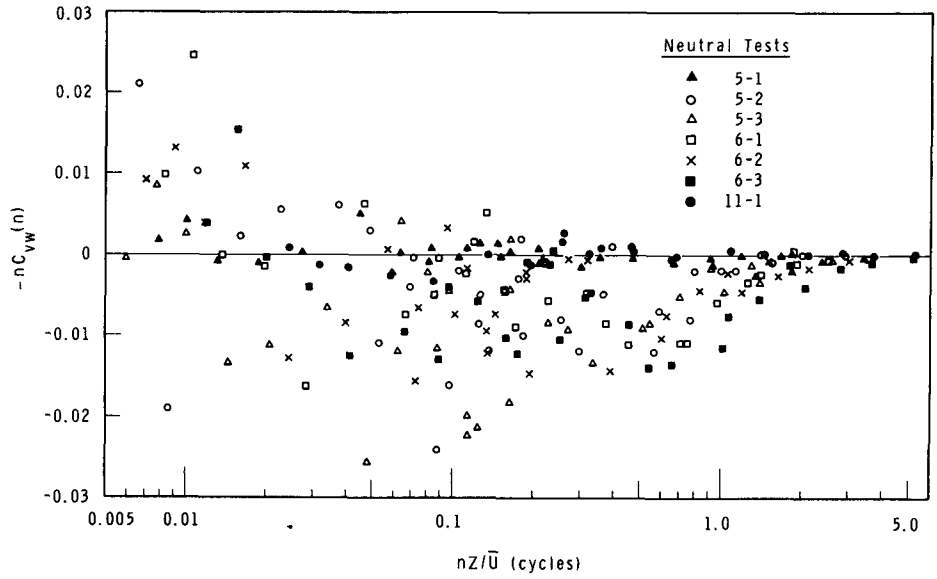

Neg 0660515-9

FIGURE 5. Cospectra Between Lateral and Vertical Velocity - Neutral Tests

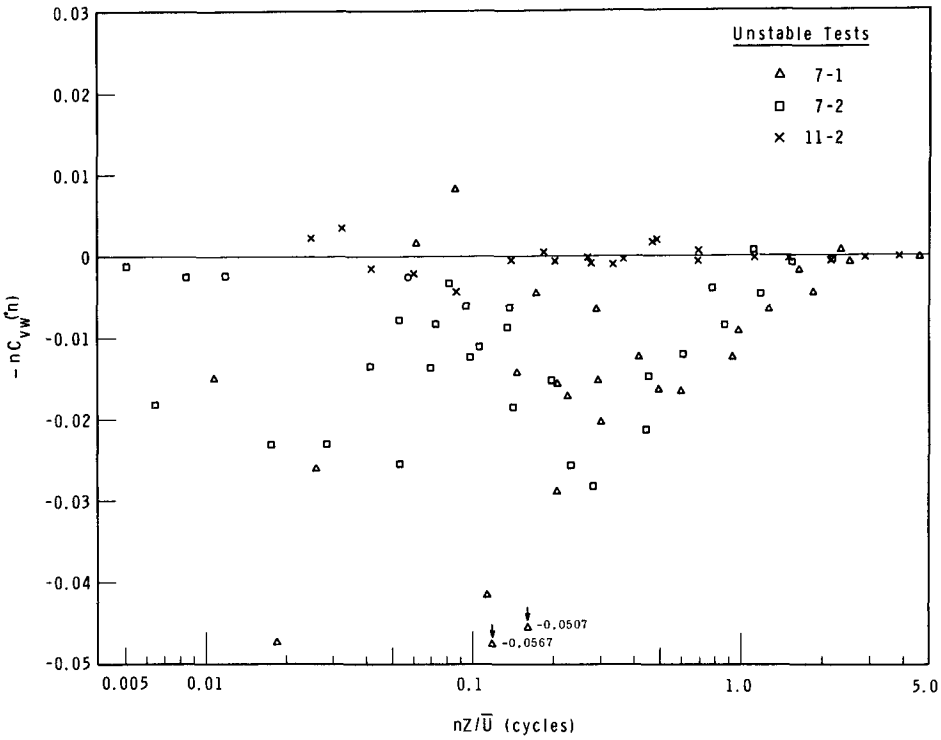

Neg 0660515-8

FIGURE 6. Cospectra Between Lateral and Vertical Velocity - Unstable Tests

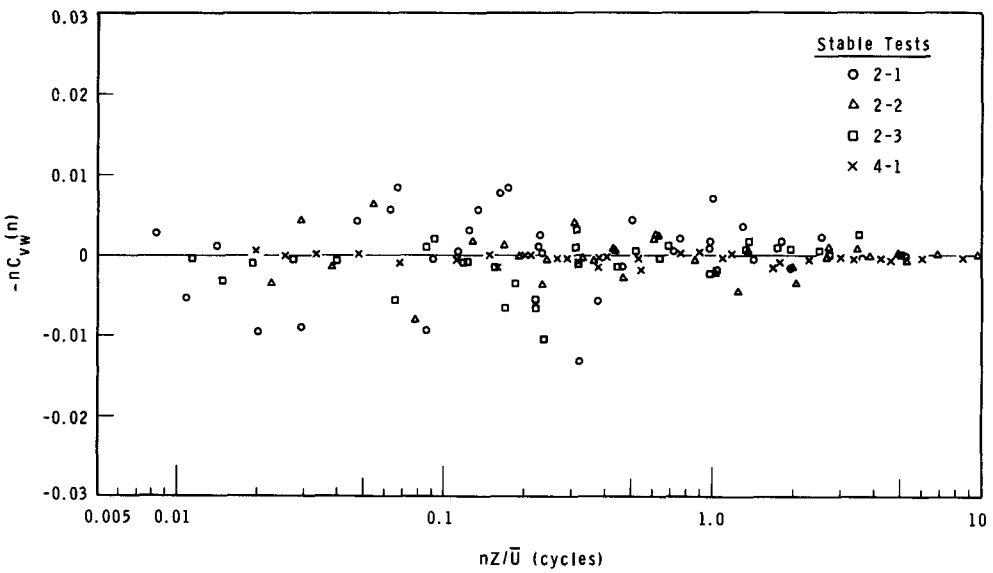

Neg 0660515-10

FIGURE 7. Cospectra Between Lateral and Vertical Velocity - Stable Tests

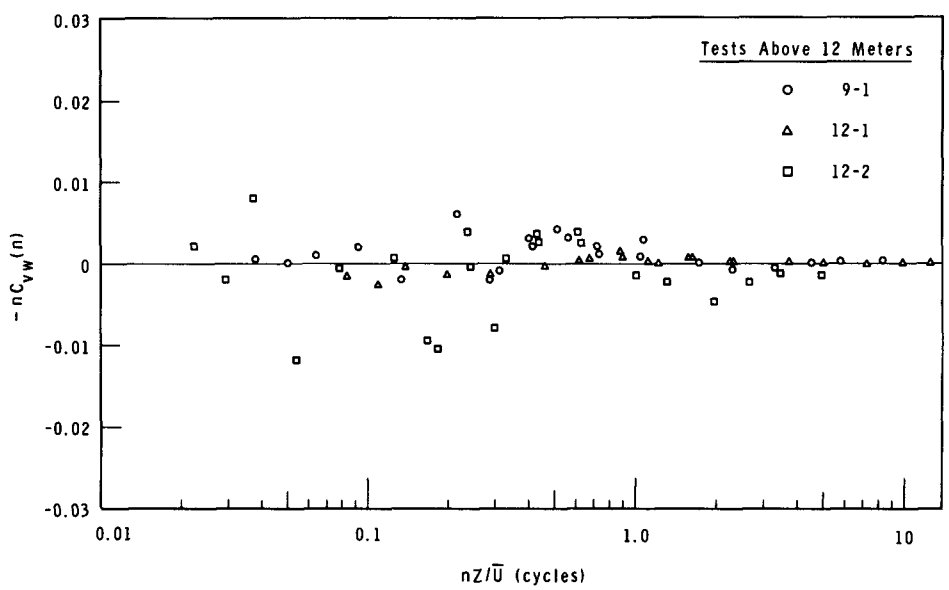

Neg 0660515-13

FIGURE 8. Cospectra Between Lateral and Vertical Velocity - Tests Above 12 Meters

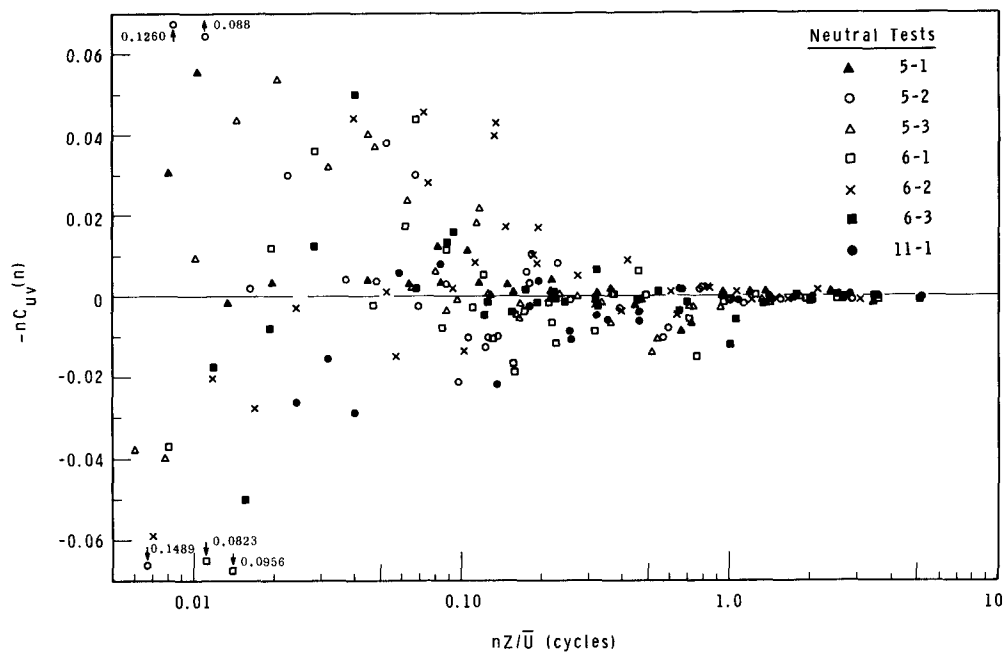

Neg 0660515-6

FIGURE 9. Cospectra Between Longitudinal and Lateral Velocity - Neutral Tests

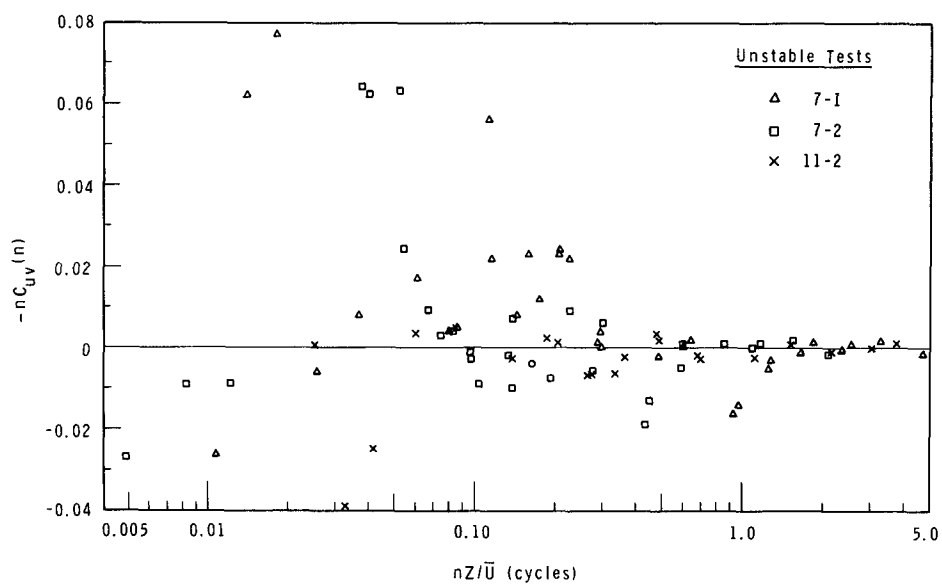

Neg 0660515-7

FIGURE 10. Cospectra Between Longitudinal and Lateral Velocity - Unstable Tests

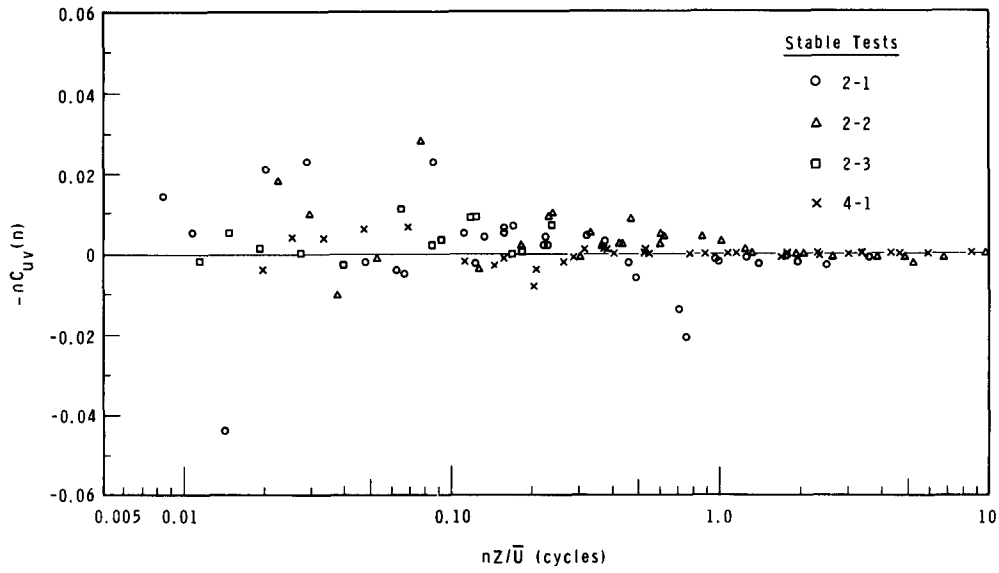

Neg 0660515-5

FIGURE 11. Cospectra Between Longitudinal and Lateral Velocity - Stable Tests

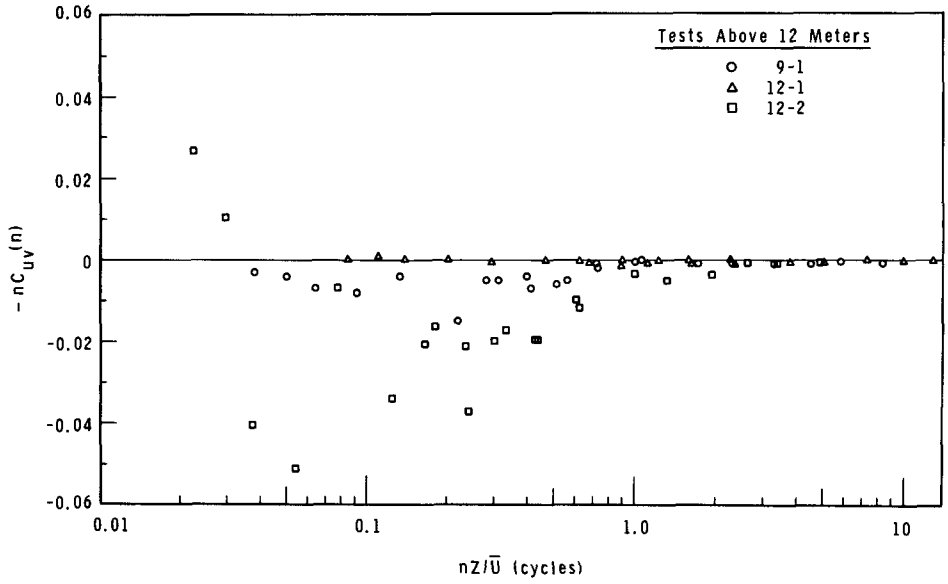

Neg 0660515-12

FIGURE 12. Cospectra Between Longitudinal and Lateral Velocity - Tests Above 12 Meters

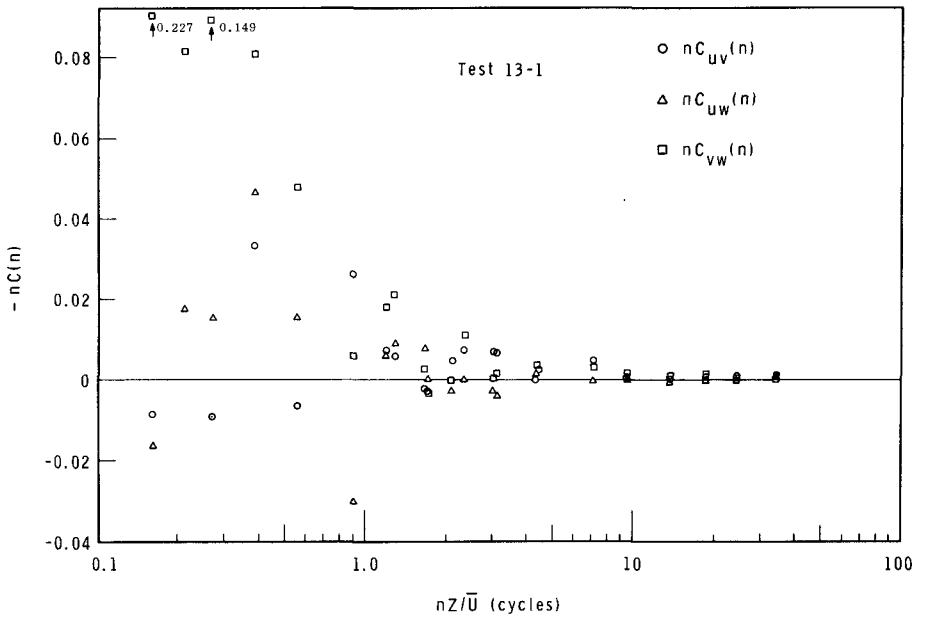

Neg 0660515-11

FIGURE 13. Cospectra for Test 13-1

low as $nz/\bar{U} = 0.1$ for longitudinal component spectra and to 0.8 for vertical component spectra.

The observation in the present study that the minus 5/3 law usually extends to lower wave numbers than the true isotropic limit (where cospectra become zero) agrees with the findings of Pond.[3] On theoretical grounds, Gifford[4] has also shown that the one-dimensional spectrum is expected to follow the minus 5/3 law below the true isotropic limit. Confirming measurements of the $\overline{u'v'}$ and $\overline{v'w'}$ cospectra are lacking in previous studies, and the $\overline{u'w'}$ cospectral measurements are few. However, Monin[5] recently reported results demonstrating the $nz/\bar{U}$ dependence, as well as stability dependence of the $\overline{u'w'}$ cospectrum which indicated that the isotropic limit occurred between $nz/\bar{U}$ values of 1 and 10, in full agreement with the results of Figures 1,2,3, and 4.

REYNOLDS STRESS RESULTS

The Reynolds stresses, calculated from the wind fluctuation data with an analog computer program, are given in Table II. With but a few exceptions, the data are not significantly different from what might be expected. The standard deviation for the flucuations of each of the wind components is divided by the friction velocity as is the mean wind speed at 3.0 m measured independently with the 80 ft tower equipment, and these ratios are listed in Table II. Though the Reynolds stresses cover a considerable range of magnitudes, the ratios demonstrate that they are consistent and reasonable. The ratio of the 3.0 m wind speed to friction velocity for neutral conditions--this ratio varies no more than ± 5% from the average ratio, except for one case--demonstrates agreement with

TABLE II. Reynolds Stresses

Stable Tests	σ_u^2	σ_v^2	σ_w^2	$\overline{u'w'}$	$\overline{v'w'}$	$\overline{u'v'}$	σ_u/u^*	σ_v/u^*	σ_w/u^*	$U_{3.0}/u^*$
2-1	1.28	0.879	0.371	-0.136	-0.00068	-0.0473	3.06	2.54	1.65	14.3
2-2	0.548	0.360	0.183	-0.0553	0.00241	-0.0111	3.15	2.55	1.82	14.3
2-3	0.255	0.126	0.132	-0.0357	0.00638	0.00583	2.67	1.88	1.92	21.7
4-1	0.206	0.104	0.0720	-0.0266	-0.000062	-0.0196	2.79	1.98	1.64	3.4†
Neutral Tests										
5-1	1.63	1.22	0.340	-0.191	-0.0106	-0.0376	2.93	2.53	1.33	12.1
5-2	2.02	0.990	0.467	-0.277	0.00329	-0.0890	2.70	1.89	1.30	12.0
5-3	2.34	1.05	0.550	-0.308	0.0307	-0.0670	2.76	1.84	1.34	12.4
6-1	1.62	0.676	0.273	-0.153	0.00743	0.794	3.25	2.10	1.34	13.8
6-2	2.22	0.864	0.424	-0.254	0.0207	-0.0117	2.96	1.84	1.29	13.1
6-3	2.03	0.862	0.552	-0.296	0.280	-0.0235	2.61	1.71	1.37	12.9
11-1	0.600	0.272	0.134	-0.0755	0.000825	-0.0418	2.82	1.90	1.33	12.0
Unstable Tests										
7-1	2.49	1.86	0.691	-0.383	0.0310	0.0246	2.55	2.20	1.34	12.1
7-2	3.02	1.81	0.890	-0.520	0.0618	-0.0391	2.41	1.86	1.31	12.5
11-2	0.479	0.317	0.113	-0.0645	0.00510	-0.0156	2.73	2.10	1.33	12.6
Tests Above 12 m										
9-1	3.00	0.178	0.154	-0.0592	0.00492	-0.0444	2.15	1.73	1.61	10.6
12-1	0.190	0.172	0.0645	-0.00765	0.0103	-0.0459	4.99	4.75	2.91	15.4††
12-2	1.09	1.16	0.475	-0.287	-0.00860	0.0710	1.95	2.01	1.29	12.0
13-1	0.865	1.72	0.845	+0.0476	0.112	-0.157				†††

†$\overline{U}$ *Missing from tower data; used wind component meter* $\overline{U}$.
††u^* *Reduced at this height.*
†††u^* *Meaningless here.*

the characteristics of the logarithmic profile where the wind speed is proportional to the friction velocity. The average ratio also leads to a roughness length of z_0 = 2.0 cm which is fairly consistent with a roughness length closer to 3.0 cm that is indicated by Hanford wind profiles. Test 6-1 may have underestimated the friction velocity somewhat because of the short length of record (13 min) so that the low frequency contributions to the $\overline{u'w'}$ correlation were poorly sampled.

The wind speed at a small height was chosen so that, for nonneutral conditions, the profile would still be close to logarithmic. The unstable cases, including Test 12-2 at 12.2 m, give essentially the same ratio as the neutral cases while the stable cases generally give values somewhat larger, indicating that the profile is deviating in the expected direction from logarithmic at 3.0 m for the stable cases. For Test 12-1 all ratios listed are large, as might be expected for such a light wind speed where the momentum flux has undoubtedly dropped off somewhat at 12.2 m.

The ratio, σ_w/u^*, is also very constant, regardless of height or wind speed, for the neutral and the 3.0 and 6.1 m unstable cases. The average value in these cases is 1.33. This value is somewhat higher than the value of 1.25 determined by Panofsky and McCormick[6] and considerably higher than the value of 1.05 found in wind tunnel investigations cited by Panofsky and Lumley.[7] However, the value here is identical to that found by Pasquill.[8] The increased value of σ_w/u^* in stable conditions noted here has not been observed in other investigations. The unstable Test 12-2 at 12.2 m gives results not significantly different from the neutral cases.

The ratios σ_u/u^* and σ_v/u^* are more variable than σ_w/u^*, but no dependence of height, wind speed, or stability is noted. The lack of dependence of the ratios σ_u/u^* and σ_v/u^* on wind speed is in agreement with previous observations, but investigators have found elsewhere a strong dependence of σ_v/u^* on stability, as well as a noticeable stability dependence for σ_u/u^*.

Some of the differences noted between the variance calculations of this investigation and other reported results can be attributed to the high-pass filtering performed in the analog computer program used in the analysis. The filter removed fluctuations with periods greater than about 8 min for the tests below 12 m and removed periods greater than about 17 min for tests above 12 m. Thus, contributions from low-frequency, horizontal mesoscale eddies were removed. If the data had not been filtered in this manner, varying amounts of low-frequency energy would have appeared in the horizontal component variances, depending on the length of record. A number of filters with various cut-off points were tried. A filter was chosen which would pass the entire vertical velocity variance and the momentum flux without limitation. Consequently, it was considered that all microscale contributions to the turbulence were included. Another difference is the large contribution of turbulent energy at low frequencies in the lateral wind component variance found at Hanford in stable conditions; whereas, investigations at other sites

have shown a marked lack of low-frequency energy for stable situations.

The $\overline{u'w'}$ covariance is large, as expected, and is systematically related to the wind speed as described above. The integrals of the product of u' and w' throughout the analysis (see Figures 14 and 15) increase at a steady rate through the tests for both the cospectral estimates and the total covariance calculations, demonstrating little statistical variability.

The $\overline{v'w'}$ covariances are small, generally less than 10% of the corresponding $\overline{u'w'}$ covariances, except above 12 m where the momentum flux has decreased,

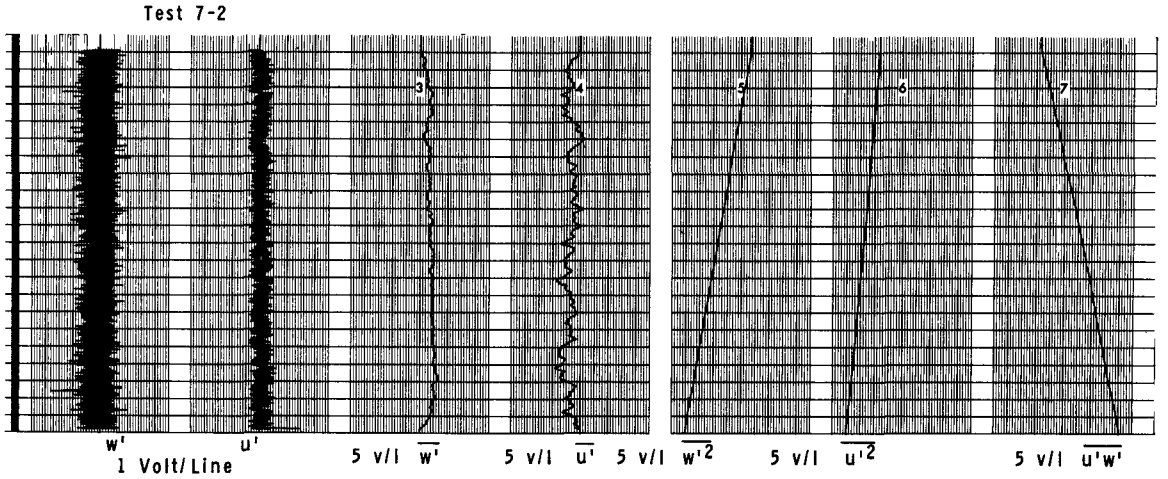

Neg 0660582-30

FIGURE 14. Reynolds Stress Monitored Results

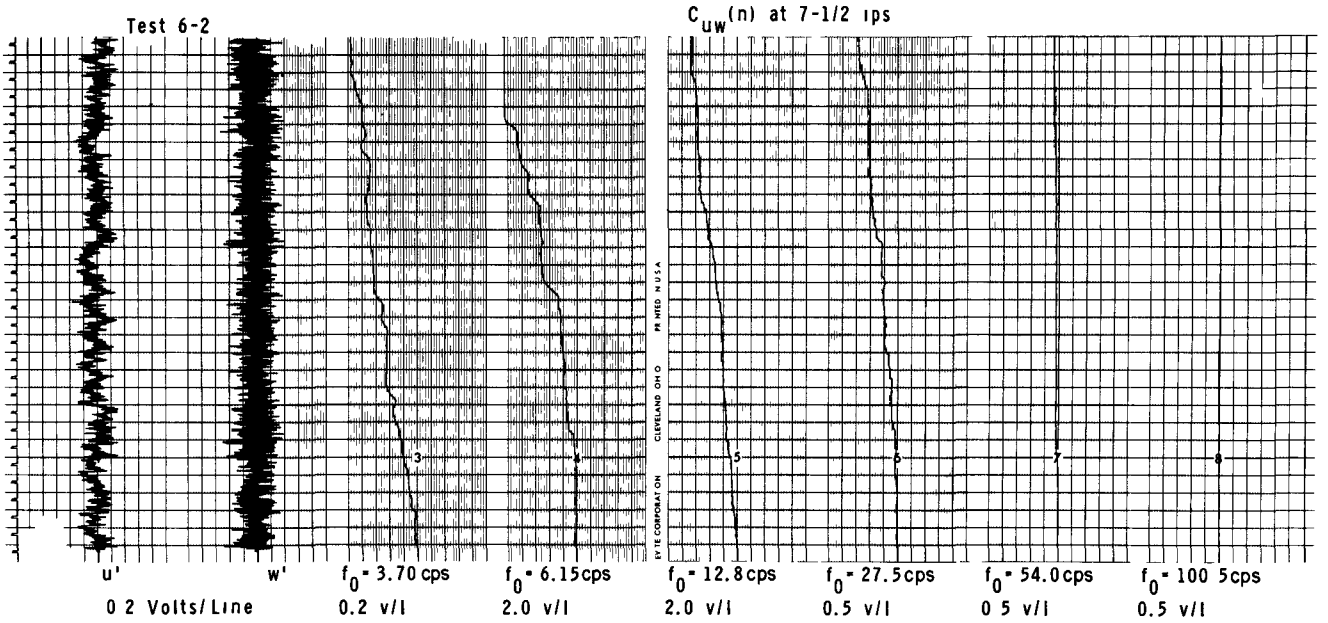

Neg 0660582-26

FIGURE 15. Cospectral Monitored Results

or for the 87 m case where $\overline{u'w'}$ is reversed in sign which corresponds to a decrease in wind speed with height. Here the $\overline{v'w'}$ stress transfers the momentum toward the surface corresponding to a wind direction shear at 400 ft. The $\overline{v'w'}$ cospectral densities are larger than might be expected from the covariance values, since in some cases positive contributions at high wave numbers are, to a large extent, balanced by negative contributions at low wave numbers. Even larger negative contributions to the total $\overline{v'w'}$ covariances, at wave numbers below those, passed by the high-pass filter as evidenced by Test 6-1 and 7-2 where the $\overline{v'w'}$ covariances were also calwithout the filter. The resulting negative covariances, -0.0864 and -0.0581, respectively, were opposite in sign to the values where the very low frequencies were filtered out; this corresponds to the required wind direction decreases with height noted between 7 and 400 ft during the testing. The integrals through the test time of the product of v' and w', monitored in the analysis of both $\overline{v'w'}$ covariance and cospectral density, showed more statistical variability than with the $\overline{u'w'}$ analysis. However, the integrals demonstrated a general trend toward the final values throughout the period of integration. Figure 16 shows the increased variability over the $\overline{u'w'}$ calculation shown previously in Figure 15 for the same test.

The $\overline{u'v'}$ covariances are quite large; but, as the cospectral distributions show, the contributions are made in a rather disorganized way, occurring both positively and negatively at larger and larger magnitudes for lower and lower wave numbers. In addition, the $\overline{u'v'}$ covariance and cospectral integrals monitored during the analysis show a distinct lack of statistical regularity, a given integral often reaching both

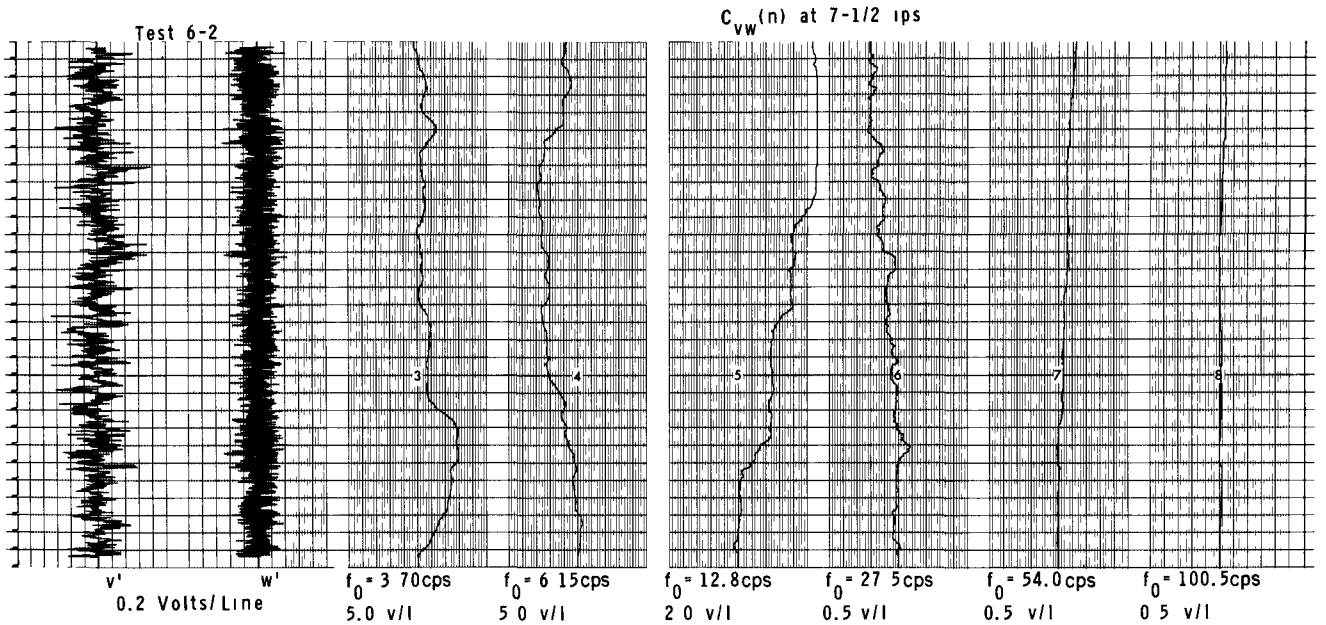

FIGURE 16. Example of Variability in Cospectral Calculation

large positive and large negative values at different points in the integration period. The variability is even greater than seen in Figure 16. Monitoring the analog computer analysis in this way provided insights into the dependability of the estimates obtained. The confidence in the stability of $\overline{u'w'}$ covariance and cospectral results (as opposed to the lack of confidence in any significance attached to the $\overline{u'v'}$ results derived from monitoring the analog analysis) could not have been supplied by any ordinary test of statistical significance.

LATERAL COMPONENT SPECTRA

The lateral component spectra are not as well organized as the vertical and longitudinal spectra. A large fraction of the total variance appears at low wave numbers in a disorganized manner as a function of $nz/\overline{U}$ and with widely varying magnitudes for neutral and unstable conditions. However, a degree of similarity is detected in the lateral spectra shown in Figures 17 through 20. All spectra generally reduce in amplitude with increasing wave number above about $nz/\overline{U} = 0.1$.

For neutral conditions, as seen in Figure 17, multiple peaks at wave numbers below $nz/\overline{U} = 0.1$ are common. For unstable conditions a range of even more consistently high spectral estimates below about $nz/\overline{U} = 0.1$ is observed in Figure 18. The stable tests demonstrate the most consistent similarity, seen in Figure 19, exhibiting a marked absence of the energy at low wave numbers found in the other stability groups. The stable group is again shifted to somewhat higher wave numbers than the neutral and unstable

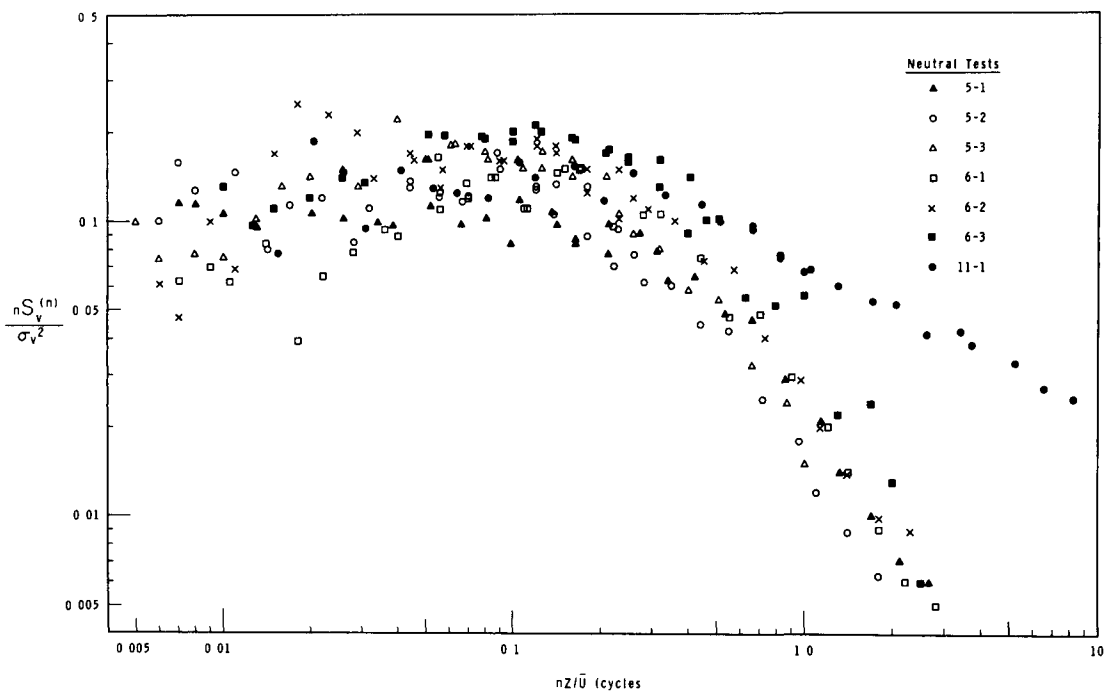

Neg 0660582-19

FIGURE 17. Lateral Wind Component Spectra - Neutral Tests

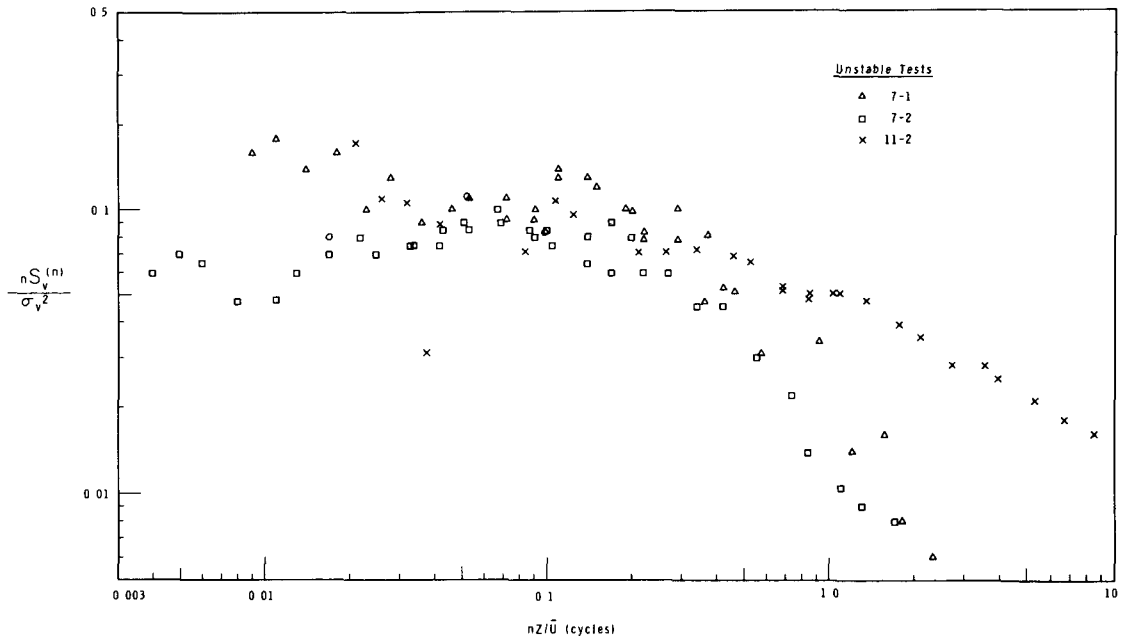

Neg 0660582-17

FIGURE 18. Lateral Wind Component Spectra - Unstable Tests

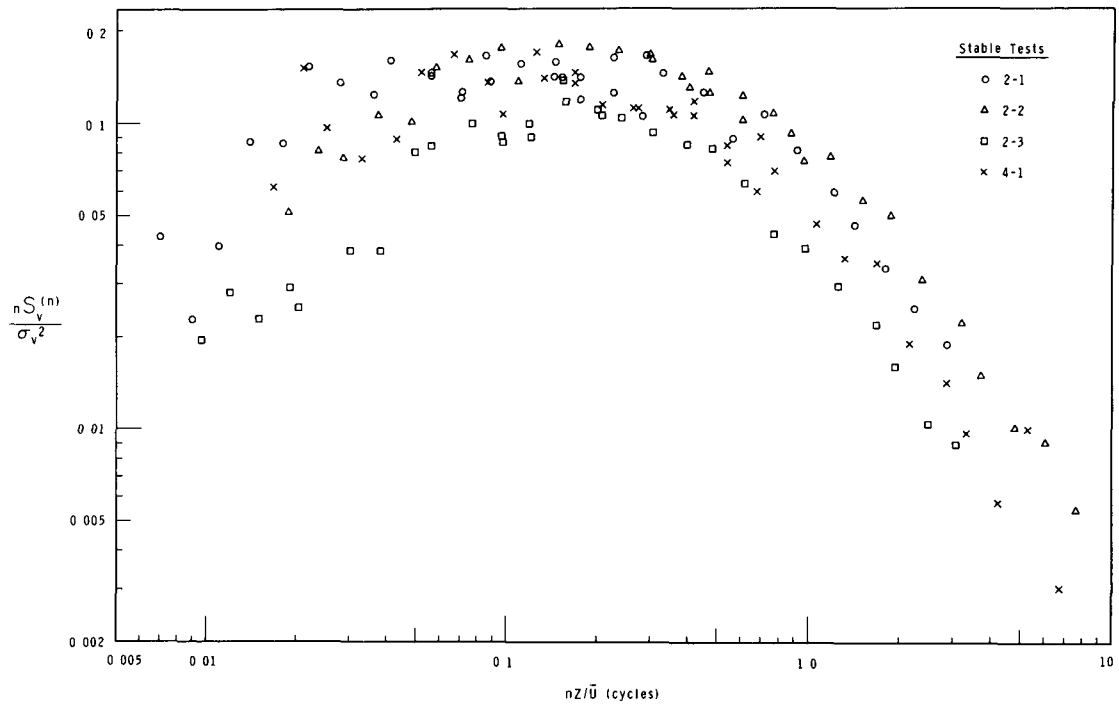

Neg 0660582-18

FIGURE 19. Lateral Wind Component Spectra - Stable Tests

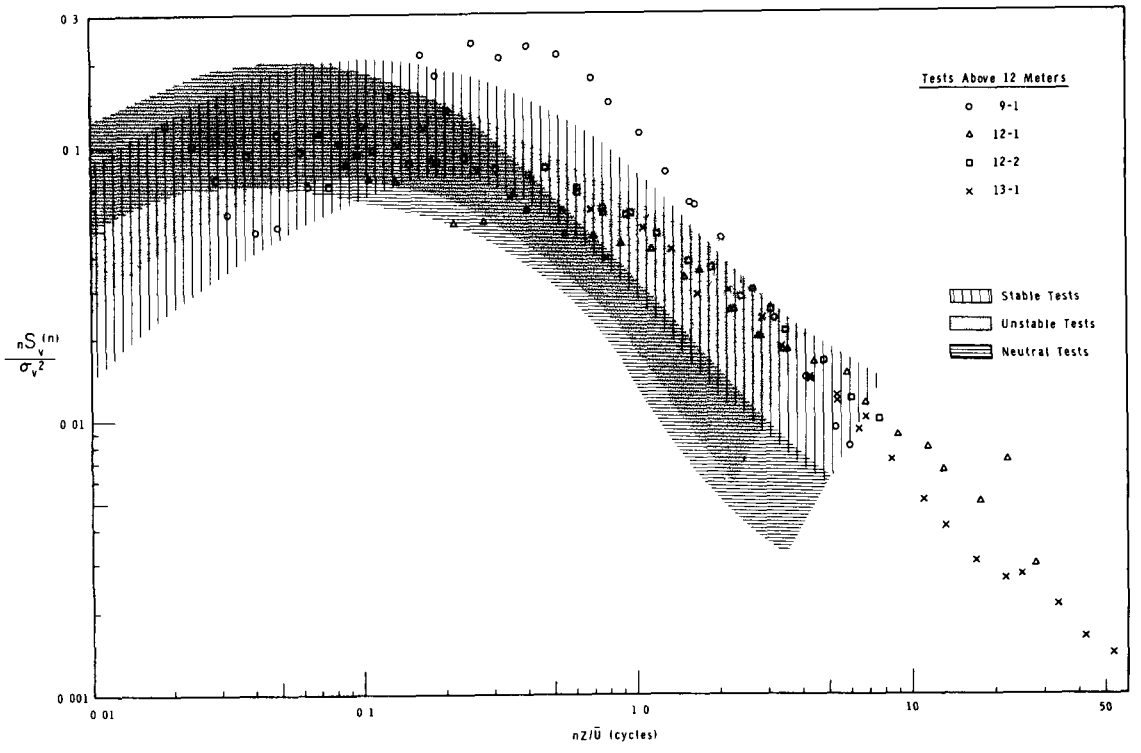

Neg 0660582-20

FIGURE 20. Lateral Wind Component Spectra - Tests Above 12 Meters

cases, and the 12.2 m stable test in Figure 20 is displaced to considerably higher $nz/\overline{U}$.

The v' component spectra are observed in most cases, from Figures 17 through 20, not to follow the minus 5/3 law at the high frequency end of the spectrum within the range of measurement. Though this is not a universal characteristic of the turbulence and could be peculiar to the particular terrain features of the Hanford site, a similar wide variability of the inertial subrange inception might be anticipated at other sites. If turbulent energy is being added within a wave number range from an external source as well as cascaded to higher wave numbers by inertial transfer, the negative slope must be less than two-thirds. However, if energy is being removed from the turbulence in a given component, the negative slope of the logarithmic plot within the range of concern must be greater than two-thirds. The observed decrease in lateral component spectral density with increasing wave number, greater than expected from inertial transfer, indicated that energy is being removed from the v' component turbulence in the wave number region where the other components demonstrate no removal or addition. Cospectral data support this contention as described in the following discussion.

A very tentative possibility for explaining the removal of energy from the v' component turbulence is the feeding of energy into the mean motion. Just as the $\overline{u'w'}$ Reynolds stress withdraws

energy from the mean motion and supplies it to the turbulence in the u' component, the $\overline{v'w'}$ Reynolds stress can work with the vertical gradient of the mean lateral component, transferring energy from the turbulence in the v' component to the mean lateral wind component. This results in the maintenance of wind direction shear. Thus the mechanical energy term, $\overline{v'w'}\ \frac{\partial \overline{V}}{\partial z}$, should not necessarily be ignored in the turbulent energy budget equation. The existence of considerable organized correlation in the $nC_{vw}(n)$ cospectral plots up to $nz/\overline{U} = 3.0$, beyond the point where the other cospectra have fallen to zero, supports the contention that this Reynolds stress is removing energy from the v' component turbulence in the same region of wave numbers. The mean wind direction shears, though the measurements were not adequate for quantitative evaluation, were of the proper sign required for feeding the mean motion. In all unstable and neutral cases during the first series of tests conducted on two consecutive days, the wind backed 10 or 15 degrees between 7 and 400 ft. The increase of the lateral mean wind component with height requires a net negative $\overline{v'w'}$ covariance, demonstrated by two calculations where the high pass filter was left out of the Reynolds stress program, allowing the covariance at low wave numbers to be included. The calculations with the filter in the program gave a positive covariance for these two cases as well as for all but one of the other tests performed on these two days, because the low frequency covariance was filtered out. The $\overline{v'w'}$ cospectra likewise show the negative correlation at low wave numbers and a positive correlation at high wave numbers. Such a distribution not only removes energy from the turbulence at the upper end of the spectrum but supplies it at low wave numbers, contributing to the considerable variability detected in the lateral component spectra.

There are exceptions to the behavior discussed above. Tests 11-1 and 11-2, in neutral and unstable conditions respectively at 6.1 m, both follow the minus 5/3 law beyond $nz/\overline{U} = 3.0$ and both have essentially no correlation between the v' and w' components over the range of frequencies filtered for cospectral density. Thus the absence of energy withdrawal from the turbulence, to support a mean lateral gradient, allows the turbulence to become isotropic at an earlier stage.

None of the stable tests show any sign of an inertial subrange even though the cospectral densities are quite small, and no organized area under the $\overline{v'w'}$ cospectral curves near $nz/\overline{U} = 3.0$ is obvious which might transfer energy out of the turbulence. However, wind direction shears, which were not adequately measured here, are often very large in stable situations and small cospectral areas might yet be effective in altering the low level of turbulence present in the stable cases.

Tests above 12 m show only a limited agreement with the minus 5/3 law. The light wind unstable case, Test 12-1, agrees quite well above $nz/\overline{U} = 1.0$ and the 87 meter case, Test 13-1, is not inconsistent with the law above $nz/\overline{U} = 10$; but the other tests deviate noticeably throughout the range of measurement.

Summarizing the significant factors of the spectra briefly, the normalized spectra for each component have a relatively simple and repeatable dependence on $nz/\overline{U}$. There are, however, differences from one component to another, which is to say that a different similarity relationship is observed for each component. This similarity is most marked for the vertical component and poorest for the lateral component. At low wave numbers the apparent similarity might be questioned because of the large variability of the estimates. All demonstrate a slight shift to higher wave numbers over the entire spectrum for stable conditions near the ground and a large shift for the stable case at 12.2 m. Also, convective peaks in the vertical component spectra are found in unstable cases above 12 m at low wave numbers, while the mechanical energy peak and the upper end of the normalized spectrum correspond to the normalized neutral spectrum. A transfer of turbulent energy to the mean flow is indicated in the lateral component spectra for many tests, shifting the lower end of the inertial subrange to higher wave numbers. Otherwise, it generally begins at about $nz/\overline{U} = 3.0$, although the minus 5/3 law for the vertical component extends down to $nz/\overline{U} = 0.8$ to 1.0 and, for the longitudinal component, down to $nz/\overline{U} = 0.2$ to 1.0.

The features of the spectra for the tests at 3.0 and 6.1 m can best be seen from pooled results for each component. These are shown in Figure 21 for the longitudinal component, Figure 22 for the vertical component, and Figure 23 for the lateral component. Average

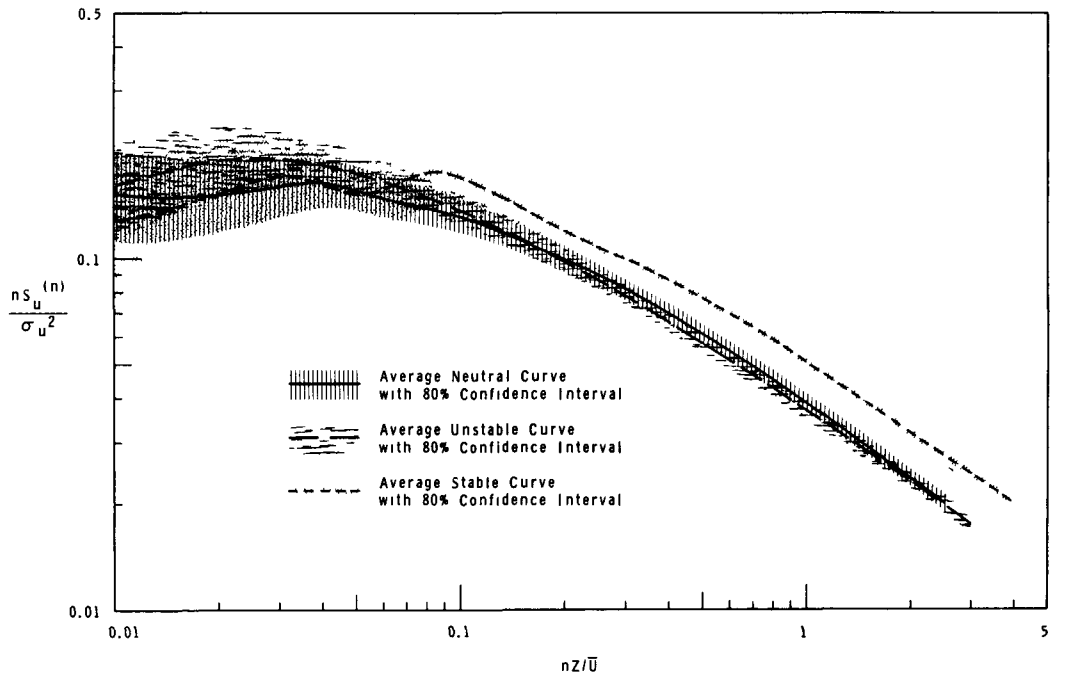

Neg 0661348-3

FIGURE 21. Average Longitudinal Wind Component Spectrum

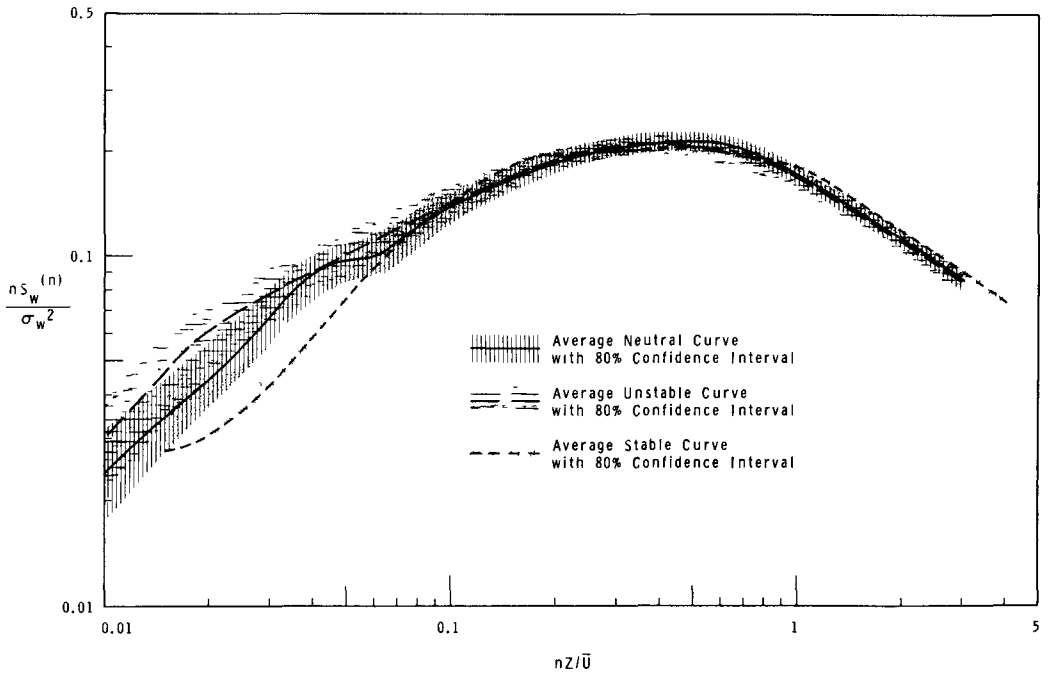

Neg 0661348-1

FIGURE 22. Average Vertical Wind Component Spectrum

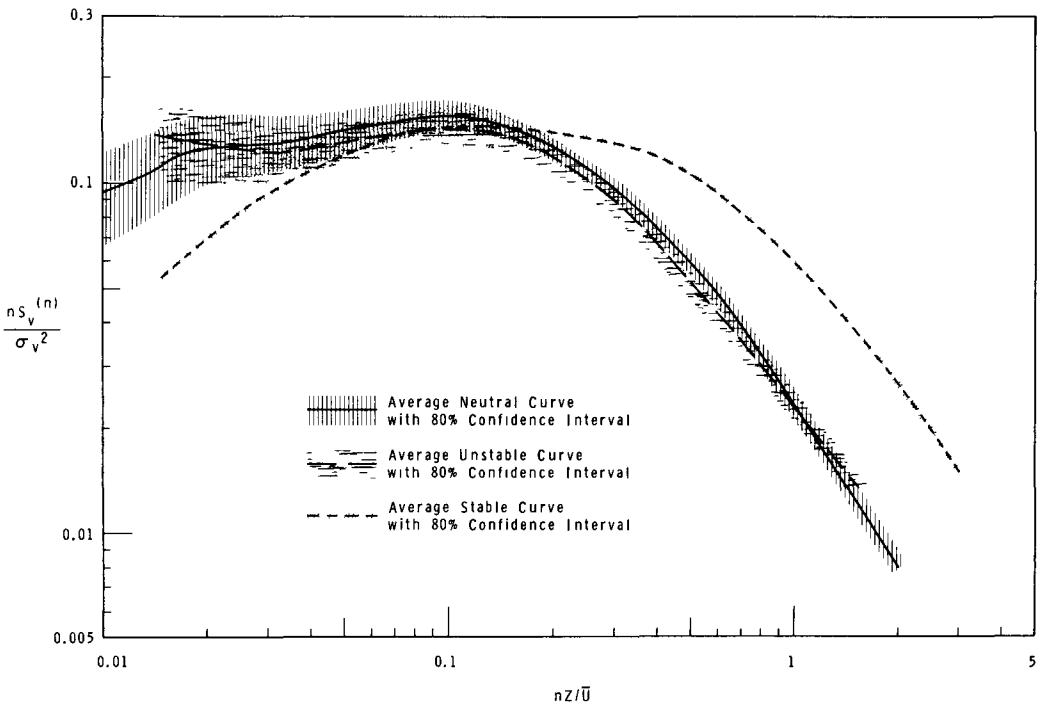

Neg 0661348-2

FIGURE 23. Average Lateral Wind Component Spectrum

curves for neutral, unstable, and stable cases are shown in each figure with the 80% confidence interval indicated with shading for each stability group, reflecting the reduced uncertainty of the data resulting from the averaging. The validity of such averaging for the lateral component spectra remains in question because it is not obvious that the similarity hypothesis applies here. Excluded from the lateral component averages for the neutral and unstable cases are Test 11-1 and 11-2, respectively, which were obviously not similar to the others. In addition to demonstrating clearly (particularly at low wave numbers) the features of the spectra previously discussed, such as the insignificant difference between neutral and unstable cases within the forced convection region and a noticeable shift to higher wave numbers for stable cases, it is also clear that the shift of the stable curves necessary to maintain similarity is not the same for all components. For stable cases, the normalized v' spectrum is similar in shape to that for neutral cases but is shifted to higher $nz/\overline{U}$ by a factor of 2.0. For the u' component, the factor is 1.5 and for the w' component the factor is 1.1.

REFERENCES

1. *C. E. Elderkin. "Spectral Distribution of Atmospheric Turbulence," Pacific Northwest Laboratory Annual Report for 1965 in the Physical Sciences, Volume 1: Atmospheric Sciences, BNWL-235 1 Pacific Northwest Laboratory, Richland, Washington, May 1966.*

2. *A. N. Kalmogoroff. "The Local Structire of Turbulence in Incompressible Viscous Fluid for Very Large Reynolds Numbers," Doklady, ANSSSR 30, p. 301. 1941.*

3. *S. Pond, R. W. Stewart, and R. W. Burling. "Turbulence Spectra in Wind over Waves," Journal Atmospheric Sciences, vol. 20. 1963*

4. *F. Gifford, Jr. "The Interpretation of Meteorological Spectra and Correlations," Journal of Meteorology, vol. 16. 1959.*

5. *A. S. Monin. "Empirical Data on Turbulence in the Surface Layer of the Atmosphere," Journal Geophysical Research, no. 67. 1962.*

6. *H. A. Panofsky and R. A. McCormick. "The Spectrum of Vertical Velocity near the Surface," Quarterly Journal of Royal Meteorological Society, no. 86. 1960.*

7. *J. L. Lumley and H. A. Panofsky. The Structure of Atmospheric Turbulence. Interscience Publishers, New York, 1964.*

8. *F. Pasquill. "Recent Broad-band Spectral Measurements of Turbulence in the Lower Atmosphere." J. Geophys. Research, no. 67, P. 3025. 1962.*

WAKE STUDIES

W. T. Hinds

A study to investigate the diffusion of pollutants around and near an obstruction, such as a building, was started in 1966. Earlier work concerning diffusion in wakes has been largely confined to wind tunnels, which provide the possibility for readily controlling the direction of the wind relative to the obstruction. Since fluctuation of wind direction is a pervasive aspect of the real atmosphere, the case of constant wind direction can only be approximated in field work. A properly designed field test is essential nonetheless, both as a proving ground for tunnel results and to investigate phenomena which are not properly or simply simulated in wind tunnel studies. Examples of such phenomina are the increased diffusion due to wind direction fluctuations and the effects of atmospheric stability.

EXPERIMENTAL DESIGN

A fairly large building, abandoned some years ago, was chosen for the experimental site. The building is about 25 m wide, 34 m long, and 11 m high, a pure rectangular paralled piped. The site has an undisturbed fetch upwind of some miles and lies on a nearly level and flat surface. The sampling arcs were surveyed around the building at distances of 30, 50, and 100 m from the building center and extending more than 300 degrees around the building. The sampling grid is shown in Figure 1.

The tracer selected was the fluorescent pigment ZnS, which has been conveniently used in the techniques developed at Hanford in past years. One modification was required in the usual procedure: the short travel times involved in reaching the nearer samplers precluded using water as the tracer carrier, so highly volatile and nontoxic trichloroethane was employed.

The wake of a building is characteristically unsteady, with strong curvature of the streamlines in the lee of the building. Tracer concentration in such conditions cannot be sampled realistically by a stationary filter such as has been used in the past for other diffusion studies. Although the effect of misorientation of the sampler with respect to the wind is not well known, it may be considerable, as indicated by Green and Lane.[1] A simple and rugged wind-oriented sampling head was therefore developed, the SOS (self-orienting sampler), and this was used in the lee of the building where unsteady flow is common.

In addition to the average concentration during the test, the time history of concentration at a point was measured by using the Real Time Sampler.[2] This unit was likewise equipped with the self-orienting sampling head to minimize misorientation errors; so equipped, the Real Time Sampler is called SORTS.

In the early stages of the study reported here, only ground level sources were used, placed as near the upwind stagnation point as possible.

THE FORM OF THE WAKE

The formation of the close-in wake behind a bluff body is familiar, and

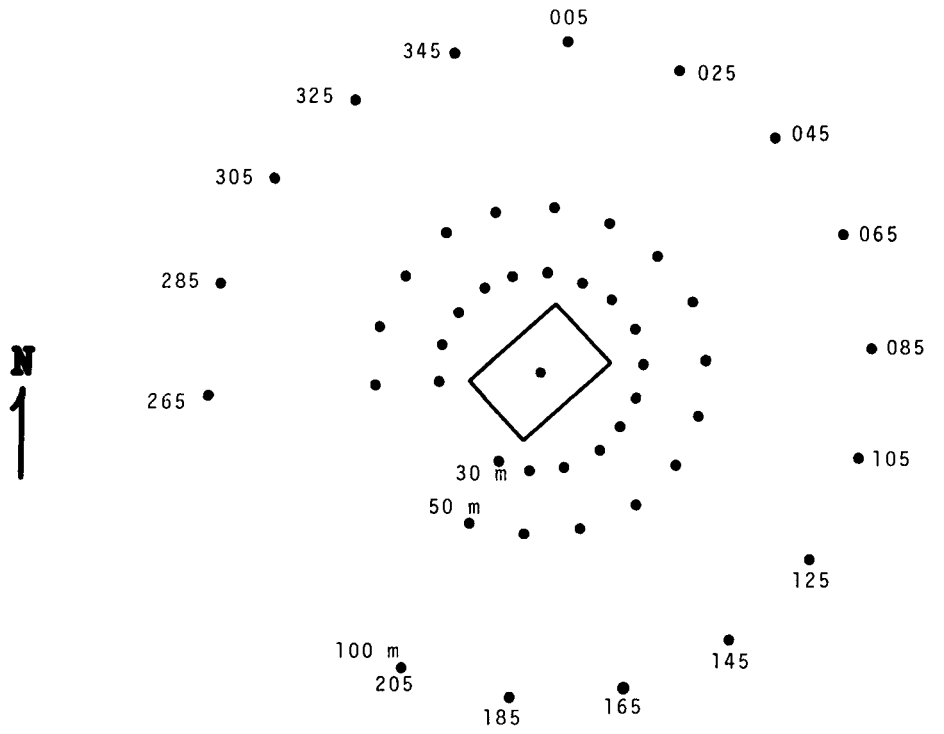

FIGURE 1. Sampling Grid for Wake Diffusion Studies

has been described several places in the literature, both in aerodynamic and in meteorological studies. The salient features here are the extent and magnitude of the "backflow" portion of the wake, the portion which results from the pressure deficit in the lee of the building.

The backflow portion of the wake is well represented by the tracer released in the upstream flow. This can be seen in Figure 2, which shows the results from a 15-min test, W-6, and a 6-min test, W-7. The isopleths of concentration are not symmetrical about the building since the source point was not precisely at the upwind stagnation point, but the general features of the wake are nonetheless indicated. There is a fairly broad region influenced by the presence of the building, and a definite minimum in the average concentration dominates the immediate area of the downwind stagnation point. In this respect, the full scale results parallel those from wind tunnel work.

The extent of the backflow portion of the wake is not defined by the concentration isopleths. Visual observation indicates that the backflow extends three to five building-heights downwind, depending on the wind speed. This is considerably larger than indicated by wind tunnel studies[3] and must be considered to be a tentative conclusion.

SHORT-TERM CONCENTRATION FLUCTUATIONS

The concentration of a contaminant in the atmosphere is not a steady entity and, depending upon the relation between the source and the receptor, may be quite variable. Two methods of indicating the magnitude of the variations are

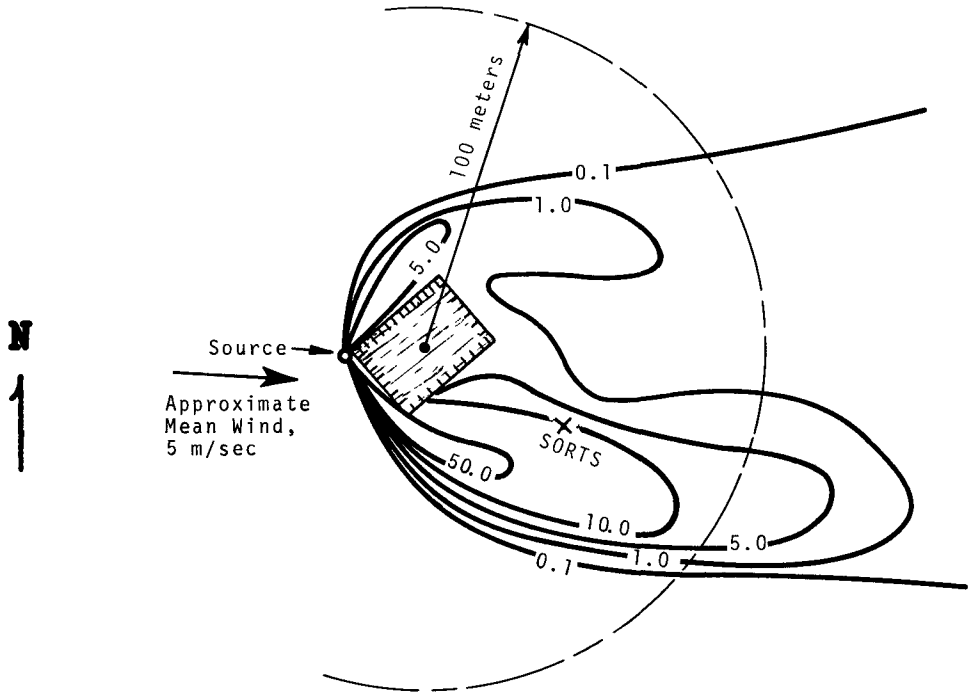

FIGURE 2(a). Concentration Isopleths for Test W-6 in Arbitrary Units

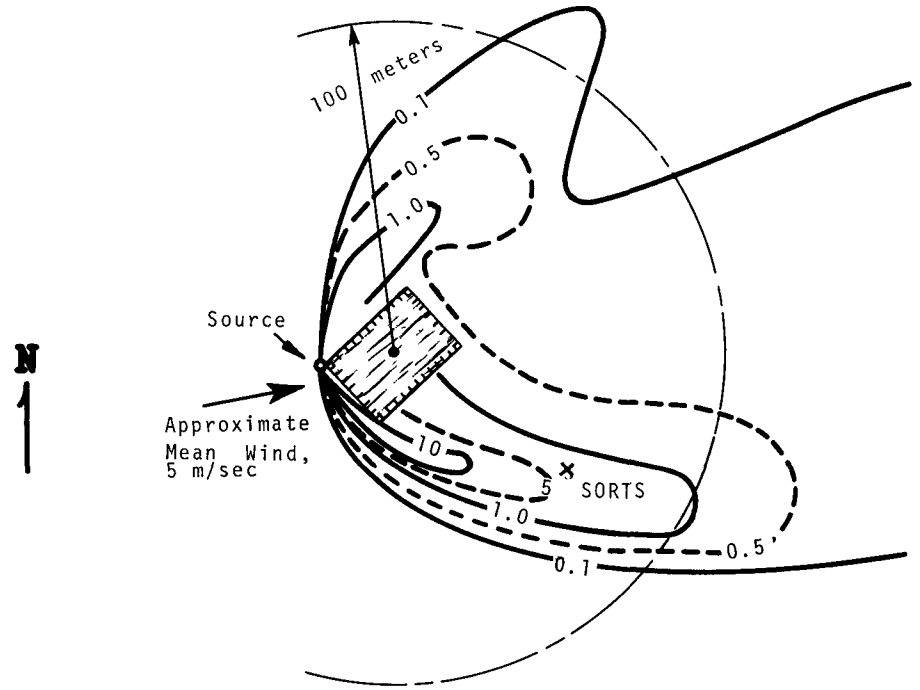

FIGURE 2(b). Concentration Isopleths for Test W-7 in Arbitrary Units

the variance of the fluctuations and the ratio of maximum concentration to average concentration. Although the variance of the concentration has some advantages in theoretical work, the "peak-to-mean" approach has been commonly used in reporting experimental work and will be adopted here.

The concentration observed during an interval of time depends upon the sampling interval. The shorter the interval, the higher the possible concentration and the greater the variety of results.

The short-term concentration fluctuations were measured in terms of basic five-second averages of concentration as determined by use of the SORTS. The range of 5-sec averages was examined for the 5-sec interval with the highest average concentration; then 10-sec intervals were searched for the highest average, then 20-sec intervals, and so on. The concentrations were then normalized to the average concentration during the test. The duration of the test (T) was divided by the time intervals appropriate for each of the concentration maxima (t). Then, a plot of X(t)/X(T) against T/t shows the dependence of the peak-to-mean concentration on the time of averaging. This is shown in Figure 3, along with curves as presented by Gifford,[4] to indicate the relation of wake concentration variability with that observed in unobstructed flow. It is clear that a power function fits well except when t approaches T. The variability in a wake is intermediate between the ground source and elevated source curves from Gifford's summary. Since the variation in any plume is accentuated by sampling away from the centerline (as shown by Gifford's two curves), it seems likely that a similar situation would be found in a wake. This appears to be the case, as inspection of the isopleths for tests W-6 and W-7 shows. The SORTS in test W-6 was somewhat more removed from the centerline of the major lobe of the wake than during test W-7, and the peak-to-mean ratios observed in test W-6 were more nearly comparable to an elevated source than in test W-7. The variation in concentration caused by the existence of the wake appears to be similar in magnitude to those caused by an elevated source. The effect of an elevated source discharging into a wake is at present unknown.

REFERENCES

1. *H. L. Green and W. R. Lane. Particulate Clouds, E&FN Spon, Ltd., London. 1957.*

2. *P. W. Nickola, M. O. Rankin, M. F. Scoggins, and E. M. Sheen. A Device for Recording Air Concentration of Zinc Sulfide Fluorescent Pigment on a Real Time Scale, HW-SA-3317. General Electric Company, Richland, Washington, January 10, 1964.*

3. *Benjamin H. Evans. Natural Airflow Around Buildings, Texas Engineering Experiment Station Report 57. College Station, Texas, 1957.*

4. *F. Gifford. "Peak to Average Concentration Ratios According to a Fluctuating Plume Dispersion Model." Inter. J. Air Pollution, vol. 3, no. 4, pp. 253-260. 1960.*

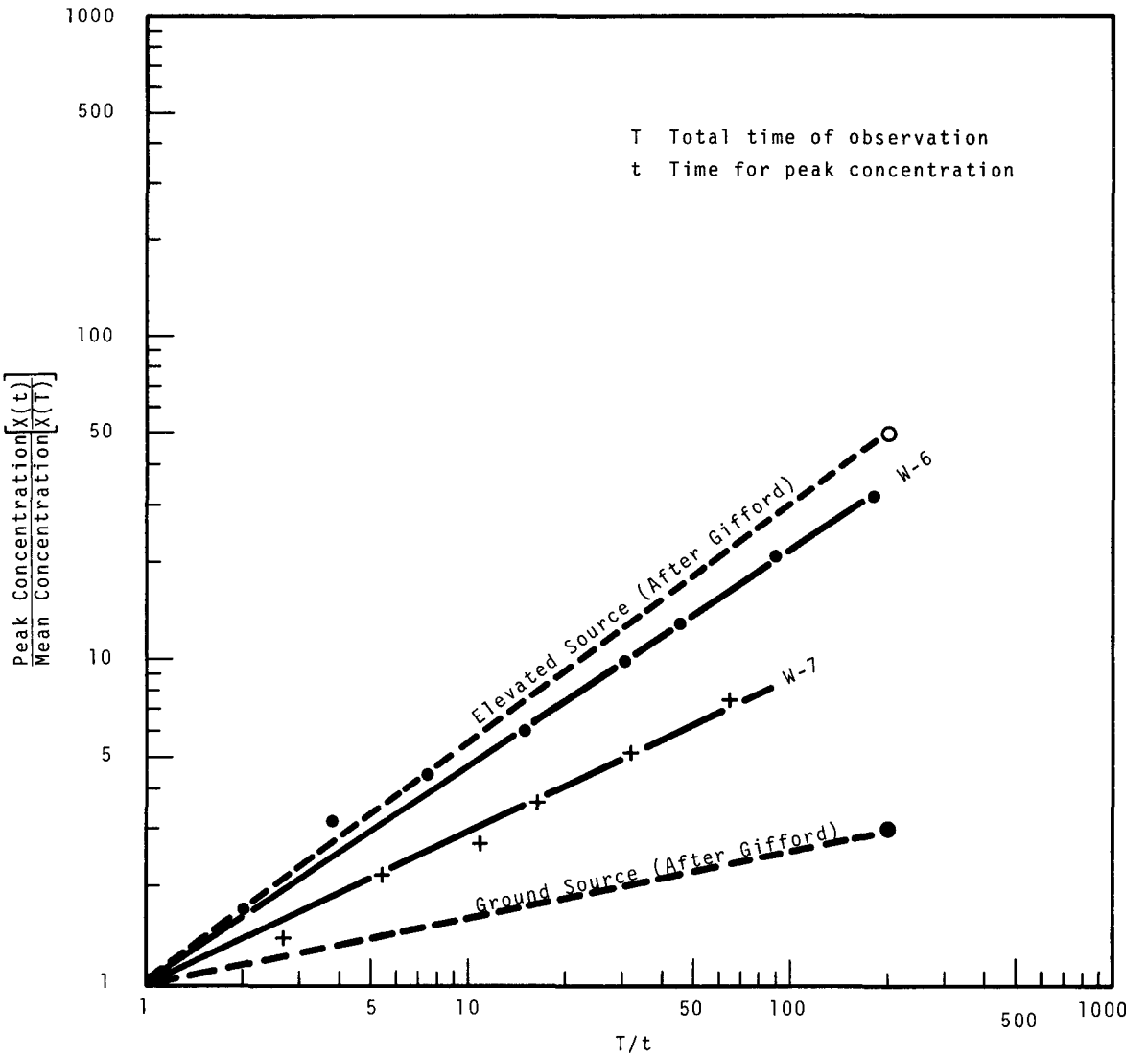

FIGURE 3. Peak-to-Mean Concentration Ratios as a Function of Averaging Time Ratio

INSTANTANEOUS PLUME DETECTION

P. W. Nickola and C. E. Elderkin

INTRODUCTION

Most techniques for sampling atmospheric tracers or pollutants involve the collection of a bulk sample over a period of minutes to days. Conclusions drawn on the basis of these samples concern mean dosages or concentrations of the sampled atmospheric contaminant for the same relatively long sampling periods. The development of a device capable of monitoring and recording concentrations of a zinc sulfide tracer on a real-time scale[1] has opened the door for more detailed information concerning the instantaneous or short term concentrations contributing to the previously investigated mean dosages or concentrations.

In 1966, a study was started into the near-instantaneous cross-wind structure of a diffusing plume as defined by a truck-mounted real time sampler (RTS) for zinc sulfide. Among the relationships being investigated are the relationship of this near-instantaneous cross-wind plume to that of the mean plume and the relationship of the observed downwind plume distribution to the source winds.

EXPERIMENTAL PROCEDURE

A real time sampler was mounted on a tripod which was fixed on the bed of a pickup truck. All power supplies, vacuum sources, and the recorder which are necessary to operate the system, were mounted on the truck. During field tracer releases of 1/2 hr duration, the truck was driven back and forth along an arc at a constant distance from the tracer source. A series of metal stakes was inserted in the ground along the arc at 3° increments; these were numbered with respect to their direction from the source and served to identify the position of the sampler as it was driven past.

An attempt was made to drive the truck at a constant rate (20 mph by the truck speedometer). The speed was a compromise between slow speeds (dictated by relatively rough arc roads and the presence of sensitive equipment on the truck) and high speeds (dictated by a desire to pass through as near as possible, an instantaneous crosswind plume distribution).

Each time the truck passed one of the identifying stakes along the arc, the event marker, which recorded at the edge of the strip chart concentration record, was activated. The traverse of the truck through the plume was terminated when the truck was well beyond the edge of the instantaneous tracer plume. This determination was made by observing the strip chart which recorded the tracer concentration.

The chart drive on the concentration recorder was set at the 6 in./min rate. This relatively high chart speed was chosen in order to define more closely the history of the concentration. An integrator on the recorder was of considerable help in subsequent reduction of the data by one-second increments.

In addition to the near-instantaneous crosswind concentration generated from the RTS data, it was possible to determine a mean crosswind concentration profile along the truck-driven arc. These data were obtained from the filters mounted on each stake along the arc. Flow through these filters was controlled by a critical flow orifice mounted in the vacuum line preceding each filter. The mass of zinc sulfide on each filter was determined by the Rankin counting technique.[2,3] A knowledge of mass, flow rate, and duration of tracer emission permitted the calculation of a concentration at each filter position.

Ideally, for comparison of the mean and instantaneous plume concentrations along an arc, the stake-mounted filters and the RTS intake should have been at the same elevation. The filters were exposed at a 1.5 m elevation. The RTS intake, however, was at an elevation of 3.0 m due to the mechanics of mounting the relatively bulky sensor firmly in a location where airflow around the moving truck would have a minimal effect.

ANALYSIS AND RESULTS

To date, three field experiments involving the moving RTS system have been completed. Although a considerably greater number of experiments will be necessary to draw any firm conclusions on the merit of this technique, let us examine some of the proposed methods of analysis and some of the results obtained from the relatively sparse data now available.

During the first field test, designated U-47, the RTS was operated along an arc 1600 m from the tracer source. As was the case in all tests to be discussed, the tracer was released from a tower at an elevation of 26 m. In the first attempt, only four traverses of the plume were obtained during the half-hour tracer generation. Figure 1 shows observed concentrations along the arc -- both the half-hour mean and the near-instantaneous values. The graphed concentrations (and all subsequent concentrations given in this report) have been normalized to a 1 g/sec emission rate.

Figure 2 gives the concentration versus crosswind distance values for Field Test U-48, a test conducted in a slightly stable atmosphere. (Tests U-47 and U-50 were conducted in unstable to neutral atmospheres.) Because traverses were made along an arc closer to the source (800 m) and because sampling procedures improved, eight traverses were possible during this field test. No tracer at all was observed during the sixth traverse; apparently the plume was completely aloft during this crosswind sampling.

During Field Test U-50, the plume was traversed on nine occasions at a distance of 800 m from the source. Tracer was observed on all nine traverses and the graph showing concentration versus crosswind distance was consequently so complex that it is not reproduced here. In one instance, the near-instantaneously detected tracer was smeared over 552 of the 630 m embraced by the one-half hr mean plume.

One parameter that may be investigated from the data generated is the crosswind integrated concentration (CWIC). In an atmosphere with no low frequency fluctuations contributing meander to the plume, the instantaneous

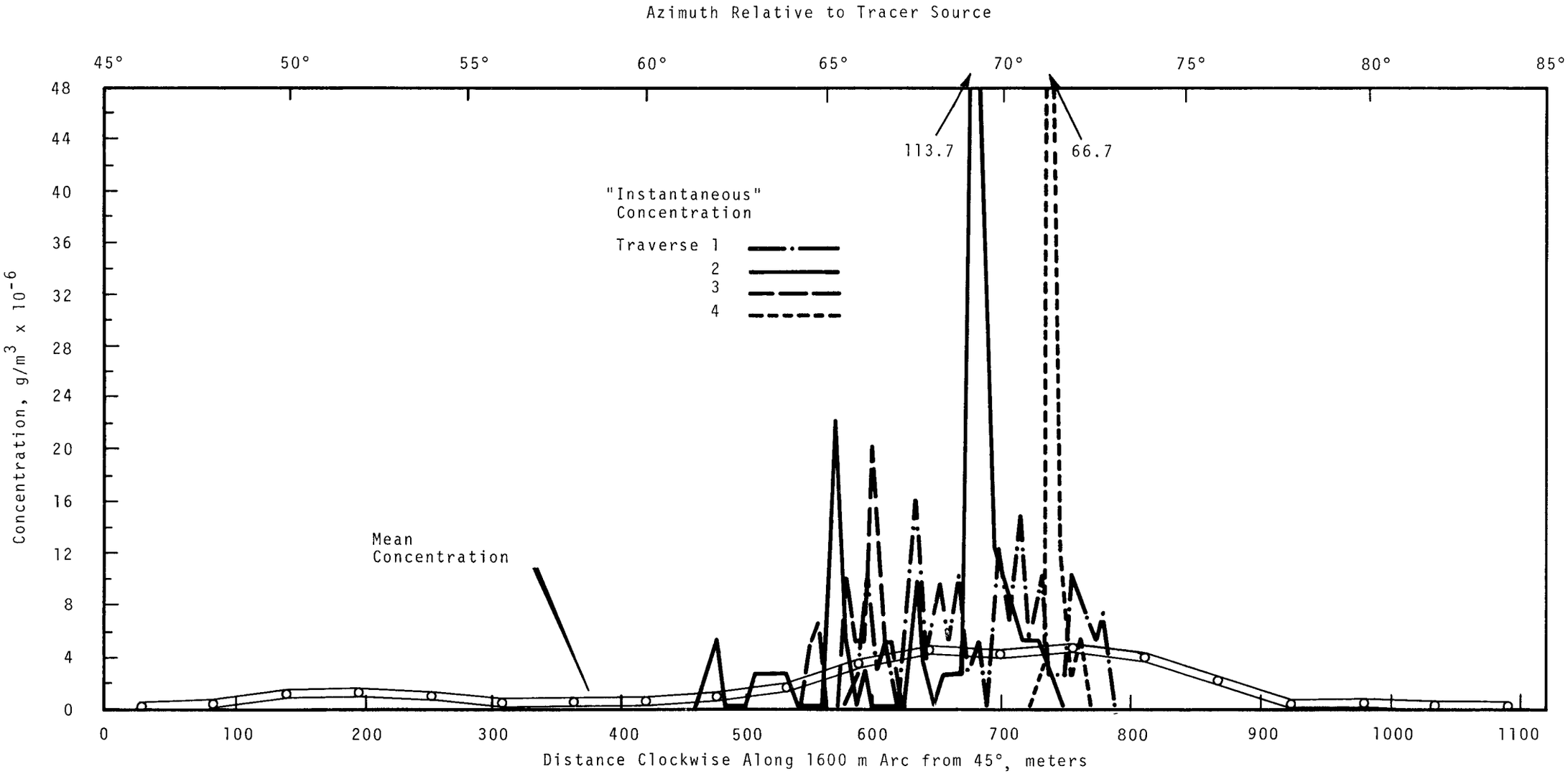

FIGURE 1. Concentration Distribution Along 1600 m Arc During Test U-47

crosswind plume concentration would be identical in location and magnitude to the mean concentration. In an atmosphere where large turbulent eddies displace the entire instantaneous plume in both the horizontal and vertical, the individual instantaneous distribution need not approximate the mean; but the mean of the instantaneous CWIC's must equal the mean CWIC for the period under consideration.

Table I presents data on CWIC values for the three field experiments. The columns headed $CWIC_i/CWIC_{30}$ list the ratios of instantaneous to 30-min crosswind integrated concentrations. Note that, although continuity demands that the mean value of this ratio be 1.00, only 5 of 21 of these ratios exceed 1.00. It is felt that this skewed distribution is real, i.e., that the majority of instantaneous CWIC values are less than the CWIC for the 30-min period. However, an occasional, particularly high instantaneous CWIC offsets several low values.

Note also that the ratio of the mean instantaneous CWIC to the 30-min value for each run is less than 1.00 in each field test (0.65, 0.55, and 0.97) although the value from Field Test U-50 is very close to 1.00. It is concluded

TABLE I. Observed Cross Wind Integrated Concentrations[a]

	Test U-47		Test U-48		Test U-50	
$CWIC_{30}$[b]	16.46		9.01		11.80	
$CWIC_i/CWIC_{30}$[c]	0.65		0.55		0.97	
Traverse	$CWIC_i$	$\frac{CWIC_i}{CWIC_{30}}$	$CWIC_i$	$\frac{CWIC_i}{CWIC_{30}}$	$CWIC_i$	$\frac{CWIC_i}{CWIC_{30}}$
1	12.55	0.76	7.14	0.79	6.26	0.53
2	19.03	1.16	2.30	0.26	13.03	1.10
3	4.47	0.27	1.48	0.16	36.51	3.09
4	6.96	0.42	8.38	0.93	1.74	0.15
5			4.05	0.45	9.94	0.84
6			0.00	0.00	5.72	0.49
7			16.02	1.78	13.60	1.15
8			0.41	0.05	6.55	0.56
9					9.99	0.85
Mean	10.75		4.96		11.48	
Median		0.59		0.35		0.84

(a) *All CWIC values in this table must be multiplied by* 10^{-4} *to obtain true integrated concentrations in* g/m^2.

(b) $CWIC_{30}$ *is the crosswind integrated concentration of the observed 30-min mean plume.*

(c) $CWIC_i$ *is the crosswind integrated concentration of the near-instantaneous plume.*

that a statistically insufficient number of traverses was made to "hit" the less frequent higher-than-average instantaneous CWIC values. If all 21 traverses are pooled, the five traversed with >1.00 ratio were not enough to raise the mean ratio to 1.00. That is, more than 5/21 (24%) of the instantaneous CWIC values must be greater than one. It may be estimated how many more of the ratios must be greater than 1 to bring the mean ratio to 1.00; from the data at hand, the estimate is about 33% which is the frequency found in Field Test U-50 where the mean ratio was 0.97.

Ratios of median instantaneous CWIC values to 30-min CWIC values are listed in Table I also. Pooling all three runs discloses a median ratio of 0.55. Examination of a frequency distribution from the pooled data suggests a modal ratio of about 0.45. These pooled median and modal values are also likely to be somewhat low for the same reason advanced regarding the mean in the previous paragraph. Further, it must be recognized that we have pooled data from these three field tests without regard to the meteorological conditions germane to each test. This can be partially excused on the basis of the minimal amount of data available at this time.

The real-time concentrations can be used to investigate other relationships between mean crosswind concentrations and the instantaneous value. As noted in the introduction, it is generally easier to measure the mean concentration for a long period of time than it is to measure the instantaneous values. One can get the mean concentrations, as shown by the bold lines on Figures 1 and 2, with relative ease. If one is concerned about what maximum concentrations to expect, the peak mean concentration ($\overline{\chi}_\rho$) is readily apparent from the bulk samples exposed during an entire experiment. For instance, in Figure 2, $\overline{\chi}_\rho$ was 4 x 10^{-6} g/m^3 at a distance of 800 m from the source.

It is obvious, however, from examination of Figures 1 and 2 that this 30 min peak mean concentration ($\overline{\chi}_\rho$) is frequently exceeded by instantaneous concentrations (χ_i) at many points. It is possible from these data to specify for a given instant the mean number of locations along an arc that one can expect to find a given ratio between χ_i and $\overline{\chi}_\rho$.

Table II presents relationships between χ_i and $\overline{\chi}_\rho$ for Field Tests U-47, U-48, and U-50. In formulating the table, a "location" is defined as an 8 m increment of distance along the arc under consideration; this is the approximate distance the sampling vehicle moved in one second. Examination of the table discloses that during Test U-47, for instance, an average of 10.0 locations along the 1600 m arc had a χ_i greater than $\overline{\chi}_\rho$. An average of 1.2 locations had an χ_i at least four times $\overline{\chi}_\rho$. The maximum observed χ_i during field test was 22.6 times the $\overline{\chi}_\rho$ value.

This type of information should be valuable in the investigation of the major concern in problems involving both chronic and short period maximum permissible concentrations.

In some situations it is easier to define the near-instantaneous distribution of concentration than it is to take stationary samples to obtain the mean crosswind distribution. An

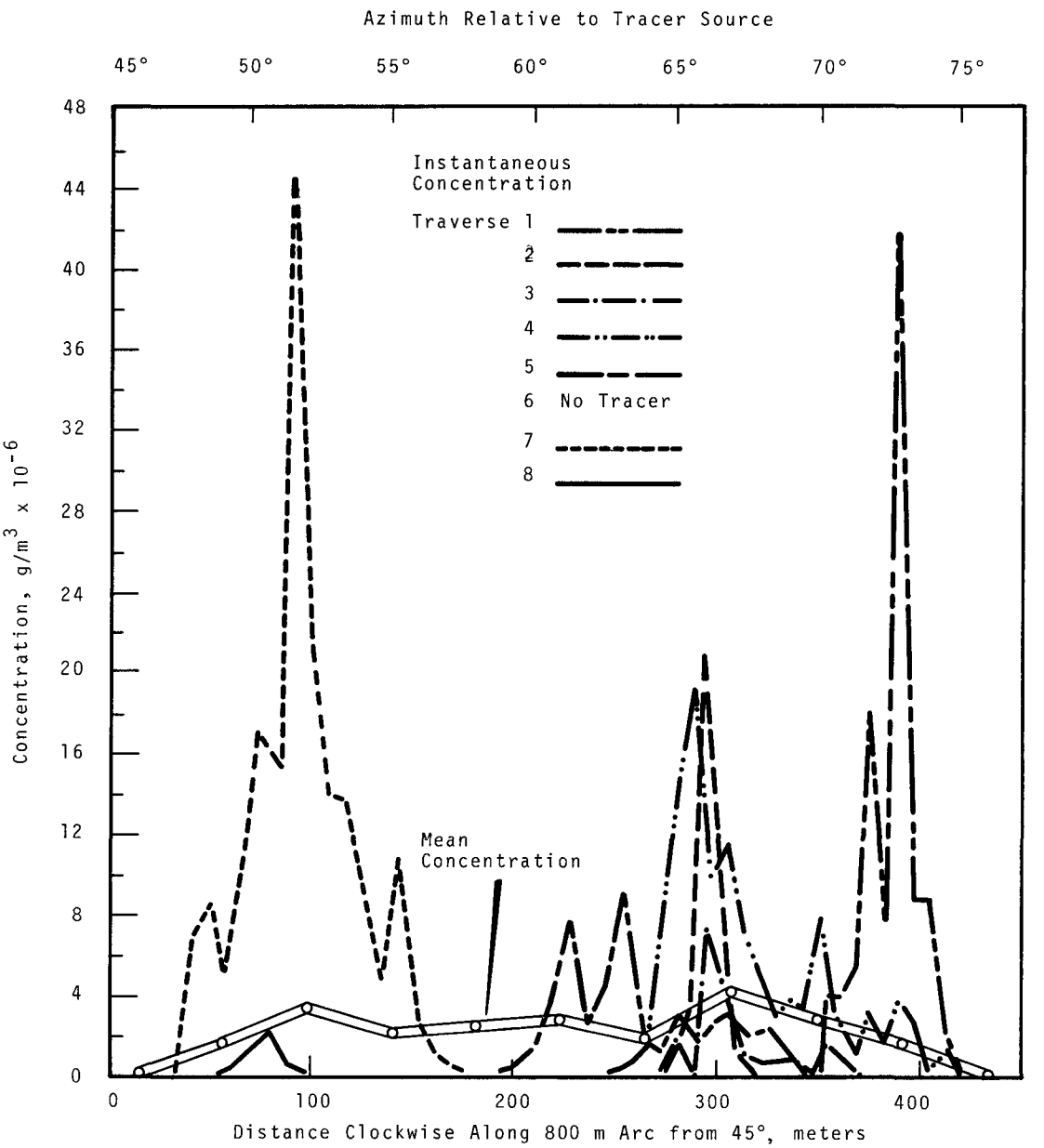

FIGURE 2. Concentration Distribution Along 800 m Arc During Test U-48

TABLE II. Mean Number of 8-m Segments of Arc for Which $\chi_i/\overline{\chi}_o$ is Greater Than or Equal to the Indicated Value

Field Test	Distance from Source, m	χ_i/χ_o Greater Than or Equal to: 0	0.5	1	2	4	4.3	8	10	11.0	16	20	22.6
U-47	1600	13.5	13.5	10.0	4.2	1.2		0.5	0.5		0.2	0.2	(a)
U-48	800	10.1	6.5	4.2	2.5	0.9		0.2	0.2	(a)			
U-50	800	21.9	11.8	6.8	2.8	0.3	(a)						

(a) *Ratio resulting from maximum* χ_i

example of such a situation is crosswind sampling by aircraft. The question arises, how well can the mean crosswind plume concentration distribution be defined by a series of crosswind traverses? Our subject field experiments can offer some clues in this direction.

Earlier in this paper some comparisons were made between near instantaneous CWIC values and 30-min mean CWIC values for Field Tests U-47, U-48 and U-50. As pointed out, the mean $CWIC_i$ must equal the $CWIC_{30}$, although the distribution of $CWIC_i$ values is skewed. It was also noted that, in the three particular cases investigated, the $\overline{CWIC_i}/CWIC_{30}$ ratios were all less than 1.00, namely 0.65, 0.55, and 0.97. Thus, although we expect before we start that the 30 min mean crosswind distribution of concentration which will be deduced from the instantaneous concentration values will be low for these cases, the resulting distributions are still of interest.

Figure 3 gives the observed mean crosswind concentrations and also the calculated mean crosswind distributions obtained from the moving RTS. As anticipated, the computed values are low. It is obvious that the computed distributions more nearly reproduce the shape of the observed distribution in Tests U-48 and U-50 than in Test U-47. In view of the increased number of traverses on these last two runs, 8 and 9 traverses versus only 4 for run U-47, this result is not surprising.

The shape of the computed distributions might be brought more closely into line with the observed by the use of running means. Certainly both shape and magnitude agreement should improve with a greater number of traverses. The results here suggest only an approach. Refinement must await the accumulation of further data.

A comparison was made between wind direction measured near the source and the pattern of crosswind instantaneous concentration distributions intercepted at 800 m during Field Test U-48. During this test, a low frequency meander in the wind direction of about one cycle per half-hour was easily identified and a similar oscillation in the instantaneous plume intercept azimuth was sought. One-minute averages of the wind direction were calculated to remove fluctuations expected to be effective in diffusion only and to leave the variation

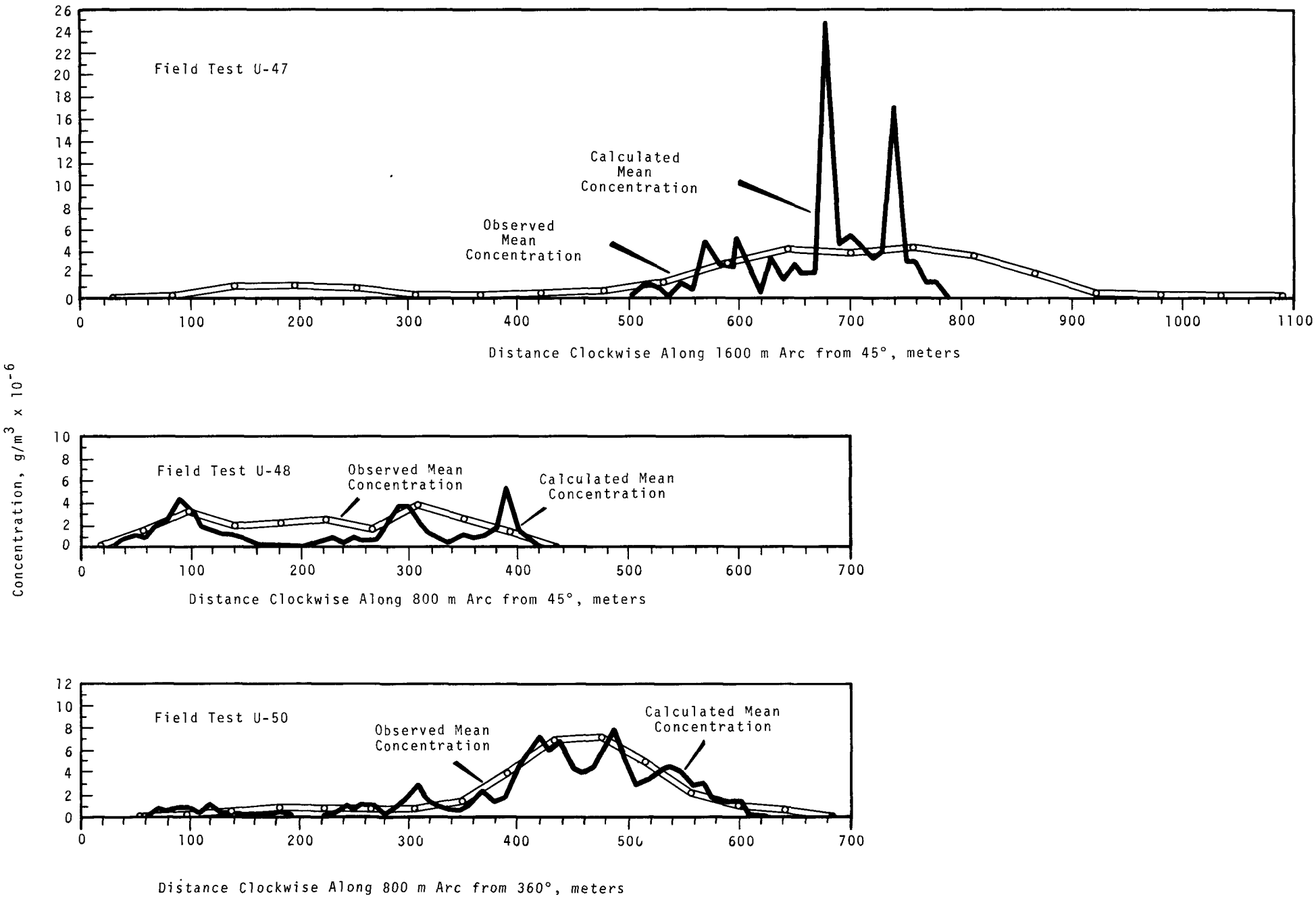

FIGURE 3. Observed and Computed Crosswind Distributions of Tracer Concentration

effective in the transport. The smoothed wind trace and the plume intercept history are compared in Figure 4. The timing of the real time sampler recording and the wind data recording were coordinated within a few seconds during the test. Thus it was possible to determine quite accurately the average travel time to the 800 m arc to be 5 1/2 min. Except for the first and the last 5 min period during the test, the wind speed was quite constant. Since the first 10 min segment of the plume was not sampled, only the last intercept gave an individual travel time different from 5 1/2 min, decreasing somewhat with the higher winds at the end of the test.

The determination of the travel times allowed the calculation of a transport speed of 2.6 m/sec, and from this an effective transport height was estimated. This was found to be close to 6 m, the logarithmic mean of the source height and the sampler height, where the mean wind was 2.7 m/sec.

The turbulence indicated by the standard deviation about the one-minute averages of wind direction was compared with the instantaneous plume width for each intercept of Test U-48. Though the approach is not rigorous, a relationship is indicated in Table III. The results reported here offer confidence that the position of the turbulent fluctuations responsible for diffusion and

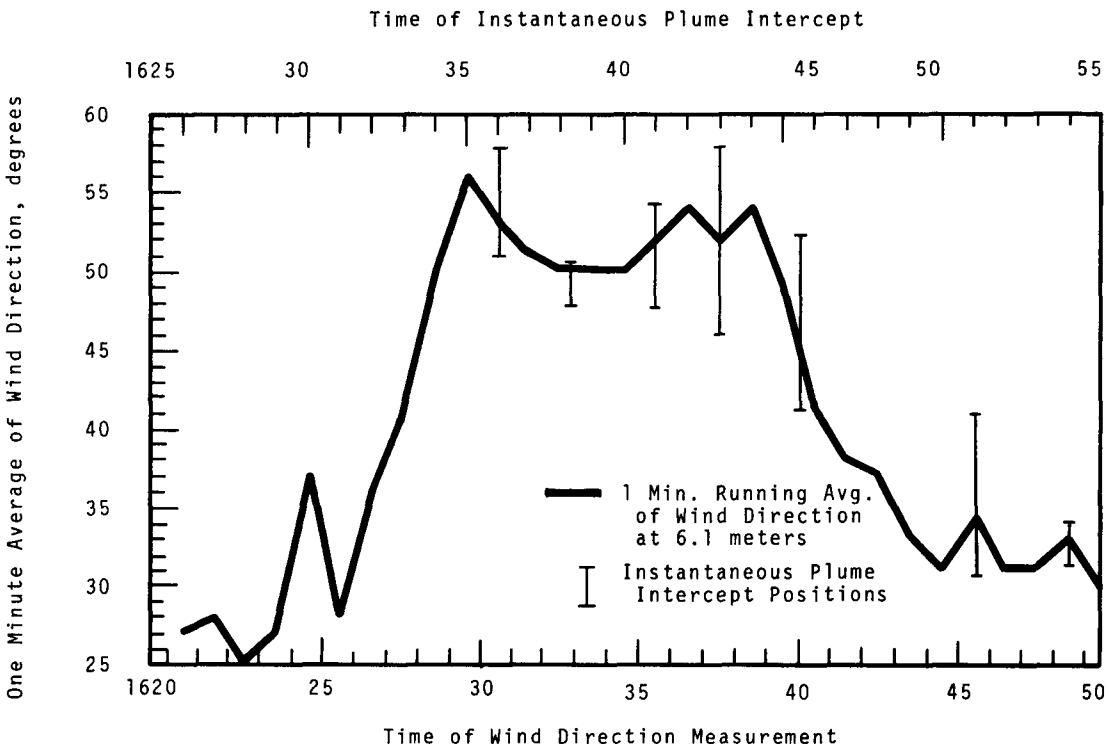

FIGURE 4. Comparison of Instantaneous Plume Locations and One-Minute Wind Direction Averages for Test U-48

TABLE III. Comparison of Instantaneous Plume Widths and Wind Variability for Test U-48

Pass Number	Instantaneous Plume Width, Degrees	Standard Deviation About One Minute Average Direction, Degrees
1	5	1.6
2	3	1.4
3	6.5	1.7
4	12	6.1
5	10	3.4
6	(no plume intercept on this pass)	–
7	9.9	3.4
8	1.5	(no wind data)

those responsible for transport of the instantaneous plume can be identified for given distances from the source. In the future work which will use both theoretical and experimental methods, the optimum relationship can be established between them.

SUMMARY

A real time tracer sampler moving crosswind through a tracer plume was used to investigate relationships between mean and instantaneous tracer concentrations. To date only three field experiments involving this technique have been carried out. Although this is not a sufficient number of tests from which to draw many firm conclusions, the tests give enough data from which to attempt various approaches that might be used to investigate long term versus instantaneous plume concentrations.

The basic data, crosswind distribution of instantaneous and mean plume concentrations, are presented.

A comparison of the frequency of instantaneous crosswind integrated concentrations which are greater than the 30-min mean crosswind integrated concentration with those that are less, reveals that about 2/3 of the values fall in the below-the-mean group.

Data are tabled which present the frequency of instantaneous values of concentration as compared to the peak mean crosswind concentration for a 30 min period.

Observed and calculated crosswind distributions are given for the 30 min mean concentration. The calculated values were generated by the moving real time sampler.

Comparisons were made of one-minute averages of wind direction and locations of instantaneous plume intercepts for one test where considerable meander made this possible. The one-minute average directions were found to persist quite well for travel to 800 m from the source, showing up quite well in the meander of the plume. Travel

time to the point of sampling led to an estimate of effective transport height near 6 m, the logarithmic mean of release and sampling heights. A relationship was indicated between the standard deviations of wind direction about the one-minute averages and the instantaneous plume widths for the individual intercepts. These preliminary results offer confidence that eventually the portion of the turbulence spectrum responsible for diffusion and that responsible for transport of the instantaneous plume can be determined as a function of distance and meteorological variables.

REFERENCES

1. *P. W. Nickola, M. O. Rankin, M. F. Scoggins and E. M. Sheen. A Device for Recording Air Concentrations of Zinc Sulfide Fluorescent Pigment on a Real Time Scale, HW-SA-3317. General Electric Company, Richland, Washington, January 10, 1964.*

2. *M. O. Rankin. Zinc Sulfide Particle Detector, HW-55917. General Electric Company, Richland, Washington, May 1, 1958.*

3. *J. J. Fuquay, P. W. Nickola, C. L. Simpson, M. O. Rankin and J. D. Ludwick. "Advances in Atmospheric Tracer Technology." Research and Development Activities in the Radiological Sciences, January through December, 1960, HW-70050, pp. 13-19. General Electric Company, Richland, Washington, January 16, 1961.*

PRECIPITATION SCAVENGING STUDIES

R. J. Engelmann and D. I. Hagen

INTRODUCTION

With the exception of improvements in the Rimrock Lake experimental site and use of larger amounts of tracers, the measurement of washout coefficients (below-cloud scavenging) for various tracers in rain and snow has continued under essentially the same experimental design as reported the preceding year.(1)

Twelve washout tests were conducted during the latter part of 1965 and 20 tests in 1966. These were multiple tracer tests utilizing one or more of bromine, iodine, silver iodide, scandium* and cesium* as tracers. Bromine and iodine were released as gases while the silver iodide and the scandium and cesium compounds were particulates.

Two tests using Hanford process plant stack gases were conducted in rains, one test in 1965 and one in 1966. These tests measure the washout of organic and inorganic forms of radioiodine vapor present in the stack effluents.

---

* *The scandium and cesium were fed to the generator as water solutions of the nitrate. The chemical composition and physical properties of the particulates released from the generator are under investigation.*

Most of the analyses of the 1965 and 1966 tests, with the exception of the late 1966 runs, were completed this year and, insofar as they are available, will be summarized here. With the exception of the scandium and cesium washout coefficients, they have also been reported elsewhere.[2,3,4]

With washout coefficients for silver iodide available, it was possible to calculate the contamination of a snowfield arising from the scavenging of silver iodide released into the atmosphere.[4] This contribution, in addition to background, must be considered when evaluating removal of silver iodide by other means such as nucleation. These calculations will be reviewed here.

From samples, taken July 20, 1965, of natural rain scavenging a dry ZnS dust, 1381 particles were counted in 302 raindrop images on diazo paper.[3] The number per drop was then normalized to the drop cross-sectional area to provide a direct measurement of the relative scavenging efficiency of raindrops of various sizes. The results were the same as the 1963 Hanford findings[5] which used artificial rain and wet-release zinc sulfide, in that the smaller raindrop is the better scavenger. The particles were not sized.

RIMROCK LAKE TEST SITE

Several operational improvements have been made on the Rimrock Lake Test Site during 1966. A small (5 x 7 ft) building was installed on the site about 200 ft from the 40 ft generation tower. This building is used for equipment storage between tests and as protection from the weather for instrumentation used during the tests. Toward the end of this year, it became clear that an additional building would be needed to satisfy increasing requirements. A larger (10 x 20 ft) farm building was ordered and will be located near the smaller building. Present plans call for the latter to house all tracer-contaminated equipment, including the generation equipment, and the larger building will contain the instrumentation. The instrumentation includes a camera modified to photograph snow crystals, an Instrument for the Measurement of Rain Electrical Charge (IMREC)*, a rain spectrum sampler using diazo paper, and wind speed and direction recorders. The new building will also be used to process the samples for transportation to the radiochemical laboratory. Previously, this had been done in a nearby motel.

Track, pulley, and winch were mounted on the 40 ft generation tower to support an elevator-platform upon which all generation equipment and wind instrumentation are located. The platform substantially reduces the amount of climbing needed during field tests, in addition to allowing generation at any height up to about 35 ft. A capability of changing generation height is advantageous when operating in varying wind speeds.

WASHOUT COEFFICIENTS FOR GASES AND PARTICULATES

The experimental procedure used to measure washout coefficients has been

* *See "Improvements in Raindrop Charge Measuring Systems" by C. A. Ratcliffe in this report.*

explained in other reports.[2,3,4] Briefly, the precipitation falling through the plume generated from an elevated source is sampled downwind on the ground. The cross-plume integrated sample is analyzed[2,4] for the tracers generated. The background concentration existing in the precipitation during the test is sampled upwind from the plume and also analyzed. If the total amount of tracer collected--less background--is denoted by Σc, the average wind speed during the test at generation height by $\bar{u}$, the sample spacing and sample area by Δy and A, respectively, and the tracer amount released by Q, then the washout coefficient--including dry deposition--is given by

$$\Lambda = \bar{u}\ \Delta y\ \frac{\Sigma c}{QA} \qquad (1)$$

for a circular sampling arc center on the generation tower.

Other information gathered during tests includes raindrop spectra or snow crystal samples, temperature and humidity, and qualitative estimates of dry deposition. This information is of value in interpreting the experimental results.

All washout coefficients obtained in 1966 are presented versus the precipitation rate in Table I for tests conducted in rain and in Table II for tests conducted in snow.

WASHOUT COEFFICIENTS FOR BROMINE AND IODINE

Gaseous iodine and bromine were released by heating their respective elemental states of crystal and liquid. In the earlier tests, typical releases of iodine and bromine were 100 g and 10 cm^3 over release times of 5 min and 30 sec, respectively. As the late 1965 and early 1966 tests were analyzed, it became clear that the releases were too small and over too short a time. Small releases led to difficulties in making a background correction since the background was often nearly equal to the sample collected under the plume, and short releases in the form of "puffs" were often brought to the ground by turbulence. For the late 1966 tests, generation times and quantities were increased for all tracers. As mentioned earlier, the results of these tests were not available by the end of 1966.

Washout coefficients for iodine and bromine in rain and snow versus the precipitation rate are given in Figures 1 and 2, respectively. The scatter in the points is probably due, in part, to the factors explained above.

Scavenging of bromine by snow is seen to be about 100 times as effective as the scavenging of iodine by snow. Since no theoretical calculations can be made for snow,[6] these numbers cannot be compared with predicted values. However, the greater scavenging of bromine as compared to that of iodine has been attributed to differing solubilities of the two gases at the surface of the snowflake.[2] If we ignore point R-15, the washout of bromine in rain is observed to be greater than that of iodine by a factor of 10 to 20, assuming a linear increase with rainfall rate.

The predicted curves for washout of iodine and bromine (Figure 1) were obtained from[6]

$$\Lambda = \pi\ Y \int Sh(D)\ N(D)\ dD \qquad (2)$$

TABLE I. Measured Washout Coefficients for Gaseous and Particulate Tracers in Rain

Test	Date of Test	Tracer	Ppt. Rate, mm/hr	Λ,(a) sec^{-1}
Z4	11-13-65	Br_2	0.64(b)	2.8×10^{-5}
Z5	11-14-65	Br_2	0.50(b)	3.9×10^{-5}
Z6	11-14-65	Br_2	0.70(b)	8.3×10^{-5}
Z9(c)	3-18-66	Br_2		
		I_2		
P4	11-24-65	Inorganic Radioiodine	0.52(b)	3.2×10^{-4}
		Organic Radioiodine	0.52(b)	3.5×10^{-6}
P6	1-5-66	Inorganic Radioiodine	0.87(d)	4.2×10^{-4}
R12	3-8-66	Cs	0.38	2.5×10^{-5}
		I_2	0.16(b)	2.5×10^{-6}
		Br_2(c)		
		Sc	0.38	6.6×10^{-5}
R13	3-8-66	Sc	0.41	9.0×10^{-6}
		I_2	0.22(b)	1.2×10^{-6}
		Br_2(c)		
		Cs	0.41	5.4×10^{-5}
R14	3-9-66	Sc	1.0	6.9×10^{-6}
		I_2	1.0	1.9×10^{-8}
		Br_2(c)		
R15	3-9-66	I_2	1.8(b)	1.6×10^{-7}
R16	3-9-66	Cs	0.76	2.7×10^{-5}
		I_2(c)		
		Br_2(c)		
R17	3-9-66	Cs	0.18	4.0×10^{-5}
		I_2(c)		
		Br_2(c)		
		Sc	0.87	9.9×10^{-5}
		AgI(e)		
R18	3-9-66	AgI	1.9	9.4×10^{-6}
R20	11-11-66	AgI(d)(c)		
R21	11-16-66	AgI(c)(d)		
		Br_2(c)(d)		

(a) *Calculated according to Equation 1.*

(b) *Calculated from raindrop size spectra taken at various times during the test.*

(c) *Radiochemical analysis not completed at close of 1966.*

(d) *Freezing rain.*

(e) *Natural background during test too high to obtain reliable washout coefficient.*

TABLE II. Measured Washout Coefficients for Gaseous and Particulate Tracers in Snow

Test	Date of Test	Tracer	Snow Type	Snowfall Rate, mm/hr Water Equiv.	Λ,(a) sec^{-1}, Measured
Z8	12-27-65	Br_2	Unclassified	0.64	2.5×10^{-5}
R1	12-28-65	Br_2	Small spacial dendrites	0.38	1.0×10^{-5}
		I_2(b)	Small spacial dendrites		
R2	12-28-65	AgI	Unclassified	0.52	1.0×10^{-6}
		Br_2(b)	Unclassified		
		I_2(b)	Unclassified		
R3	12-28-65	Br_2	Small spacial dendrites	0.05	1.2×10^{-6}
		I_2	Small spacial dendrites	0.05	3.0×10^{-8}
R4	12-29-65	Br_2	Powdered snow	0.7	5.0×10^{-8}
		I_2	Powdered snow	0.7	7.4×10^{-8}
		AgI	Powdered snow	0.7	3.0×10^{-7}
R5	12-29-65	Br_2	Small spacial dendrites	0.48	1.4×10^{-6}
		I_2	Small spacial dendrites	0.48	1.8×10^{7}
		AgI(b)	Small spacial dendrites		
R6	12-29-65	Br_2	Unclassified	0.56	2.1×10^{-5}
		I_2(b)	Unclassified		
		AgI	Unclassified	0.56	1.3×10^{-6}
R7	12-29-65	Br_2	Small powdered snow	0.07	9.6×10^{-8}
		I_2(b)	Small powdered snow		
		AgI(b)	Small powdered snow		
R8	12-30-65	AgI	Unclassified	0.27	3.7×10^{-7}
		Br_2	Unclassified	0.27	1.6×10^{-6}
		I_2	Unclassified	0.27	9.4×10^{-9}
R9	2-28-66	Br_2(b)	Powdered snow		
		I_2(b)	Powdered snow		
		AgI	Powdered snow	0.27	1.1×10^{-6}
R10	2-28-66	Br_2(b)	Powdered snow		
		I_2	Powdered snow	0.67	5.5×10^{-8}
		AgI	Powdered snow	0.68	2.8×10^{-6}
R11	3-1-66	I_2	Powdered and planar dendrites	0.07	3.7×10^{-8}
		Sc	Powdered and planar dendrites	0.1	5.5×10^{-5}
R19(b)	11-11-66	AgI	Granular snow		
R22(b)	12-6-66	AgI	Unclassified		
		Br_2	Unclassified		
R23(b)	12-6-66	AgI	Spacial dendrites		
		Br_2	Spacial dendrites		
R24(b)	12-7-66	AgI	Small spacial dendrites		
		Br_2	Small spacial dendrites		
R25(b)	12-7-66	AgI	Rimed spacial dendrites		
		Br_2	Rimed spacial dendrites		
R26(b)	12 7 66	AgI	Rimed spacial dendrites		
		Br_2	Rimed spacial dendrites		
R27(b)	12-8-66	AgI	Spacial dendrites		
		Br_2	Spacial dendrites		

(a) *Calculated according to Equation 1 in text.*

(b) *Radiochemical analysis not completed at close of 1966*

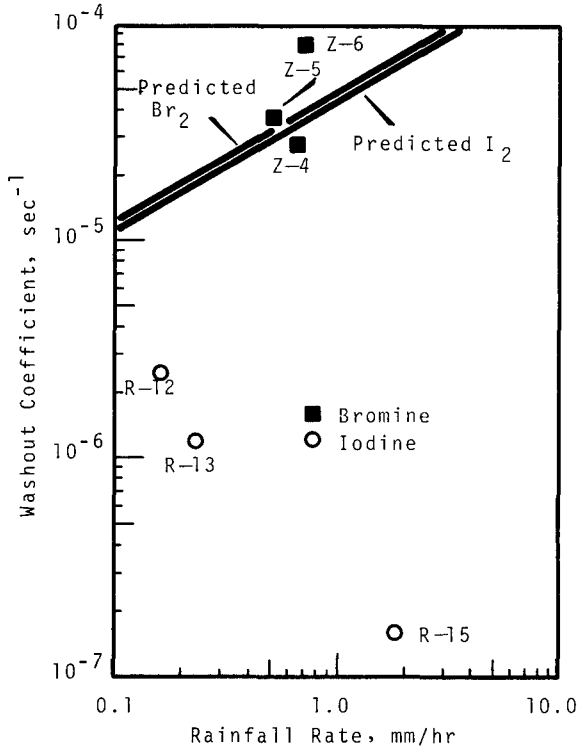

FIGURE 1. Washout Coefficients for Bromine and Iodine Gas in Rain

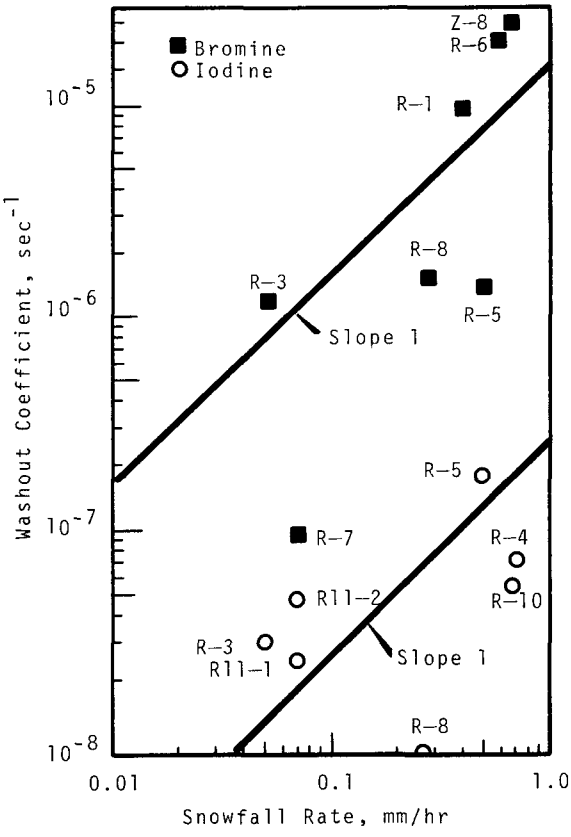

FIGURE 2. Washout Coefficients for Bromine and Iodine Gas Versus Snowfall Rate (water equivalent)

where Y is the diffusivity for iodine or bromine in air, Sh(D) is the Sherwood number and N(D) is the space density (drops per volume per diameter interval) of raindrops. Equation (2) is derived assuming resistance to mass transfer in the gas phase only (i.e., the drop is a perfect sink). The N(D) for the Figure 1 curves were obtained from Indian and Hanford rain spectral data.[6]

It is clear that the bromine washout coefficients verify the theory within a factor of 2. This is to be expected on the basis of a moderate solubility of bromine in water. On the other hand, the theoretical predictions for iodine are a factor of 10 higher than the observed washout coefficients. Since iodine is 1/100 as soluble as bromine, it is expected that resistance to mass transfer at the droplet-air interface and in the drop itself would be more important than for bromine. In fact, it appears that for iodine, resistance to mass transfer is determined by the liquid phase rather than the gas phase,[7] and the washout coefficients would be lower than predicted by Equation (2).

Finally, the data in Figures 1 and 2 show that the washout coefficients for both gases in rain are a factor of 10 higher than those for snow for the same precipitation rate.

WASHOUT COEFFICIENTS FOR HANFORD PROCESS PLANT RADIOIODINE VAPOR

The washout coefficients in rain for Hanford Process Plant inorganic radioiodine vapor (present as free iodine and hydrogen iodide) are presented in Figure 3, along with previously measured washout coefficients in snow.[3]

The inorganic washout coefficients are a factor of 10 greater than predicted by Equation (2) as shown in Figure 1, and two orders of magnitude greater than the iodine washout obtained from the Rimrock tests for similar precipitation rates.

To explain these high numbers, it has been concluded[3] that the process plant washout is not of free gas, but of small fog droplets which contain most of the radioiodine and are formed from stack exhaust moisture condensing in the cool outside air. That this conclusion is plausible can be seen by comparing the predicted washout of 20 to 40-micron diameter droplets with the measured inorganic iodine washout coefficients in Figure 3.

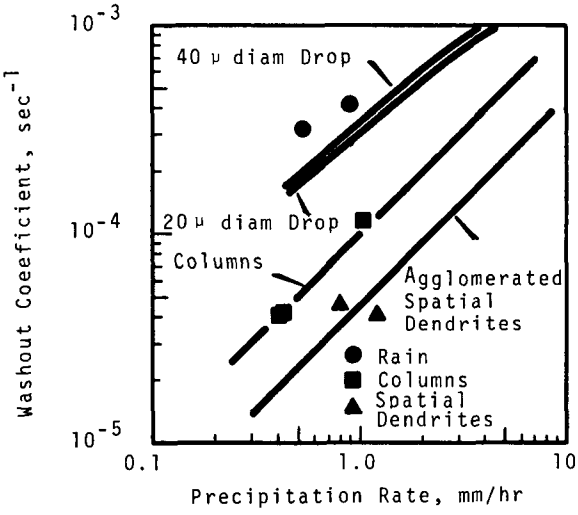

FIGURE 3. Washout Coefficients of Inorganic Iodine in Process Plant Stack Gases for Rain and Snow

Organic forms of radioiodine (present as organic iodides) were scavenged only about 1% as effectively as the inorganic, but there was too little captured to allow calculation of coefficients.

WASHOUT COEFFICIENTS FOR PARTICULATES

Four washout coefficients measured for scandium particulates in rain and one in snow and four washout coefficients for cesium particulates in rain are presented in Figure 4. Six washout coefficients for silver iodide in snow and one in rain are presented in Figure 5.

These particulates were generated from a propane-burning silver iodide generator called the "Skyfire Generator", a type used routinely in cloud-seeding work.[8] The tracers were generated from the following solutions: 16.125 g of silver iodide, with sufficient sodium iodide, per liter of acetone; 1 g scandium nitrate per liter of water; and 1 g of cesium nitrate per liter of water. The scandium and cesium particulates generated from these solutions are believed to be mixtures of the oxides and nitrates. Size distributions for the scandium, cesium, and silver iodide particulates have not yet been obtained although the silver iodide is believed to be of submicron size.[9]

The low washout coefficients of silver iodide in rain and snow are a result of the very low inertia of submicron particles. The latter tend to follow the streamlines of the air past the snowflake or raindrop. That there

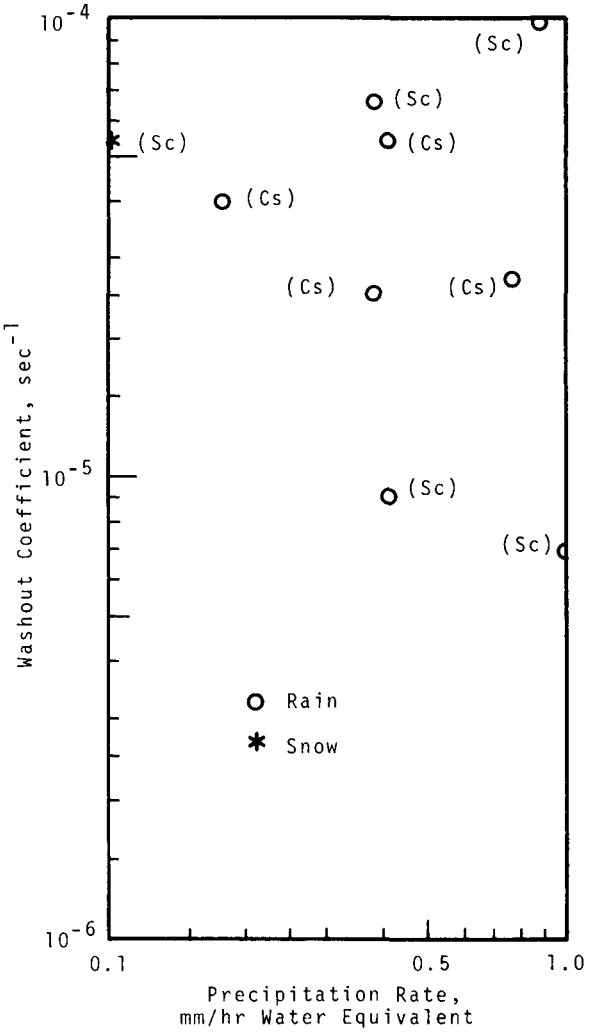

FIGURE 4. Washout Coefficients and Sc and Cs Particulates in Rain and Snow

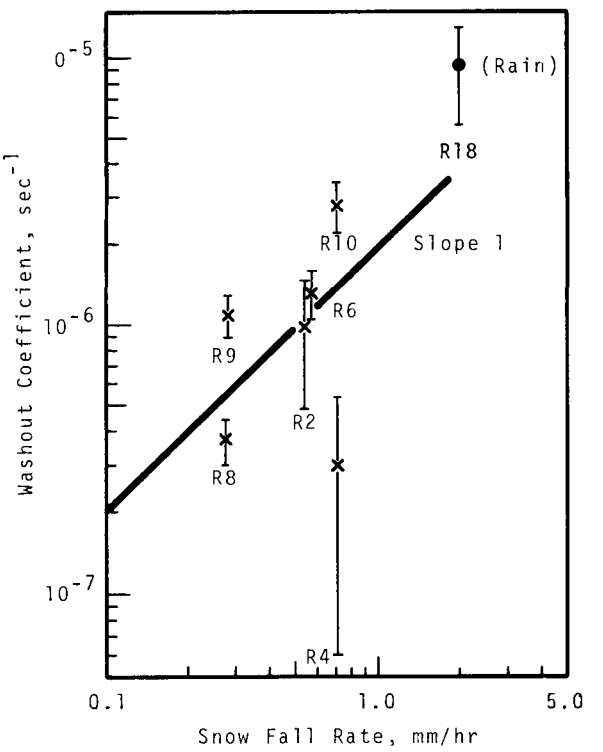

FIGURE 5. Washout Coefficients for Silver Iodide in Rain and Snow Versus Precipitation Rate (Water Equivalent). The Range About Each Point Indicates Estimated Corrections for Background

is any collection at all may be attributed to electrical forces. An instrument designed to measure rain and snow electrical charges (IMREC) will soon be available to supplement these studies.*

As seen from Figures 4 and 5, particulates are washed out in snow about the same as in rain for a given precipitation rate. This is in contrast to a much lower washout of gases in snow than in rain.

WASHOUT CONTRIBUTIONS TO NATURAL BACKGROUND OF SILVER IODIDE IN SNOW

In evaluating the effectiveness of cloud-seeding techniques from the silver iodide content of snow collected in the seeding area, possibilities of removal of silver iodide by means other than nucleation must be considered. Measured washout coefficients for silver iodide in snow (Figure 5) indicate that removal by washout is small but not insignificant.

* *See "Improvements in Raindrop Charge Measuring Systems" by C. A. Ratcliffe in this Report.*

Calculations have been made for the amount of silver iodide which will be deposited in the snow through washout. This, in addition to the normal background, must be exceeded before removal by other means can be postulated. The calculation is based on two assumptions.

1. The washout rate varies linearly with snowfall rate and the snows during the tests will be similar to those at other locations.
2. The silver iodide plume concentration has the shape of a normal distribution with its standard deviation being a function of downwind distance according to $\sigma_y = 0.2\ x^{0.8}$ where σ_y and x are in meters. The equation is a kind of composite of experimental diffusion data for 30-min long releases at Hanford, Washington.

The "area within a washout isopleth" has been previously calculated[6] using the second of the above assumptions. The results of this calculation give $\omega\bar{u}/Q\Lambda$ versus area where ω and Q are the deposition and generation rates, and $\bar{u}$ is the average wind speed. Because both the volume of snow water and the washout coefficient vary linearly with precipitation rate according to the first assumption, the washout coefficient may be eliminated with the results shown in Figure 6. The ordinate, $C\bar{u}/Q$, is the concentration of silver in the snow water, times the wind speed, normalized to the silver release rate. For example, if the contamination level of interest were 2×10^{-11} g/ml of snow water, then a release rate of 200 g/hr in a wind of 5 m/sec will contaminate 10^8 m^2 of snowfield. Thus, washout is

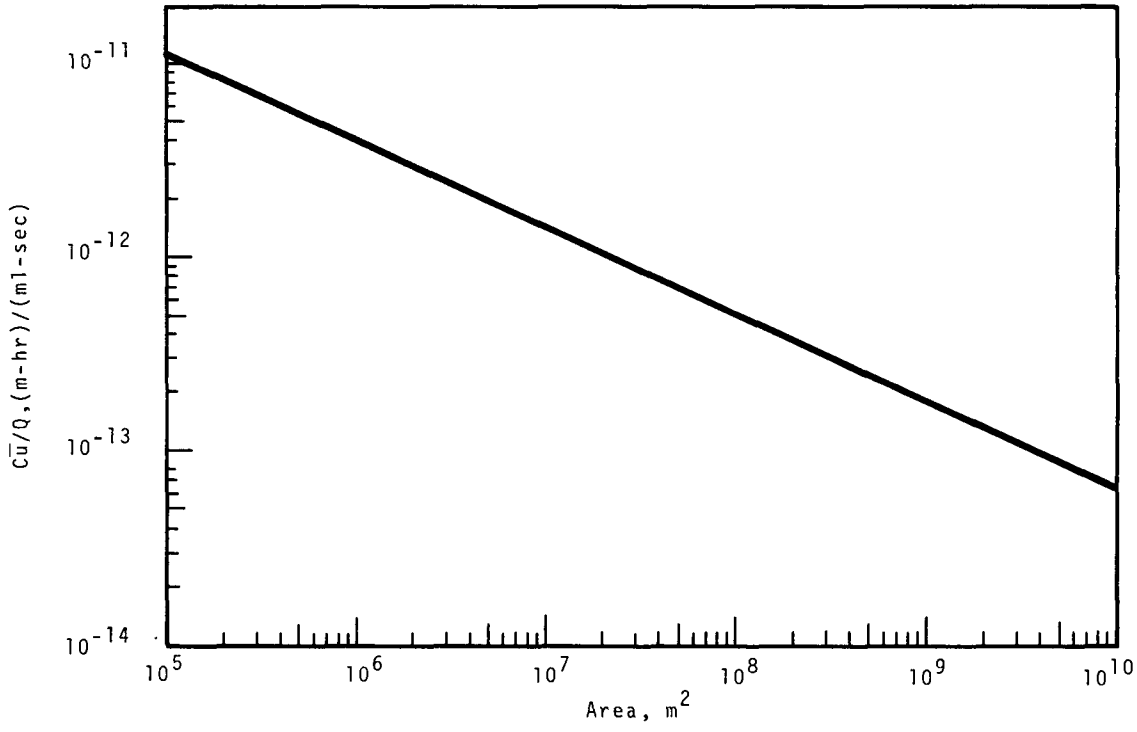

FIGURE 6. Area of Snowfield Contaminated to the Concentration C or more, from a Release Rate of Q of AgI in a Wind of $\bar{u}$

capable of doubling a normal background of 2×10^{-11} g/ml over an area of 100 km^2.

During the conduct of the silver iodide washout tests, several samples of snow were taken for the determination of silver backgrounds and the results are presented in Table III.

REFERENCES

1. *R. J. Engelmann and D. I. Hagen. "Precipitation Scavenging Studies," Pacific Northwest Laboratory Annual Report for 1965 in the Physical Sciences, BNWL-235 1, pp. 1-7. Pacific Northwest Laboratory, Richland, Washington, 1966.*

2. *R. J. Engelmann, R. W. Perkins, D. I. Hagen, and W. A. Haller. Washout Coefficients for Selected Gases and Particulates, BNWL-SA-657 and APCA 66-118, Pacific Northwest Laboratory, Richland, Washington, 1966.*

3. *R. J. Engelmann and R. W. Perkins. "Snow and Rain Washout Coefficients for Process Plant Radioiodine Vapor," Nature, vol. 211, no. 5044, p. 61. July 2, 1966.*

4. *R. J. Engelmann, D. I. Hagen, W. A. Haller, and R. W. Perkins. Washout Coefficients for Silver Iodide, BNWL-SA-798. Pacific Northwest Laboratory, Richland, Washington, 1966.*

5. *R. J. Engelmann. "Rain Scavenging of Zinc Sulfide Particles," J. Atmos. Sci., vol. 22, pp. 719-727. 1965.*

6. *R. J. Engelmann. The Calculation of Precipitation Scavenging, BNWL-77, Pacific Northwest Laboratory, Richland, Washington. July, 1965.*

7. *V. Griffiths. "Use of Sprays as a Safeguard in Reactor Containment Structures," Nuclear Safety, Winter 1964-65, pp. 186-194 and 209-210. 1965.*

8. *D. M. Fuquay. "The Project Skyfire Cloud Seeding Generation," Final Report, Advisory Committee on Weather Control II, pp. 273-277. 1957.*

9. *N. H. Fletcher. The Physics of Rainclouds, Cambridge University Press. 1962.*

TABLE III. Silver Background in Snow at Rimrock Lake, Washington

Date	Time (PST)	C, g/ml x 10^{-11}	Remarks
12-28-65	2230	1.7	Snow gathered from fresh snow surface
2-28-66	1700	0.47	Snow gathered from fresh snow surface
3-8-66	0900	1.1	Snow gathered from fresh snow surface
3-8-66	0900	2.1	Snow gathered from fresh snow surface
3-9-66	0945	7.4	Snow caught in several bag-lined baskets
3-9-66	1030	4.8	Snow caught in several bag-lined baskets
3-9-66	1100	6.6	Snow caught in several bag-lined baskets

REAL TIME SAMPLING OF AIRBORNE TRACER WITH AIRCRAFT

W. L. Dotson, P. W. Nickola and M. A. Wolf

INTRODUCTION

This discussion covers progress during 1966 toward development of the instrumentation and techniques for improved aircraft sampling of a phosphorescent, airborne tracer.

The first part of this discussion, "Evolution of the Aircraft Sampling Equipment," describes the process of adaptation of the concept to an Airborne Real Time Sampler (ARTS) installation and the subsequent modifications which were required to provide a meaningful system. Possible future improvements to the system are discussed.

"ARTS System Evaluation" considers some of the problems in the interpretation of the recorded data and the limitations in application of the ARTS as revealed in an evaluation during a diffusion field test. Several guidelines for the ARTS utilization and for discrimination between true and false signals are presented.

The last part, "Operational Application of the ARTS System," discusses results of a test designed to examine the potential contribution of the ARTS system to diffusion studies. Determinations of tracer position and distribution were made and compared with surface observations of tracer and meteorological parameters. Additional insights into the physical description of a diffusing plume are noted.

EVOLUTION OF THE AIRCRAFT SAMPLING EQUIPMENT

W. L. Dotson

A device for monitoring and recording atmospheric concentrations of an airborne zinc sulfide tracer[1] was developed at Hanford and employed in the field in 1963. A natural extension of the experimental work with this zinc sulfide real time sampler was the early attempts to carry this device aloft in an aircraft as an Airborne Real Time Sampler (ARTS). Some aircraft have proved difficult to adapt to because of the lack of a suitable electrical power source. However, continuing emphasis on diffusion research has provided an incentive to use aircraft which could provide both the payload capability and suitable electrical power. But, the translation of a piece of equipment developed for ground operation to an airborne instrumentation package has not been a straightforward task.

The original airborne package has been described in a prior document.[2] The equipment is designed to cause a zinc sulfide atmospheric tracer to phosphoresce, to monitor the phosphorescence, and to record a signal proportional to the phosphorescence. The signal can be calibrated in terms of atmospheric concentration of the tracer.

Two sampling heads--consisting primarily of an ultra-violet radiation source, a light trap and a photomultiplier tube--were mounted in the radome compartment of the Battelle-Northwest Beechcraft Queen Air. A set of two, modified 9 in. venturi was mounted on the right hand radio compartment access door and connected to the sampler heads to provide a vacuum source. The photomultiplier signal was carried back to the cabin and electronically processed for strip chart recording. One sampler head was in use at a time with the other available as a spare.

The two sampler heads were found not to be identical in operation. The left hand (number one) sensor was found to be more sensitive than the other by a factor of about ten. A change in photomultipliers did not significantly alter the relative sensitivity of the systems and reworking the solenoid-controlled airflow system similarly had no effect.

The program dictated that a series of field tests be commenced using the number one sensor head while a thorough study of the instrument problem was carried out concurrently. The results of this study are incorporated in the system now employed on the Queen Air as described in the following.

Much data had been collected using sensor head number one and it was decided that no significant changes would be made to that unit. The number two unit was completely remade.

The first effort was devoted to providing identical and effective, simultaneous air flow through the units. This was accomplished by installation of two additional and identical venturi heads on the left side of the aircraft. The tubing connecting the sensor heads to the venturi vacuum source was reworked. Particular care was taken to insure unrestricted flow by use of gently curved bends and adequately sized tubing. Ball valves were installed in each system to provide a positive check and a means of regulation.

One plaguing problem was the uncertainty as to the actual flow rates in the sensor heads during flight. A vacuum gauge inserted in the flow line permitted monitoring of the vacuum during airborne sampling, although no direct measurement of flow rate was possible. While on the ground, control of vacuum to the in-flight value and simultaneous direct measurement of flow rate was possible. The inference that identical ground and in-flight vacuum readings specified identical ground and inflight flow rates was open to considerable doubt. To overcome this deficiency, a matched and calibrated pair of Cox Instrument Model GL 12 flow raters with Series 700 indicators were installed. These have proven to be of great value and more so after the ball valves (in the nose) were fitted with remote controls for airborne operation. Now the precise desired flow rate for each sensor can be obtained while airborne.

One of the problems had been the inability to calibrate the sensor while airborne. A solenoid-controlled calibrated light source was therefore installed in the number two sensor head and this has proved to be successful.

In order that both systems could be operated simultaneously, the power supply and recording systems were duplicated. This has been satisfactory and

several runs have been completed with dual recordings being made. This has resulted in development of a feeling of increased confidence that the data are real and that definitive numbers are being obtained.

There are several problems that still exist. The first is that of radio transmission interference in the recorded data. Another is the inability of the present instrument to operate in the presence of liquid water in the atmosphere. An occasional high noise background and spurious signals are as yet unexplained. Finally, the photomultiplier sensitivity changes with temperature. Although the previously-mentioned calibrated light source does permit in-flight calibration checks and adjustment, drift between checks may still exist.

These problems prompted the development of a semi-quantitative bulk sampler device. This is simply a probe connected to a filter holder and thence to a venturi vacuum source; a flow rater is provided. The probe is mounted in the fore part of the cabin through a window on the left side. A Plexiglass tube, 6 in. in diameter, provides a means of access for filter change.

The problems that yet remain are under active study. A complete new design of the sampler should eliminate most, if not all, of them. The radio interference problem should be overcome by increased shielding of the signal leads and the development of an electronic ground dedicated to the instrumentation. The moisture problem should be eliminated through the new development wherein the ambient atmosphere is excluded from the electronics by means of optical filters. The high noise background, spurious signal, and temperature drift should be eliminated by pairing the photomultiplier tubes and electronic coupling to provide a comparative rather than a direct reading. In this scheme, one tube looks at the air flow and the other at a dark chamber. The latter is then a constant reference for comparison. This new instrument is in final design.

ARTS SYSTEM EVALUATION

P. W. Nickola

The major problems associated with operation of the airborne zinc sulfide tracer detection system have been discussed in the previous paragraphs. However, these difficulties have not precluded the use of these samplers and a considerable amount of data has been generated with the ARTS system.

As previously noted, the atmosphere frequently contains contaminants which phosphoresce or in some other manner simulate the phosphorescent effect of zinc sulfide in the ARTS system. This "noise" varies from day to day and from location to location. An estimate of the noise to be expected during a field diffusion experiment can be obtained by operation of the ARTS system prior to release of tracer and in the same locale where tracer sampling is to be done. An extreme amount of noise can, and has on occasion, prevented use of the system.

In any event, some subjectivity is involved in chart interpretation. Some signals can be discarded immediately by an experienced chart reader as being "non-typical" in appearance. Other sig-

nals are debatable, and still others result unquestionably from zinc sulfide.

The ARTS system can be evaluated by examination of the results fom a specific field experiment. This test differs from that to be discussed in "Operational Application of the ARTS System" such that in the present test, no definite pretest flight plan was in effect. The aircraft merely searched out tracer where it could be found. Figure 1 maps the results of an experiment in which the Queen Air aircraft was so used. Tracer was generated from point A for a period of one-half hour. The dashed lines emanating from the generation source show limits of the tracer as found on the network of ground-based filter samplers. These samplers were not in use beyond about 9 km from source point A. The double

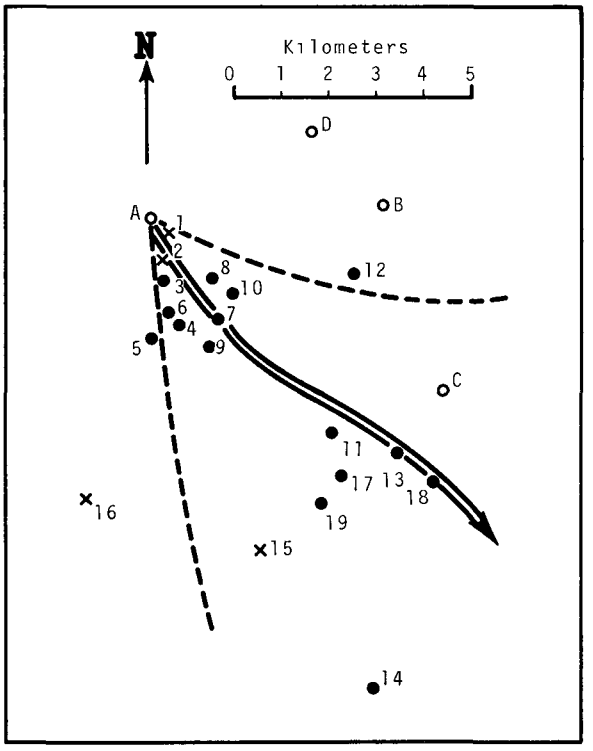

FIGURE 1. Distribution of Surface Level and Aloft Tracer Samples

line arrow specifies the "centerline" of exposure for these ground samples. The individually numbered points show the projection to the surface of intercepts of the aircraft with tracer. The intercepts are numbered in their order of occurrence. Questionable intercepts are denoted as x, confident intercepts are solid dots.

Further information concerning each intercept is given in Table I. The first column lists Intercept Number. The Normalized Peak Concentration is derived from the highest point reached by the pen on the ARTS recorder during the occurrence of an intercept (> indicates that the recorder was driven full scale). It is desirable to obtain not only peak concentrations, but also mean or integrated concentrations over the duration of an aircraft traverse through the tracer plume. Sometimes this is possible. In the experiment under consideration, it generally was not. The tracer plume was apparently so divided into many discrete "puffs" that the character of the recorded signal was usually a series of nearly instantaneous "spikes" superimposed on a mean background signal level.

Duration, in seconds, is also listed, this is defined as the length of time between the first and last spikes on the chart as the aircraft traversed through an area where tracer was observed.

Since the aircraft travels at about 60 m/sec during sampling, a multiplication of the duration (in seconds) by 60 will give the distance in meters that the aircraft traversed during a tracer intercept. Inasmuch as the aircraft did not always fly normal to the

TABLE I. Aircraft Tracer Intercepts

Tracer Intercept Number	Normalized[a] Peak Concentration, g/m^3	Duration in Seconds	Sampling Location: Altitude, ft MSL	Sampling Location: Altitude, ft Above Surface	Sampling Location: Distance from Source, km	Tracer Speed: Min, m/sec	Tracer Speed: Max, m/sec
1[b]	2.6	2	500	250	0.5	2.2	∞
2[b]	>5.4	4	500	200	0.9	3.1	∞
3	9.9	5	620	220	1.3	3.0	∞
4	>20	9	1100	600	2.3	3.4	∞
5	2.7	6	1500	1100	2.5	2.9	∞
6	>6.2	32	1100	650	2.0	2.0	∞
7	3.9	12	1500	800	2.6	2.0	∞
8	>6.6	26	1500	1050	1.9	1.3	∞
9	8.1	5	1500	850	3.0	1.8	∞
10	4.3	12	1500	1050	2.4	1.0	3.4
11	>6.7	38	1600	500	6.0	2.3	7.9
12	3.5	63	1500	600	4.5	1.5	3.7
13	2.8	13	2000	1250	7.2	2.1	4.5
14	0.79	9	2500	1900	10.9	3.1	6.3
15[b]	0.60	41	3000	1500	7.3	1.9	3.8
16[b]	1.1	36	1500	750	6.0	1.4	2.3
17	>2.0	82	1500	800	6.8	1.4	2.3
18	5.3	115	1000	250	8.2	1.6	2.6
19	3.4	96	800	100	7.0	1.1	1.6

(a) *Normalized to 1 g/sec emission rate. Concentrations listed must be multiplied by 10^{-6} for true concentration.*

(b) *Questionable tracer intercept.*

expected tracer plume during this experiment, this distance cannot be interpreted as a crosswind instantaneous plume width. For that matter, even if each aircraft traverse were normal to the plume axis, the concentration and width would vary considerably except, perhaps, under conditions of strong mixing. An attempt to define widths and concentrations at different distances and elevations would require a series of crosswind traverses at each of the desired locations to obtain statistical significance.

The Sampling Location in the table lists the aircraft altitude and its distance from the source at each intercept. In flight, it was the duty of an observer in the co-pilot seat to make notes on aircraft location, altitude, and heading at convenient landmarks, and to activate an event marker on the ARTS chart as the aircraft passed over these landmarks. In the current test, an attempt was made to plot each intercept location at the midpoint of its duration--not where the aircraft initially or finally detected the tracer.

As seen in Table I, tracer intercepts were made only to a distance of about 10 km from the source during this particular field experiment. In other tests, tracer has been confidently intercepted to distances greater than 40 km. However, present tracer generation capabilities, "average" atmospheric dilutions, and ARTS sensitivities generally preclude sampling beyond 20 or 25 km from the source.

Under Altitude in the table are listed the aircraft elevations above mean sea level(determined by the aircraft altimeter) and above the mean land surface elevation in the vicinity of the aircraft traverse. The fact that the differences between MSL and above-surface values are far from constant points out that the terrain over which this experiment was carried out had considerable relief.

The last two columns in the table list the minimum and maximum speeds with which a puff of tracer would have had to move to arrive at the actual point of aircraft intercept. The Min column makes the assumption that the sampled aircraft intercept was the first puff out of the generator. A knowledge of the time at which the intercept was detected and its distance from the source permits this speed computation. Obviously any puff of the tracer emitted from the generator after the initial puff would have to travel at a greater mean speed to get to the intercept point at the time of measurement. The puff which would have to move the fastest to get to the point of intercept would be the last puff from the generator. The Max column lists the speed which this last puff would have had to travel to qualify as the tracer intercepted by the aircraft. The Max Tracer Speed computation results in infinite or absurdly high speeds being required if the aircraft intercept takes place before, at, or shortly after the last puff has been generated. As time after generation increases, the Max speed value becomes more meaningful and, with the accompanying Min value, can place reasonable limits on the mean speed required for the sampled tracer to get from source to intercept location. These speeds and directions may imply an effective transport height.

During this test, tracer was generated between the hours of 1435 and 1505 PST. The ARTS sampling equipment was in operation at 1434 PST and continued to function until 1620 PST. Intercept No. 1 occurred at 1439, and Intercept No. 19, the last for this test, was made at 1618 PST.

Measured surface winds at the tracer source and at locations B and C were in agreement with the plume centerline as shown on the accompanying map for the field test. They were 305 to 315° at 2 to 3 m/sec. Speeds aloft, as measured by upper air soundings at location D, were 1 to 3 m/sec throughout the period of aircraft tracer intercepts. Thus the computed Min Tracer Speeds listed in the accompanying table appear to be in good agreement with the measured winds.

Note that most of the aircraft tracer intercepts were south of the centerline of the ground-level tracer plume. This observation is consistent with observed upper winds at location D. These winds veered from about 310° throughout the surface to 1000 ft MSL layer to 30 to

80° at the 3000 ft MSL elevation. Intercept 12 is an apparent anomaly in location; but it must be admitted that coordination between aircraft location and ARTS chart was less than ideal during this test, a test among the first with airborne sampling. Plotted Intercept 12 (and others) may be somewhat displaced from the true location.

Temperature soundings at location D showed an unstable atmospheric layer (-1.2 °F per 100 ft) from the surface up to about 700 ft MSL. From 700 to 1700 ft MSL, the atmosphere was relatively stable (-0.2 °F per 100 ft), although there was no temperature inversion. Above 1700 ft MSL, the atmosphere had a near adiabatic lapse rate throughout the layer of aircraft sampling. An examination of Sampling Altitude in the accompanying table shows that the tracer penetrated readily into the relatively stable layer--even as close to the source as Intercept 4 at 2.3 km, if the location D soundings were typical of the aircraft sampling zone.

Intercepts 17, 18, and 19 were made during traverses in a deep east-west canyon. Note the lengthy duration of these intercepts. It can be speculated that aerodynamic effects along the north ridge of the canyon may have induced tracer to mix uniformly into the canyon. An aircraft traverse through the canyon would be expected then to produce a nontypical intercept record. No definite answer is evident from the data at hand, but the expanded zone of tracer is an interesting fact pointed out by use of the ARTS.

Several traverses at greater than 1500 ft MSL were made between Intercepts 9 and 10 with no tracer interception. It would seem that the maximum vertical extent of the tracer at about 3 km was 1500 ft MSL. Between Intercepts 11 and 13, traverses at 2100 and 2200 ft MSL were flown with negative results. This suggests a maximum vertical tracer extent of 2000 ft MSL at about 5 to 7 km. As evidenced by significant Intercept 14, tracer extended to at least 2500 MSL at a distance of 11 km.

OPERATIONAL APPLICATION OF THE ARTS SYSTEM

M. A. Wolf

A diffusion test was performed on the evening of September 2, 1966 to examine the operational utilization of the Airborne Real Time Sampler (ARTS). This test was conducted on the Hanford stable course under neutral conditions. The surface (4-5 ft) tracer release extended from 1742 to 1843 PST with a seven minute interruption from 1749 to 1756 PST due to malfunction of the tracer generator.

Support of the airborne operations was provided by surface sampling at 1.50 m height on arcs 1, 2 and 4, (at distances of 200, 800 and 3200 m respectively). Arc 4, 200-ft tower samplers were operated also. Meteorological support consisted of wind velocity and temperature data from the standard levels of the 400 ft Meteorological Tower at the source.

During the test, conditions were quite steady. The wind remained near 10 knots from 310° throughout the period. The temperature structure, unstable immediately before and stable immediately after the test, was neutral

during the operation. Twenty-one aircraft traverses (numbered alphabetically) of the tracer plume yielded ARTS instantaneous and integrated values. The integrated values are shown as a function of plume transit time in Figure 2 where it is suggested that traverses E, H, K' and U are not representative of the plume. Though not clearly established, it is suspected that these four traverses were above the main portion of the instantaneous plume; each was at a greater height than the average of the others at comparable distances. The significance of this is discussed in greater detail in the following. Therefore, the analysis of aircraft sampling is restricted to the remaining 17 tranverses which are circled in Figure 2. Pertinent data from these traverses are presented in Table II.

The aircraft was operated in a manner designed to determine the vertical and horizontal crosswind extent and concentration of the tracer at several distances from the source. All traverses were flown nearly normal to the plume to yield true instantaneous

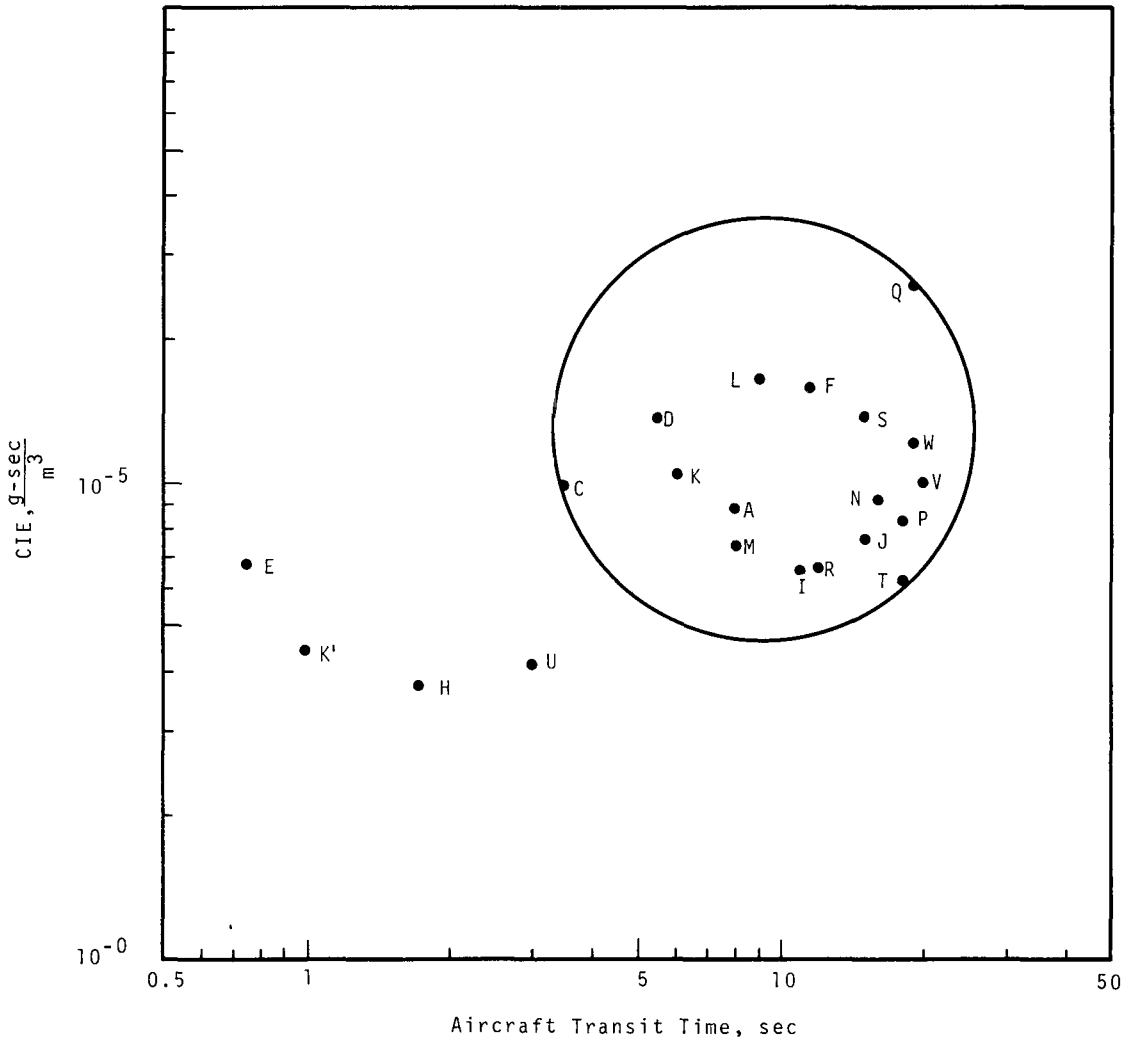

FIGURE 2. Aircraft Cross-wind Samples

TABLE II. Pertinent Aircraft Sampling Parameters

Pass	Time (PST)	Distance Downwind, m	Ht Abv SFC, ft	Direction of Pass	Intercept Distance South of Reference, m	CIE, g-sec-m^{-3}	Intercept Duration, sec	χ_{p}, g-m^{-3}
A	1801:04/01:12	3200	200	S	1680/2210	8.88×10^{-6}	8.0	4.48×10^{-6}
C	1805:48/05:51.5		50	S	704/897	9.92×10^{-6}	3.5	1.24×10^{-5}
D	1807:01/07:06.5		150	N	515/817	1.37×10^{-5}	5.5	1.24×10^{-5}
F	1811:23/11:34.5		300	N	562/1194	1.59×10^{-5}	11.5	1.66×10^{-5}
I	1820:31/20:42		400	N	264/869	6.59×10^{-6}	11.0	7.70×10^{-6}
J	1822:29/22:44		200	S	(a) 268/752	7.60×10^{-6}	15.0	6.77×10^{-6}
K	1825:13/25:19		220	N	539/869	1.04×10^{-5}	6.0	8.14×10^{-6}
L	1827:35/27:44		150	S	604/1216	1.66×10^{-5}	9.0	1.40×10^{-5}
	Average		210			1.12×10^{-5}	8.7	1.03×10^{-5}
M	1832:44/32:52	6900	150	S	2210/2754	7.37×10^{-6}	8.0	7.82×10^{-6}
N	1835:18/35:34		100	N	2170/3050	9.20×10^{-6}	16.0	6.35×10^{-6}
P	1838:22/38:40		200	S	2550/3775	8.29×10^{-6}	18.0	4.95×10^{-6}
Q	1841:41/42:00		300	N	1945/2990	2.62×10^{-5}	19.0	1.14×10^{-5}
R	1844:41/44:53		300	S	2680/3496	6.64×10^{-6}	12.0	5.87×10^{-6}
	Average		210			1.15×10^{-5}	14.6	7.28×10^{-6}
S	1847:52/48:07	12500	200	NE	2612/3540	1.38×10^{-5}	15.0	1.10×10^{-5}
T	1851:11/51:29		200	SW	3295/4408	6.22×10^{-6}	18.0	3.55×10^{-6}
V	1857:36/57:56		300	SW	3480/4717	1.01×10^{-5}	20.0	1.15×10^{-5}
W	1901:30/01:49		50	NE	2575/3750	1.22×10^{-5}	19.0	1.27×10^{-5}
	Average		190			1.06×10^{-5}	18.0	9.69×10^{-6}

(a) *Distance north of reference*

width. Though a large number of traverses at various heights and distances was desired, fewer were permitted by the time limitations imposed by the arrival of darkness. Table II shows that a minimum of four successful traverses was made at each of the three distances and that each distance was traversed over a vertical range of at least 200 ft. The fact that the tracer was sampled at 300 ft on four occasions but was also missed between 250 and 340 ft on four occasions indicates that the mean height of the plume top was about 300 ft. There was no indication that this top height varied with distance. Also to be noted in Table II is the fact that no organized variation in crosswind integrated exposure nor peak concentration was noted either with height or with distance. Both of these points are significant in the comparisons of the observations with diffusion theory.

During each traverse a fiducial point was placed on the real time sampler chart to enable subsequent location of the plume intercept with reference to the ground. Calculation of intercept position from these references was done through incorporation of aircraft heading and airspeed and the speed and direction of the wind near flight level. The resultant intercepts are plotted in Figure 3 as a function of time and displacements from the stable course radial along which the centerline of the average plume was observed on the Arc 4 surface samplers. For each distance, the envelope of these traverses can be interpreted as defining the horizontal form of the instantaneous tracer distribution at the time of observation.

The envelope is well defined by the traverses at 6900 m, where each one encountered the plume, and demonstrates a periodicity of about 7 min. Though this period was not initially apparent in the intercepts at 3200 and 12,500 m, Figure 3 shows that it is not inconsistent. The ratio of the width of the instantaneous plume to that of the mean plume, for the time presented, is about two for the 6900 and 12,500 m distances, and for the shortest distance also if the two large excursions are disregarded. The width of the mean plume on the surface at 3200 m, where comparison is available, is nearly identical with the width of the mean plume aloft.

There is ample reason to question traverses A, C, and D all of which are nontypical of the 3200 m traverses. It was noted earlier that no tracer was generated from 1749 to 1756 PST. The corresponding time period at the 3200 m sampling distance is 1800 to 1807 PST, considering existing winds. Apparently, the tracer sampled in traverse A was released just prior to shutdown and that sampled in traverses C and D was released soon after restart. However, with no indications of atypical atmopheric conditions, these traverses were retained. No reason is apparent for the displacement of traverse A.

The character of the source wind direction, its period, and amplitude was considered in relationship to the instantaneous plume to see if similarities existed. Figure 4 presents the results of taking successive three-minute averages of the wind direction and converting these angular displacements to crosswind displacements at the downwind distances of interest. An average period of about 7 min is noted

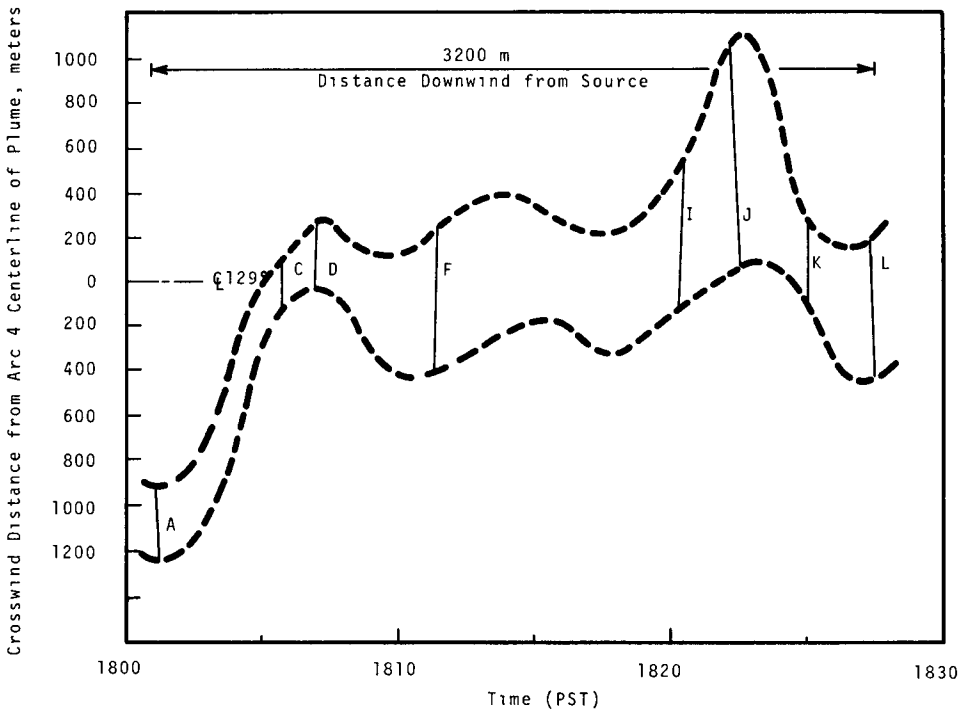

(a)

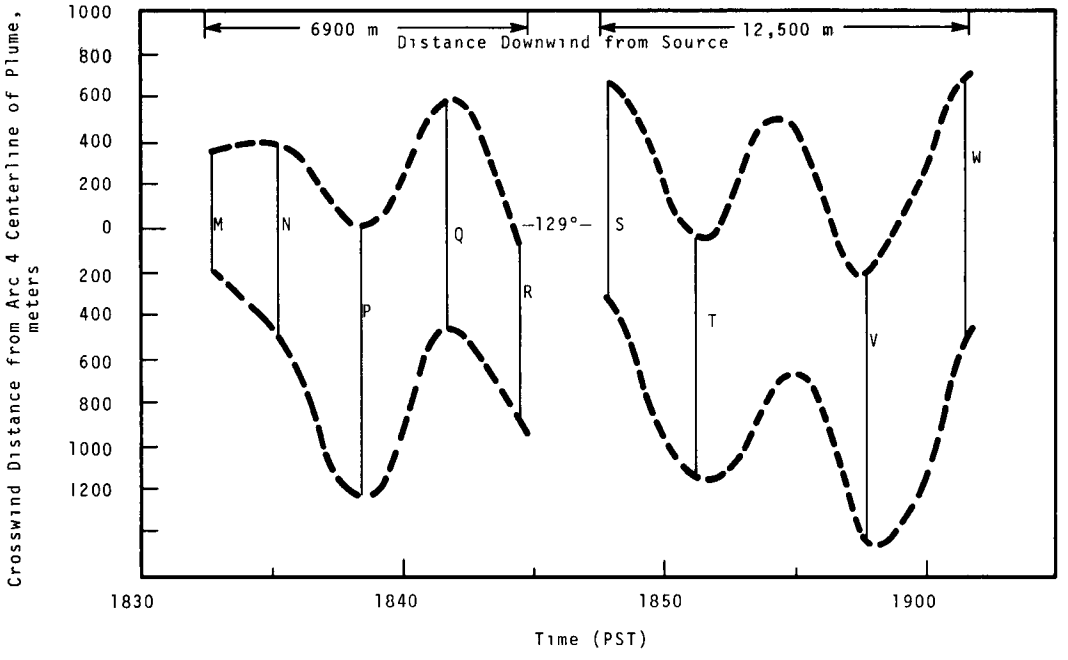

(b)

FIGURE 3. Aircraft Intercepts of Tracer Plume

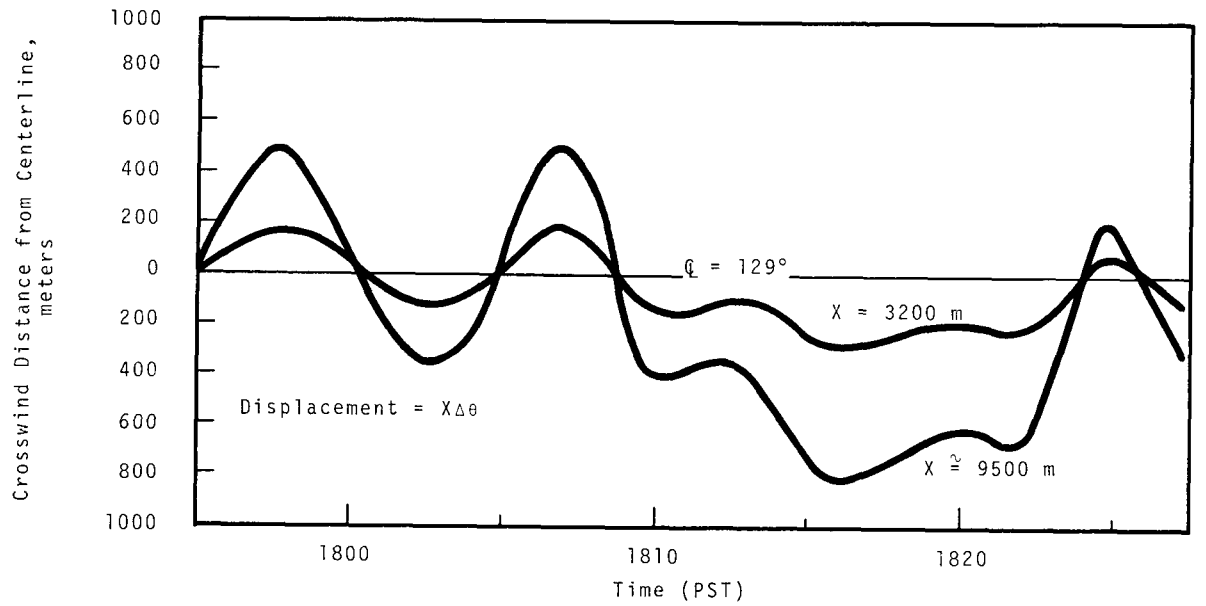

FIGURE 4. Typical Downwind Displacement of Instantaneous Plume Centerline (℄) Predicted by Three-Minute Averages of Source Wind

here also. Furthermore the displacements indicated in Figure 4 are very nearly equal to the displacements of the instantaneous plume centerline at comparable distances. It is concluded, therefore, that traverses of the downwind plume can provide a detailed description of the shape of the instantaneous plume and may even serve as a research tool in investigating the relationship of the plume to the source characteristics.

Another research application, touched on earlier, is the relationship of the mean plume width to the instantaneous plume width. This is displayed graphically for this test in Figure 5. As discussed, the crosswind projected width of the envelopes of the instantaneous plumes defined by the aircraft traverses are very nearly double the instantaneous widths. The projected envelope width, plotted in Figure 5, is seen to correspond extremely well to the surface width which when defined as six times the observed σ_y, is bounded by the crosswind positions at which 1% of the central peak is found.

Moreover, the lateral growth of the tracer plume, in the interval of distance examined, is seen to lie between a linear relationship with distance and an $x^{0.5}$ relationship, the latter relationship probable at distances on the order of 15 miles.

To this point we have discussed only that information which is derived from using the ARTS as a tracer detector. Beyond this application is its measurement capacity since both instantaneous peak concentrations and crosswind integrated exposures are recorded. Comparisons of airborne and surface measurements are possible at the 3200 m arc which was common to both surface and aircraft operations. In addition

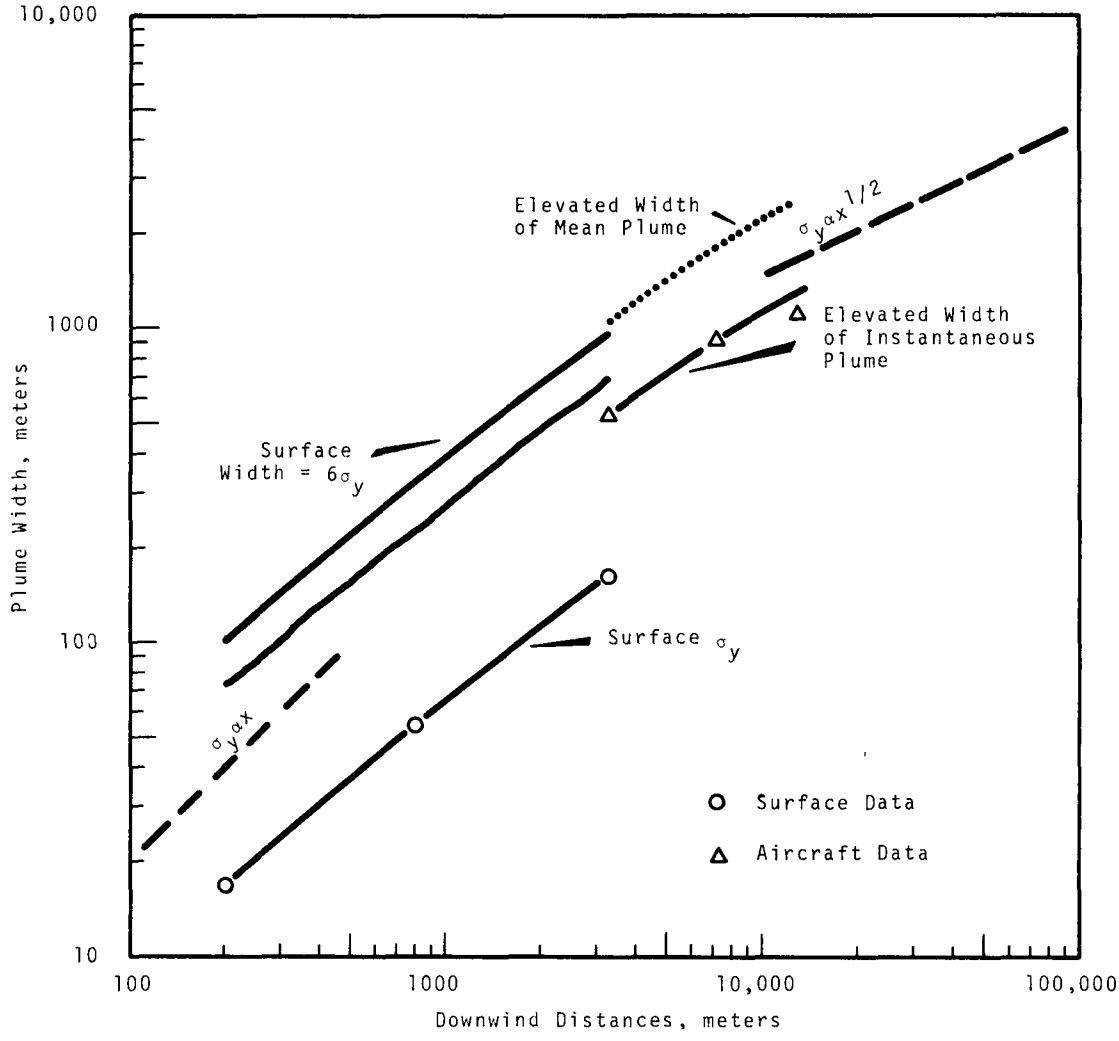

FIGURE 5. Plume Dimensions

to comparison with each other, comparisons with diffusion theory can also be made.

It is necessary to examine all available information from this test to ascertain the representativeness of the data and to select the proper models for comparison. It was noted earlier that aircraft measurements showed the mean height of the apparent upper boundary of the tracer to be at 300 ft and that no organized variation in tracer concentration with height or with downwind distance would be detected. The surface measurements are likewise examined for clues to the vertical distribution of tracer, the lateral distribution already being identified as approximately Gaussian. Figure 6 presents the tracer distribution throughout two of the Arc 4 towers on the 122 and 130° radials. There is little evidence of a Gaussian distribution, rather there is support

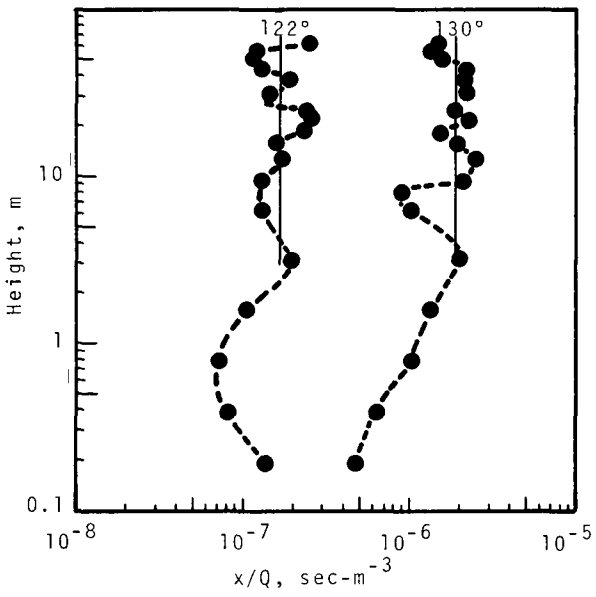

FIGURE 6. Vertical Distribution of Tracer on Arc 4 Towers

for the observation of vertical invariance derived from the aircraft traverses. The profiles of Figure 6 also suggest that deposition may be instrumental in reducing the exposures below a height of about three meters.

It is assumed that representative crosswind values for nondepositing, vertically invariant distributions are given by the depth-weighted averages derived from the towers. Such values for the 122 and 130° towers are determined as 1.67×10^{-7} sec-m^{-3} and 1.88×10^{-6} sec-m^{-3}, respectively. Their respective ratios to the surface sampler measurements on corresponding radials are 1.33 and 2.17, which may indicate that deposition is proportional to concentration. The observed peak on the Arc 4 surface samplers is corrected by 2.17 since the peak occurred near 130°, but the crosswind summed exposure is corrected by the average value, 1.75. In this way the peak χ/Q is determined as 3.01×10^{-6} sec-m^{-3} and the crosswind summed exposure becomes 2.29×10^{-2} g-sec-m^{-3}. Before considering these measurements further, it is well to discuss the models for comparison.

The assumed model appropriate to a continuous point release and containing only a lateral Gaussian distribution is given by

$$\chi = \frac{Q\, e^{-0.5(y/\sigma_y)^2}}{\sqrt{2}\,\pi\,\bar{u}\,H\,\sigma_y} \quad \frac{g}{m^3} \qquad (1)$$

Equation (1) can be integrated with respect to y to give the crosswind integrated concentration

$$CIC = \frac{Q}{\bar{u}\,H} \quad \frac{g}{m^2} \qquad (2)$$

In the above equations Q is the rate of release of tracer material (g-sec^{-1}), y is the distance laterally from the plume axis (meters), $\bar{u}$ is the mean windspeed at the source (m-sec^{-1}), H is the height of the uniformly mixed layer (meters), and σ_y is the lateral standard deviation of the tracer(meters).

The exponential term of Equation (1) becomes unity when the peak value which occurs on the axis is considered. It is common to write Equations (1) and (2) in terms of unit source strength so that the left hand sides are expressed as χ/Q and CIC/Q, respectively.

Equations (1) and (2) are appropriate to both surface and elevated sampling. The only term which has different values for the two situations is σ_y which as noted earlier has a value appropriate to the instantaneous width for comparison with the aircraft measurements and a value appropriate to the mean width for comparison with surface measurements. The surface-determined width value for σ_y at Arc

4 is 164 m. The aircraft-determined width value is 90 m if the average instantaneous width at Arc 4 is taken as 6 σ_y. The height of the mixed layer is taken as 95 m (approximately 300 ft) as noted earlier. A total of 1333 g of tracer was released at a rate of 0.412 g/sec into a wind of 5 m/sec. Substitution of these values into Equations (1) and (2) provides the following results:

$$(\chi/Q)\ \text{ACFT} = 9.36 \times 10^{-6}\ \text{sec-m}^{-3}$$
$$(\chi/Q)\ \text{SFC} = 5.14 \times 10^{-6}\ \text{sec-m}^{-3}$$
$$(\text{CIC/Q})\ \text{ACFT} = 2.10 \times 10^{-3}\ \text{sec-m}^{-2}$$
$$(\text{CIC/Q})\ \text{SFC} = 2.10 \times 10^{-3}\ \text{sec-m}^{-2}$$

The above values, then, are those to be expected for the assumptions made and the inputs used.

Returning now to the values observed at the surface samples, the χ/Q value of 3.01×10^{-6} sec-m^{-3} is directly comparable; but the integrated value is crosswind summed exposure. It becomes comparable when it is multiplied by the distance interval of the samplers, divided by the sampling time, and then normalized to unit source strength by division with Q. Thus,

$$\frac{\text{CIC}}{Q} = \frac{(\text{CSE})(\Delta y)}{Qt} = \frac{2.29 \times 10^{-2}\ (55.8)}{(0.412)\ (3240)}$$
$$= 9.57 \times 10^{-4}\ \text{sec-m}^{2}$$

The aircraft measurements are much the same in that the measured average peak of 1.03×10^{-5} g-m^{-3} is divided by the source emission rate to give an E/Q value of 2.50×10^{-5} sec-m^{-3}, but the $\frac{\text{CIC}}{Q}$ is somewhat more complicated. The integrated value recorded in the aircraft is the crosswind integrated exposure; and, to convert it to CIC/Q, it is multiplied by the speed of traverse across the tracer and divided by Q. Thus,

$$\frac{\text{CIC}}{Q} = \frac{\text{CIE}}{Q} V = \frac{1.12 \times 10^{-5}\ (61.8)}{0.412}$$
$$= 1.68 \times 10^{-3}\ \text{sec-m}^{-2}$$

All values, calculated from the models and measured in the air and on the ground, are listed in Table III for comparison. It is seen that for the (CIC/Q), which was the same calculated value for both surface and air, the aircraft measurement is greater by a factor of 1.75. For χ/Q, the aircraft measured value is 4.56 greater than the surface value even after allowance is made for its lesser width. It may be that the instantaneous peak is poorly related to the instantaneous cloud width as measured, or it may be that the assumption of complete mixing over 95 m in the vertical is extreme for the instantaneous distribution. Whatever the reason for the rather large discrepancy between the measured and calculated χ/Q for the aircraft, it is beyond the scope of the data from this limited operation to resolve it.

TABLE III. Comparisons of Diffusion Theory and Observations

	χ/Q ACFT	χ/Q SFC	(CIC/Q) ACFT	(CIC/Q) SFC
Measured	2.50×10^{-5}	3.01×10^{-6}	1.68×10^{-3}	9.57×10^{-4}
Calculated	9.36×10^{-6}	5.14×10^{-6}	2.10×10^{-3}	2.10×10^{-3}
Ratio $\left(\frac{\text{Measured}}{\text{Calculated}}\right)$	2.67	0.585	0.800	0.456

The operational value of the ARTS clearly established in diffusion studies is certain to increase with additional use and understanding. Further tests will be conducted to extend the knowledge and insight gained in this test and, thereby, to generate more reliable models for describing diffusion to large distances where variations in the vertical can no longer be ignored.

REFERENCES

1. *P. W. Nickola, M. O. Rankin, M. F. Scoggins and E. M. Sheen. A Device for Recording Air Concentrations of Zinc Sulfide Fluorescent Pigment on a Real Time Scale, HW-SA-3317. General Electric Company, Richland, Washington, January 10, 1964.*

2. *P. W. Nickola. "Instrumenting of the Queen Air Aircraft for Sampling of a Zinc Sulfide Atmospheric Tracer." Pacific Northwest Laboratory Annual Report for 1965 in the Physical Sciences, Volume I: Atmospheric Sciences, pp. 11-13, BNWL-235 1. Pacific Northwest Laboratory, Richland, Washington, May 1966.*

SELECTED METEOROLOGICAL ANALYSES OF PLUMBBOB NUCLEAR TESTS

W. E. Davis and R. J.Engelmann

INTRODUCTION

Until now, a thorough meteorological analysis has not been performed on specific nuclear shots in the Plumbbob nuclear test series. Such an analysis may reveal information on the transport of the nuclear debris. With the aid of ground samples, information may also be gained on the geological availability and distribution of particles in the fallout pattern.

Shot Smoky was selected for such an analysis because ground fallout samples existed and there was an abundance of pibal and additional radiosonde data. Also Shot Smoky had two areas of anomalous higher dose (hot spots) in its fallout pattern.

ISENTROPIC ANALYSIS OF SHOT SMOKY

An analysis of stream functions on isentropic surfaces (surfaces of constant potential temperature) was performed to aid in the investigation of the horizontal and vertical transport of the nuclear debris.

The stream functions were computed through the use of a MIDAS computer program.[1] Radiosonde data used for the computations were provided by the U. S. Weather Bureau and the 6th Weather Wing, Air Weather Service. From these computations, the streamline analysis was performed. However, since the stream-analysis was not smooth, an error analysis was used to explain, in part, the irregularities.

To determine the random error in the stream function due to the instruments, personnel, etc., at a particular location (observational error), a statiscal analysis on original data taken at Vandenberg AFB was performed.

A set of 50 data points for 300° θ (potential temperature) level from four radiosonde stations located within a radius of four miles was used for the error analysis. The set of data at the sites was acquired from seven hourly radiosondes on two separate days. Three of the sites were operated by the 6th Weather Squadron (mobile), 6th Weather Wing, Air Weather Service, and one site was operated by the U. S. Weather Bureau.

First the soundings were used for stream function calculations after assuming that there were no effects due to time or space variations. Then, the data were tested for changes due to differences in time of measurement (time error) and for systematic bias at the individual sites (location error). The observation, location, and time errors were combined to give a total error for a single observation. On the first day, one of the Air Force sites was omitted, as well as any hour which had an observation missing. On the second day, the first time period was omitted. This was done to obtain a "balanced" design for each day(i.e., no missing values).

The calculations gave a computed standard observational error of 0.02 to 0.04 x 10^7 cm^2-sec^{-2} (Table I). This random error in the stream function can be expected at other radiosonde stations.

Aneroid barometers were used at three of the sites. Since comparison of pressure data from the barometers at each site indicated that they were in error, the stream function data were corrected to remove the pressure error. This was done by computing a single pressure versus height curve applied to all locations for each time period. A corrected surface pressure was taken off the pressure height curve for each of the four sites. The result of the error analysis of the corrected data was that the observational error remained the same while the location error was approximately halved.

The next step was to apply the error analysis to the meteorological data taken during Shot Smoky. It was assumed that the United States Weather Bureau sites with better instrumentation such as mercurial barometers would have a small location error.

It was assumed that data from the sites operated by the 6th Weather Wing for Operation Plumbbob had the same errors as the uncorrected data in the previous error analysis. Thus, it was concluded that the data obtained by them could be used only as a guide to possible values of the stream function. The latter conclusion was reached because of the large combined error for a single observation of 0.071 to 0.095 x 10^7 cm^2-sec^{-2} (Table I). The Weather Bureau data, on the other hand, would have a combined error of 0.03 x 10^7 cm^2-sec^{-2}.

With these errors in mind, we reanalyzed the charts. The stream line analysis of the stream function was considerably smoother, although there

TABLE I. Errors in the Stream Function Data $\Delta\Psi_{300} \times 10^{-7}$ *(cm²-sec⁻²)*

	Observational Error	Location Error	Time Error	Combined Standard Error for a Single Observation
Original Data				
6-10-66	0.039	0 060	0.000	0 071
6 13 66	0 020	0.093	0.000	0.095
Pooled Error	0.030			
Corrected Data[a]				
6 10-66	0 04	0.038	0 000	0.056
6 13 66	0.018	0 032	0.012	0.04
Pooled Errors	0.026			
Corrected Data[b] Without Weather Bureau Site				
6 13 66	0.012	0.014	0.016	0.025

(a) *One pressure height curve was used to find surface pressure at all sites.*

(b) *Calculations were not made for 6-10-66 due to small sample.*

were indications (e.g., from Salt Lake City) that larger errors than just observational error assumed for the United States Weather Bureau, could exist.

The isentropic trajectories were then constructed on potential temperature surfaces. The trajectories were taken to track the position of the nuclear cloud. The end points of the trajectories were adjusted under the assumption that the energy equation on isentropic surfaces be conserved.[2]

A confirmed trajectory was found when the path of an air parcel on the 330° θ surface passed over a position in Wyoming where a "pilot report" indicated the existence of an orange cloud, which was presumed to be a fallout cloud. The trajectory is shown in Figure 1. The observation corresponded to the height and the time of travel of the cloud predicted by the trajectory.

Isentropic trajectories also may be used to find a large scale vertical air mass movement.[3] It was hoped that the relatively dense radiosonde network would allow an investigation that would reveal smaller scale vertical motions affecting the close-in fallout. However, due to the large errors in the streamfunctions and, thereby, in the heights of the potential temperature surfaces, only macroscale motions could be revealed. These vertical motions were found to be quite small for this particular case.

AREA WITHIN AN ISOPLETH

A graph of the dose per yield (in kiloton) versus area within an isopleth

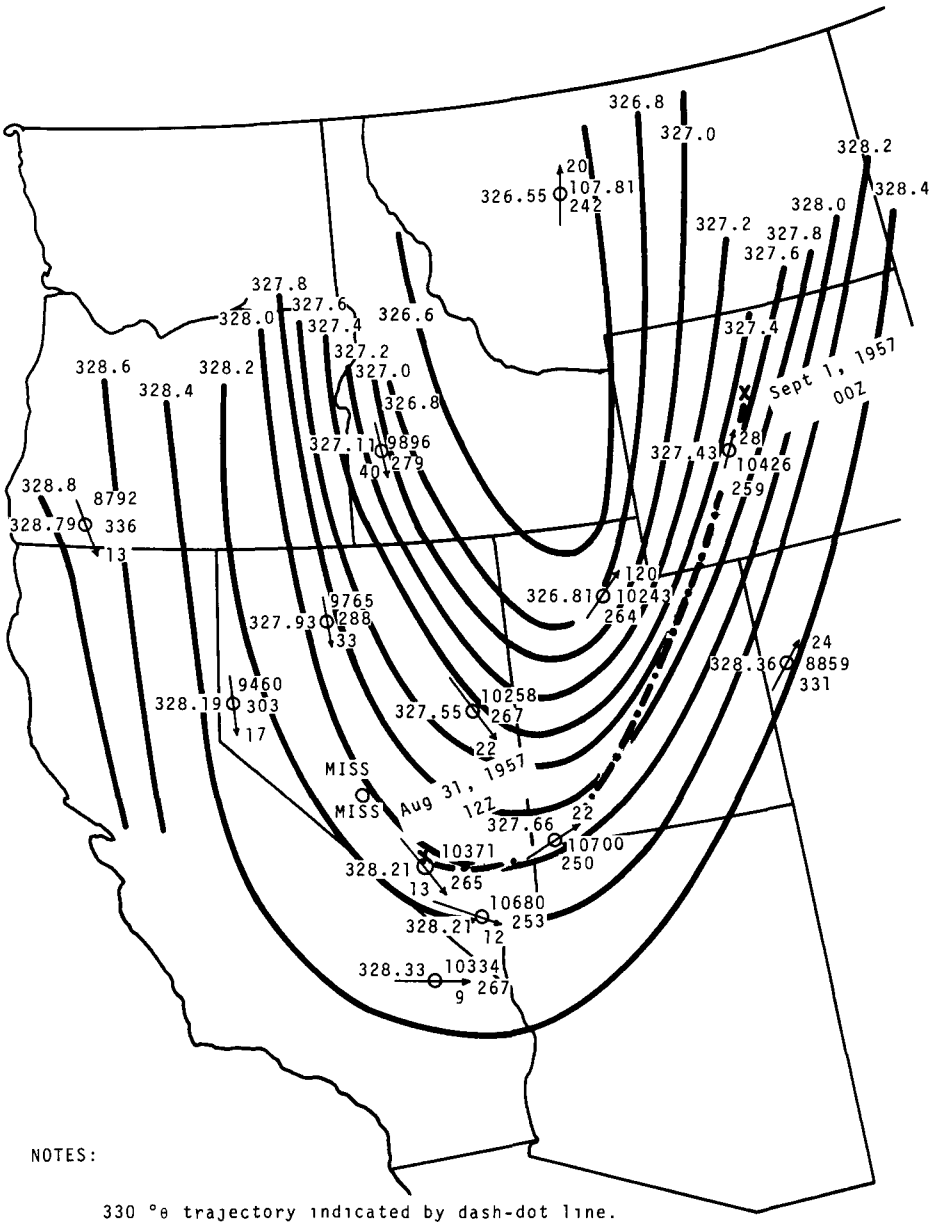

FIGURE 1. 330° θ (Potential temperature) Surface Sept. 1, 1957, 00Z (Greenwich meantime)

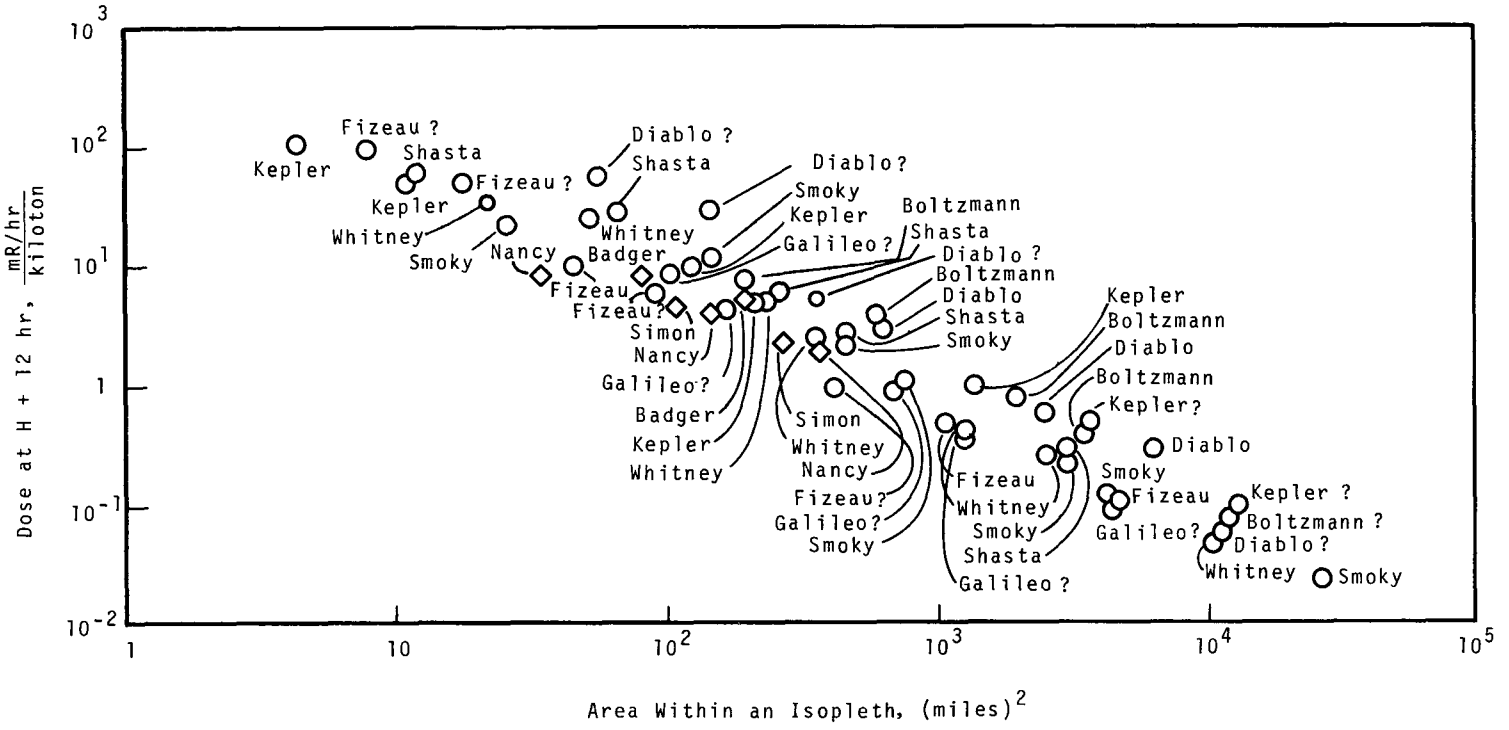

FIGURE 2. Upshot-Knothole Shots Indicated by Diamonds. Points in Question Indicated by (?)

was plotted for the tower shots of Plumbbob and the Upshot-Knothole series (The dose was calculated for shot time plus twelve hours, so that the effects of decay could be removed.) The slope of the logarithmic plot of these parameters in Figure 2 was found to be -1.15 by the method of least squares.

When the Plumbbob data[4] alone were considered and those points which were rough estimates of the area were removed, a slope of -1.08 was calculated.

Curiously, Nickola and Nutley[4] found a similar area-dosage relationship for diffusion from a continuous point source at the ground. These isopleths had slopes of -1.09 for stable Richardson numbers to -1.14 for unstable Richardson numbers.

There were large changes in the individual slopes of the dose per yield versus area within an isopleth for close-in fallout from individual tower and balloon shots in Plumbbob. An attempt was made through the use of wind speeds at various layers in and below the nuclear cloud to explain the change in slope. The results of this investigation are not yet conclusive and the work is continuing. Figure 3 shows the wind speeds at the base of the cloud versus the slope (dose per kiloton versus area within an isopleth). It appears that there may exist some correlation between the parameters.

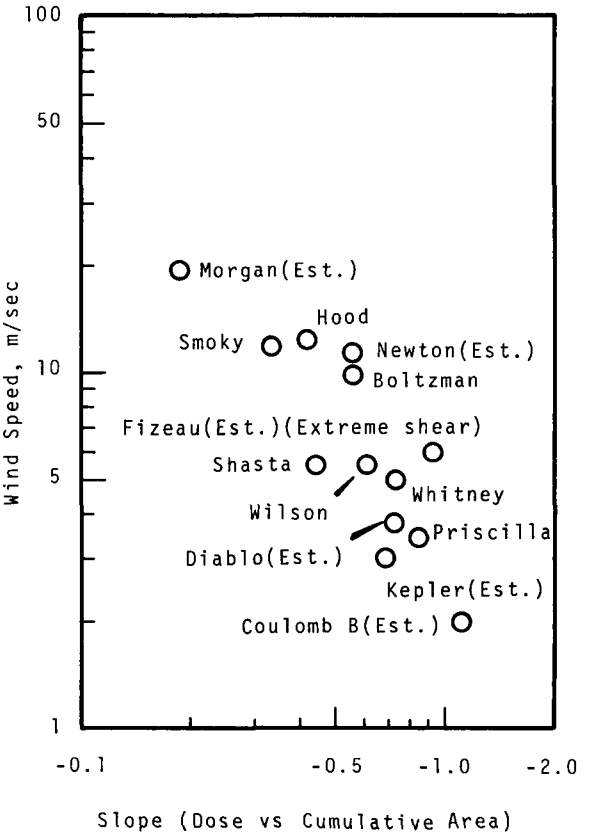

FIGURE 3. Wind at Base of Cloud Versus Slope of Dose Versus Area

REFERENCES

1. *R. J. Engelmann and W. E. Davis. Low-Level Isentropic Trajectories and the MIDAS Computer Program for the Montgomery Stream Function, BNWL-441. Pacific Northwest Laboratory, Richland, Washington, 1967.*

2. *E. F. Danielson. "Trajectories; Isobaric, Isentopic, and Actual," Journal of Meteorology, vol. 18, no. 4, pp. 479-486. August 1961.*

3. *Elmar R. Reiter and J. D. Mahlman. "Heavy Radioactive Fallout Over the Southern United States, November, 1962." Transport Processes in the Atmosphere Leading to Radioactive Fallout, Progress Report No. 1, Technical Paper No. 58. Department of Atmospheric Science, Colorado State University, September 1964.*

4. *P. W. Nickola and N. E. Nutley. "Area Dosage Relationships Downwind of a Point Source," Hanford Radiological Sciences Research and Development Annual Report for 1964, BNWL-36. Pacific Northwest Laboratory, Richland, Washington, 1965.*

IMPROVEMENTS IN RAINDROP CHARGE MEASURING SYSTEMS

C. A. Ratcliffe *

Improvements made in the earlier equipment are in transducer design, better charge sensitive amplifier stability, and easier field adjustment and operation. The transducer was modified to be more tolerant of breezes during the rain or snow shower being sampled. The charge sensitive amplifier was improved to provide higher gain, more stability, and an easier adjustment procedure than previously. Different cabling, connectors, and power supply arrangements have made field operation and maintenance simpler, especially when the ambient temperature is low.

DISCUSSION

Earlier work on this system was reported[1] a year ago. Work this year has been directed toward improved operation of the system, both electrically and mechanically.

Perhaps the most important change was the redesign of the transducers. The old transducer was a large canister (barrel) containing the inductor rings used for the measurement. It operated well but was intolerant of any breeze which caused the raindrop fall to be very different from vertical. The new transducer has the inductor rings mounted close to the top of the shielding enclosure box and closely spaced together. A cylindrical vertical shield is seen in Figure 1. This physically shields against existing electric fields. A shorter cylindrical shield is also sometimes used.

The charge sensitive amplifiers were changed to incorporate a commercial operational amplifier. This provided more gain, smaller current consumption and easier adjustment. Greater stability with time and temperature was also achieved.

A new power supply, also shown in Figure 1, provides voltage regulated power, and has batteries with longer life and a greater temperature range of usefulness. Better connectors and fittings are incorporated, simplifying field use and repair, particularly at low temperatures and during snow showers.

Laboratory calibration shows that the inductor ring-charge amplifier combination produces one volt of output for about 3.2×10^{-12} coulomb. Using a post amplifier with a gain of 28 gives one volt of output for 1.1×10^{-13} coulomb. On the chart recorder we can discern (at 0.5 V/cm) 0.1 V with ease, for a sensitivity of about 10^{-14} coulomb. The recorder cannot be used at arbitrarily high gain, however, as during rain showers there are many charged particles suspended in the air, giving a background having considerable variation or drift. The chart must be able to handle the drift plus the anticipated signals, each with either polarity referred to zero.

Field measurements during snow showers at White Pass, Washington, indicated that almost all of the flakes bore negative charges ranging from 2×10^{-14} to 2×10^{-13} coulomb. Rain showers near Richland, Washington, produced drops with both polarities and

* *Instrumentation Section, Applied Physics and Electronics Department*

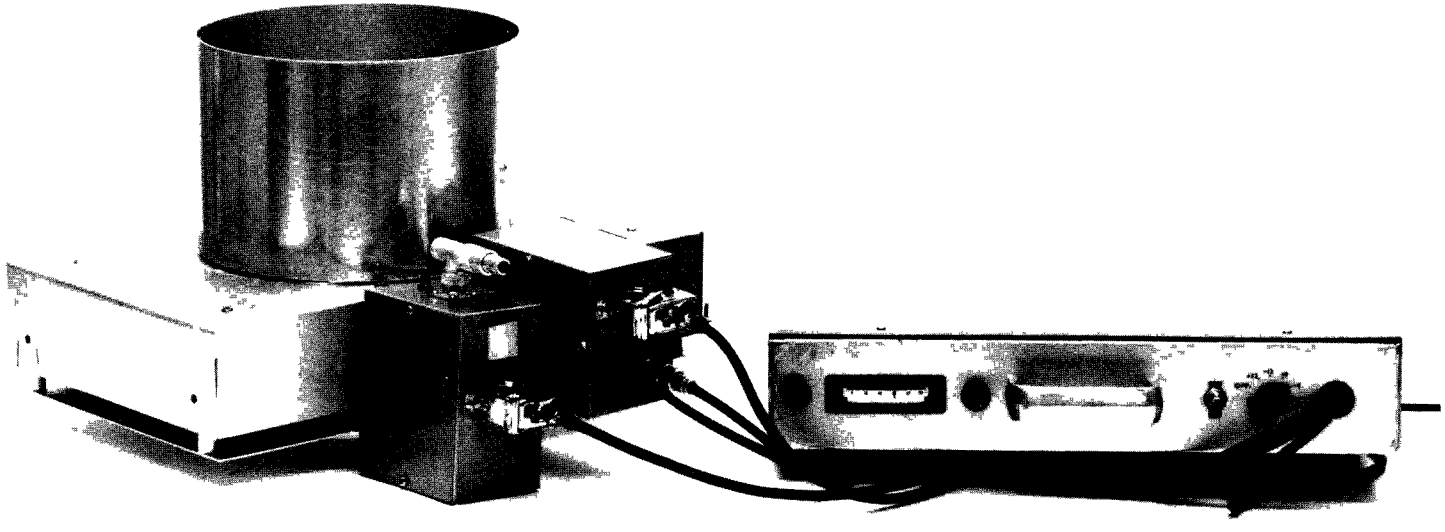

Neg 067447-1

FIGURE 1. Raindrop Charge Spectrometer Transducer and Power Supply

many uncharged drops. Charge magnitudes observed were from 10^{-14} to 10^{-12} coulomb.

Further field work is planned to obtain more spectra and to improve the speed measuring capabilities of the apparatus.

REFERENCES

1. *C. A. Ratcliffe and N. C. Hoitink. "Raindrop Charge and Velocity Measurement Techniques," Pacific Northwest Laboratory Annual Report for 1965 in the Physical Sciences, Volume 4: Instrumentation, p. 21, BNWL-235 4. Pacific Northwest Laboratory, Richland, Washington, 1966.*

IDENTIFICATION AND MEASUREMENT OF HYDROGEN CHLORIDE GAS IN THE ATMOSPHERE BY SPECTROPHOTOMETRIC AND RADIOMETRIC ANALYSIS

J. D. Ludwick*

INTRODUCTION

The radionuclides released from nuclear testing and nuclear plant operation include inert gases, reactive gases, and particulate materials. The reactive gases may deposit downwind on exposed surfaces. Depletion of downwind air concentrations by such a mechanism makes uncertain the worthiness of diffusion predictions, if the model were based on particulates or on a less reactive gas. For this reason, techniques were wanted for the release, collection, and determination of hydrogen chloride gas in the atmosphere. A very sensitive technique was needed to measure the long distance air concentrations and any fluctuations that might occur because of reactions between the gas and particulate phases. The nature of the mechanism of removal of this gas from the atmosphere could then be investigated.

Several analytical methods were available for the determination of chloride in excess of 5×10^{-6} g chloride per sample: these include coulometric, turbidimetric, controlled potential titration and colorimetric techniques. A few methods are described in the literature utilizing spectrophotometric analysis in the range of 10^{-7} to 10^{-6} g per sample. None of these techniques appeared suitable for measurement of chloride ion in the anticipated range of 10^{-8} to 10^{-5} g per sample.

Several unrelated analytical techniques are based upon the interference of one material with the fluorescence or the photometric absorption spectra of another. Several fluorescent materials were studied but the chloride ion failed to extinguish the emission satisfactorily.

* *Radiological Chemistry, Radiological Sciences Section*

Larger quantities (>10^{-6} g) of chloride ion reduced the fluorescence of quinine sulfate, for example; but none of the methods provided the necessary sensitivity for our needs.

A study was made of the interference of chloride with certain light-absorbing materials. It was expected that interference could be obtained in a spectrophotometric procedure involving dithizone and its silver complex, silver dithizonate. A technique was developed utilizing this principle which detected as little as 1 x 10^{-8} g of chloride. The sensitivity of this method was excellent, but it required the dilution of the more concentrated chloride solutions and was, therefore, not satisfactory for field us.

Efforts were then made to develop a simpler method by which almost any field-collected chloride sample could be analyzed. A reasonably sensitive radiometric technique was developed involving precipitation of the chloride with ^{110}Ag, thus tagging the chloride precipitate.(1) The method is sensitive to less than 2 x 10^{-7} g of chloride ion and is readily adaptable to routine operation.

THE RADIOMETRIC CHLORIDE METHOD

In developing the method, standardized chloride solutions were treated with suitable volumes of silver nitrate solution tagged with ^{110}Ag. The solution with the precipitated AgCl was then centrifuged and filtered through a 50 mμ membrane filter. The precipitate was washed and counted. A series of measurements using this technique indicated rather poor precision for the very small precipitates, many of which were invisible to the eye. The time involved in filtering each sample was also prohibitive.

This procedure was modified to take an aliquot of the supernatant solution for gamma analysis, rather than attempting to recover the precipitate. A direct correlation was found between the amount of chloride in the sample and the ^{110}Ag activity in the solution. If a standard silver solution containing the proper specific activity of ^{110}Ag is used, there is no upper limit for chloride determination, and as little as 2 x 10^{-7} g can be rapidly measured.

HCl GAS FIELD SAMPLER

To sample hydrogen chloride gas from the atmosphere, a scrubber-column collector was designed and assembled. Two glass scrubber-columns were arranged in series with each sampler. Fifteen milliliters of 0.05N Na OH solution was introduced into each column of the sampler, all glassware and solutions having first been washed with Cl^- -free water. The inlet air to the sampler was filtered through a 5μ membrane-type filter for collection of any particulate materials; chloride could be determined in the collected material if desirable. Air flow control through the system was accomplished with a critical orifice calibrated to pass 0.1 ft^3/min. A gasoline-driven air pump was used to operate the sampler.

FIELD TESTS

Two field tests using HCl gas were conducted over the Meteorology Grid

network. The HCl gas emission was controlled by a valve on a pressure cylinder. About 5 pounds of HCl was released over a period of 10 minutes in each test. Twelve samplers were arranged downwind on the two innermost arcs located 200 and 800 meters from the source.

A commercial portable HCl gas sampler was evaluated for analytical sensitivity. The instrument, a Billion-Air Analyzer, (Model No. 706P—Mine Safety Appliance Co., Pittsburgh, Pa.) was moved along the meteorology arcs as emission HCl took place. The instrument was sufficiently sensitive to detect and measure the HCl at the 800 meter distance. Real-time measurements made with the portable instrument agreed with analytical results of chloride content from the field collectors by the radiometric technique described. The peak field concentration of HCl gas at 800 meters corresponded to an air concentration of about 2×10^{-7} ppm.

REFERENCE

1. *W. J. Driscoll, B. F. Scott, and E. A. Huff. "Exploration of Radiometric Methods for Industrial Process Control", TID 11306. Nuclear Chicago Corp., Chicago, Illinois, 1961.*

KRYPTON-85 AS AN ATMOSPHERIC TRACER

J. D. Ludwick*

A study of ^{85}Kr as an atmospheric tracer was completed. The gas can be released in a puff or in a continuous stream. Downwind samples of air containing the tracer were readily analyzed by beta-counting, and real-time measurements could be made routinely.

INTRODUCTION

Particulate tracer materials, although useful in predicting the behavior of other particulates, have some limitations as tracers for air diffusion measurements. They are, of course, affected by gravitational attraction; however, more seriously, tracer depletion occurs due to ground effects. Also, since it is difficult to generate a particulate material in any precise size distributions, the diffusion models derived from particulate data are subject to reaction or adsorption as downwind travel takes place.

In a search for an atmospheric tracer with more suitable characteristics, it was determined that the chemically-inert radioactive gas, ^{85}Kr, best fitted the various needs.

* *Radiological Chemistry, Radiological Sciences Section*

EXPERIMENTAL

An experimental survey was undertaken to determine the most advantageous combination of radiation detector and rare gas radioisotope. Laboratory experiments were conducted to test the efficiency of various detectors in atmospheres containing radioactive rare gases.

Figure 1 illustrates the physical arrangement of these tests. The detector was held at the top of a 7 ft stand fitted with a sliding block through which the gas and the elecrical connections were led. The neck of a large meteorological balloon was fitted over the sliding block, and a small amount of helium gas was introduced for partly inflating the balloon. Next a known amount of the tracer gas under test was introduced, and the balloon was filled with air to a size sufficiently large to simulate the atmospheric condition such that the distance from detector to wall was greater than

Neg 0662469-1

FIGURE 1. Experimental Gas Atmosphere Chamber

the normal air range of the radiation to be measured. After filling, the mixture of gases was exhausted in steps, and measurements were made of the counting rate versus radius of the balloon. In this way, concentrations of the tracer were related to the effects on the detector.

Several xenon and krypton radioisotopes were tested for possible application to the tracer problem; and various detectors, organic crystals, plastic scintillators, thin NaI(Tl) crystals, and various end window Geiger detectors were tried. Each inert gas radioisotope was calibrated for specific activity by measurement of a known volume of the gas in a liquid scintillation spectrometer described previously.(1) Results from these tests indicated the suitability of the ^{85}Kr isotope for measurement with a large-window beta detector, since the beta energy of this isotope (0.69 MeV) was sufficient to penetrate the rugged window necessary to prevent detector damage under some of the expected field conditions. In practice, a 4 mg/cm^2, Amperex Model 18546 Geiger counter with 51 mm diameter end-window was used.

In the field, the detectors are housed in a 7 in. length of thick-wall lead pipe which acts both as a radiation and an environmental shield. Also housed inside the pipe is an electronic booster circuit to prevent loss of the signal in traversing the cable distance from field location to recording equipment location. Each sampler is fitted with a removable front face cover to prevent window damage when not in use. The samplers were bolted to the existing stakes in the present meteorological arcs for testing.

Two field tests have been conducted over the course of the Hanford Meteorological Grid. Two prototype field beta detectors were strategically positioned downwind from the source along the 200 m arc. A cylinder containing 4 Ci of ^{85}Kr was pressurized with a small amount of inert krypton and a much larger quantity of argon carrier gas. The mixture was released at a controlled rate for 110 sec, and data from the samplers were taken by dual scalers and recorded every 15 sec. These preliminary data indicate the potential of this real-time analytical method for studying and defining atmospheric diffusion phenomena. Figure 2 illustrates the results from the most recent of these tests.

CONCLUSIONS

Krypton-85 appears to satisfy most of the criteria necessary to make it a nearly ideal tracer for wind diffusion experiments. Its ease in handling, decay characteristics, detectability, and half-life make it compatible with the unusual demands of unpredictable field experiment programming. It is reasonably priced ($10.00/Ci) and can be obtained in suitable containers ready for instantaneous release in any necessary amount. Its chemical inertness allows it to follow the diffusion process precisely. After proper dilution of the tracer gas in a pressure cylinder, any source strength can be

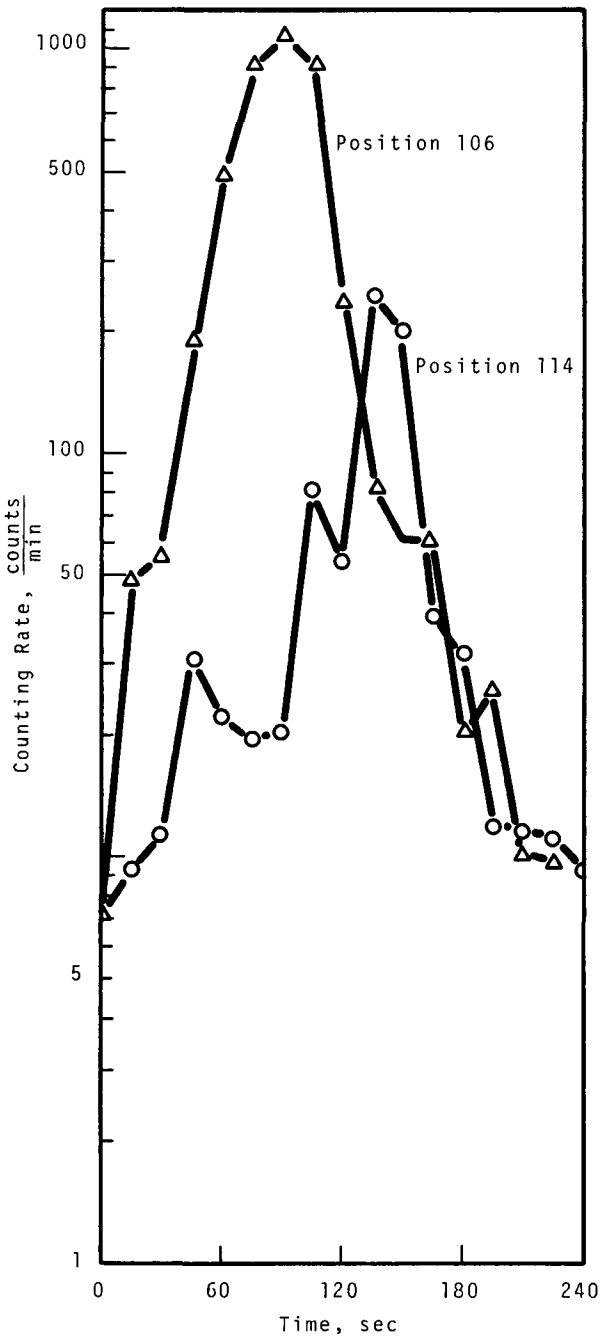

FIGURE 2. Real-time Concentration Analysis of Downwind ^{85}Kr Gas (Field test no. 2, 200 meters)

released at a controlled rate. With the proper selection of electronic measuring equipment, data from the field samplers can be relayed instantly and displayed, if desired, at a central counting station.

REFERENCE

1. *J. D. Ludwick. "Xe^{133} as an Atmospheric Tracer", J. Geophys. Res. 71, 4743-8(1966)*

EVALUATION OF ELEMENTAL TRACERS AND NEUTRON ACTIVATION ANALYSES IN ATMOSPHERIC PRECIPITATION STUDIES

W. A. Haller*

The washout of aerosols or gases by snow or rain has been measured under field conditions[1,2,3] where a known quantity of a tracer was released at a known height in the air, and the amount of washout on an arc subtending the plume was measured. The amount of tracer deposited on the arc was determined from that collected in equally-spaced plastic lined precipitation collectors. The amounts of tracer found per unit volume of water were generally in the parts-per-billion range or lower, thus requiring a sensitive analytical method. Neutron activation and multidimensional gamma-ray analysis provide the necessary sensitivity[4] with a minimum of chemical operations.

Since collection of the particulates that serve as nucleation sites for the formation of rain and snow and of dust particles scavenged by the falling precipitation is unavoidable, an essential factor in the selection of a tracer was that its natural abundance in the rain or snow should be lower than the amount of tracer that would be scavenged during the experiment. A good estimate of this background from such sources during the experiment may be obtained by the simultaneous collection of a blank precipitation sample upwind from the test site and comparing with the collections associated with the release of the tracer. Where contamination occurs from relatively large amounts of dirt which are picked up with the precipitation, the trace element background is drastically increased as seen, for instance, in Table I.

Iodine and bromine were released as gases in the molecular state by rapidly heating them in large evaporating dishes. Following collection in the field, the test samples were transferred from collection containers to Vycor beakers; about 2 ml of doubly-distilled concentrated ammonium hydroxide was added; and the mixture was evaporated to a few milliliters. This was then transferred to a 30 ml Vycor crucible, evaporated to about 0.1 ml, and transferred to 6 mm ID vitreous silica ampoules using several washings of doubly-distilled water containing 0.01 ml of doubly distilled NH_4OH. Following neutron irradiation, the ^{128}I was extracted with carbon tetrachloride and precipitated as AgI for measurement of the 0.445 MeV gamma ray by standard gamma-ray spectrometry. The iodine in the sample was calculated by comparing its ^{128}I content with that of a standard iodine solution irradiated together with the sample. The bromine measurements required the same preirradiation treatment as the iodine, but no chemical separation was required after the irradiation. The water samples were simply evaporated on a standard counting dish and the ^{82}Br determined by direct counting on a multidimensional gamma-ray spectrometer[5] utilizing triple coincidence of the 0.777, 0.82 and 1.044 MeV gamma rays. Results of a test-run

* *Radiological Chemistry, Radiological Sciences Section*

appear in Table II and show washout-to-background ratios for bromine of approximately 4. An increase by a factor of ten in the amount of bromine released would be needed to obtain washout measurements of sufficient accuracy. The washout-to-background ratios for iodine ranged from approximately 6 to 50 which is in the proper range of precision for most of our washout measurements.

Silver, scandium, cesium, and strontium were tested for use as particulate tracers. Particulates were produced in a standard propane-burning, silver iodide generator (the "Sky Fire Generator") which is a type used routinely in cloud seeding work. Aqueous solutions of scandium nitrate, cesium nitrate, and strontium nitrate were used while the standard acetone mixture was used for the silver iodide. Following collection of the rain or snow from the field, the samples were placed in Vycor beakers which had been cleaned by leaching with hot concentrated nitric acid. One milliliter of doubly-distilled nitric acid was added to each sample and they were evaporated to approximately 0.1 ml. They were then quantitatively transferred with doubly-distilled HNO_3 to 6 mm ID vitreous silica ampoules. The samples were irradiated to an integrated neutron flux of about 10^{19} neutrons/cm^2, then stored

TABLE I. Trace Element Concentrations in Precipitation Samples

Particulate, mg per 100 ml precipitation	Trace Element, Nanogram/100 ml				
	Sb	Ag	Zn	Co	Sc
> 10	16	30	240,000	760	44
> 10	8.4	7.9	140,000	1200	66
< 0.1	1.6	0.2	500	1.8	0.2
< 0.1	1.5	0.2	660	3.0	0.1

TABLE II. Washout of Gaseous Tracers

Tracer	Approx. Amount Released	Daughter Determined	Background,(a) Nanogram/100 ml	Washout, Nanogram/100 ml
Br	10 ml	^{82}Br	1.0	4.2
Br	10 ml	^{82}Br	0.7	3.8
Br	10 ml	^{82}Br	1.8	7.9
I	100 g	^{128}I	0.35	2.1
I	100 g	^{128}I	0.02	1.0
I	100 g	^{128}I	0.05	0.49

(a) *Taken concurrently with sample*

for 15 days to allow the ^{24}Na and ^{82}Br to decay. The ampoules were opened, the samples removed by washing with 8N nitric acid and dried on a standard counting dish. The radionuclide concentrations were measured by multidimensional anticoincidental shielded gamma-ray spectrometry.[5] The amount of tracer in the sample was calculated by comparing the radionuclide content with that of the standard solution irradiated with the samples. Results of these determinations appear in Table III and indicate that washout-to-background ratios for cesium, scandium, and AgI range from 2 to 12. To reduce the effect of background variation, the amount of tracer released during the tests should be increased by a factor of 5. Strontium has such a high natural background that at least two orders of magnitude increase in its release would be required for its successful use as a tracer.

REFERENCES

1. *R. J. Engelmann, R. W. Perkins, D. I. Hagen, and W. A. Haller. Washout Coefficients For Selected Gases and Particulates, BNWL-SA-657 Pacific Northwest Laboratory, Richland, Washington, April 15, 1966. Also APCA 66-118.*

2. *R. J. Engelmann and D. I. Hagen. "Precipitation Scavenging Studies," Pacific Northwest Laboratory Annual Report for 1965 in the Physical Sciences, Volume 1: Atmospheric Physics, pp. 1-7, BNWL-235 1. Pacific Northwest Laboratory, Richland, Washington, 1966.*

3. *R. J. Engelmann, D. I. Hagen, W. A. Haller, and R. W. Perkins. Washout Coefficients For Silver Iodide, BNWL-SA-798. Pacific Northwest Laboratory, Richland, Washington, August 4, 1966.*

4. *R. W. Perkins and D. E. Robertson. "Selective and Sensitive Analysis of Activation Products by Multidimensional Gamma-Ray Spectrometry," Proceedings, 1965 International Conference: Modern Trends in Activation Analysis, College Station, Texas, April 19-22, 1965.*

TABLE III. Typical Washout of Particulate Tracers

Tracer	Released, g	Daughter Determined	Gamma Rays Measured	Background,(a) Nanogram/ 100 ml	Washout, Nanogram/ 100 ml
Cs	0.26	^{134}Cs	0.603 0.797(b)	4.2	9.7
Cs	0.25	^{134}Cs	0.603 0.797(b)	1.4	7.6
Cs	0.10	^{134}Cs	0.603 0.797(b)	4.4	9.6
Sc	0.10	^{46}Sc	1.118 0.892(b)	0.2	2.2
Sc	0.03	^{46}Sc	1.118 0.892(b)	0.2	0.3
Sc	0.24	^{46}Sc	1.118 0.892(b)	0.4	0.6
Sr	0.06	^{85}Sr	0.515	1100	1500
Sr	0.38	^{85}Sr	0.515	3600	2600
Sr	0.22	^{85}Sr	0.515	800	2100
AgI	1.4	^{110}Ag	0.706 0.656 1.560(c)	2.0	4.2
AgI	1.2	^{110}Ag	0.706 0.656 1.560	1.0	12.0
AgI	0.5	^{110}Ag	0.706 0.656 1.560	1.1	7.9

(a) *Measured concurrently with sample.*

(b) *Coincidence measurement.*

(c) *Triple coincidence measurement.*

5. *R. W. Perkins. "An Anticoincidence Shielded-Multidimensional Gamma-Ray Spectrometer," Nuclear Instruments and Methods, vol. 33, pp. 71-76, 1965.*

COSMIC RAY PRODUCED RADIONUCLIDES AS TRACERS OF ATMOSPHERIC PRECIPITATION PROCESSES

N. A. Wogman*, C. W. Thomas*, J. A. Cooper*,
R. J. Engelmann and R. W. Perkins*

During the past few years, numerous cosmic ray spallation products of atmospheric oxygen, nitrogen, and argon have been found in aerosols and rainwater.[1] Some of the long-lived radionuclides, with half-lives greater than one week, have been useful in defining tropospheric and stratospheric mixing rates. The shorter-lived isotopes with half-lives of minutes to hours have a potential in defining the precipitation scavenging mechanisms. By use of highly sensitive multidimensional gamma-ray spectrometers, the two short-lived cosmic-ray produced radionuclides ^{38}Cl (37.3 min) and ^{38}S (2.9 hr) were discovered in rainwater[2] and techniques for the measurements of three other short-lived radionuclides ^{34m}Cl (32.4 min), ^{39}Cl (55 min), and ^{24}Na (15.0 hr) in precipitation were developed. For their measurement the chlorine isotopes are precipitated from rainwater samples of 2 to 100 liter volumes, while the ^{38}S and ^{24}Na are contained in the residue from evaporation of the water samples. The five radionuclides are then measured by direct counting on a multidimensional gamma-ray spectrometer[3] which has two 11 in. diam by 6 in. thick NaI(Tl) crystals serving as the principal detectors. The concentrations of these radionuclides observed in various rain samples are listed in Table I. The concentrations in rainwater of the various cosmic ray produced radionuclides vary with precipitation rate. During periods of light rain with accompanying small drop sizes, the number of condensation nuclei per unit liquid volume is high, resulting in a high concentration of radionuclides.

The ratios of these five radionuclides provide information on the scavenging rate and removal efficiency of the atmospheric aerosols to which they are attached, while the absolute concentrations of these radionuclides provide information on the average altitude of the air mass from which

* *Radiological Chemistry, Radiological Sciences Section*

TABLE I. Cosmic Ray Produced Radionuclides in Rainwater[a]

Date	Precip. Rate, cm/hr	Collect. Time, min	Vol, liters	Disintegrations/min/liter				
				^{39}Cl	^{38}Cl	^{34m}Cl	^{38}S	^{24}Na
6-15-64	(b)	(b)	60					0.70 ± 0.2
6-17-64	(b)	(b)	6.64					2.22 ± 0.25
6-18-64	(b)	(b)	14.32					0.59 ± 0.09
7-29-64	(b)	50	5.10	200 ± 17	147 ± 15	(b)	13 ± 5	2.0 ± 0.2
8-01-64	(b)	50	3.50	15 ± 3	9 ± 5	(b)	(b)	(b)
8-12-64	(b)	5	2.20	62 ± 12	42 ± 13	(b)	(b)	2.3 ± 0.4
1-14-66	0.255	30	30.16	24.4 ± 1.1	20.4 ± 2.1	0.3 ± 0.1	1.22 ± 0.16	0.227 ± 0.017
1-28-66	0.0767	44	13.32	60.5 ± 1.6	45.3 ± 3.0	0.7 ± 0.2	2.07 ± 0.31	2.06 ± 0.08
2-01-66	0.316	25	97.87	37.2 ± 0.8	22.9 ± 1.5	0.5 ± 0.1	1.85 ± 0.14	0.608 ± 0.019
2-12-66	0.0515	40	25.50	108.7 ± 2.0	82.7 ± 3.4	1.1 ± 0.2	8.24 ± 1.5	6.14 ± 0.13
2-13-66	0.0638	37	29.20	93.5 ± 1.6	60.5 ± 2.5	1.4 ± 0.2	3.29 ± 0.67	1.77 ± 0.10
1-26-67	0.155	40	76.80	59.2 ± 1.3	43.9 ± 2.3	0.9 ± 0.3	1.11 ± 0.16	1.06 ± 0.03
1-26-67[c]	0.0384	40	19.0	181.6 ± 3.2	113.9 ± 4.9	1.5 ± 0.4	(b)	1.07 ± 0.12

(a) *± values are the standard deviation for the measurement.*

(b) *Not determined.*

(c) *End of rain 1-26-67.*

precipitation formation occurred. The distribution of the isotope production rates within the atmosphere can be calculated from cosmic-ray energy and intensity data and from theoretical expressions for high energy spallation yields.[4] In addition, the atmospheric concentrations or production rates are being experimentally obtained between sea level and the middle stratosphere by aircraft sampling. The principal feature of this distribution is a continual increase of production rate from sea level to about 12 km which varies somewhat with geomagnetic latitude. The wide variation observed in the ratio ^{38}Cl (37.3 min) to ^{24}Na (900 min) in the rain samples is indicative of the "in-cloud" time spent by the condensation nuclei; this is a major cloud physics parameter. The lowest ^{38}Cl-to-^{24}Na ratios were observed during the beginning of a rain storm while the highest ratios were observed near the end. This suggests that the initial precipitation occurs from a slow formation of droplets in the cloud allowing much of the initially-present ^{38}Cl to decay; whereas, the final precipitation results from relatively rapid droplet development.

This technique provides a unique method for studying fallout rates and mechanisms and permits the investigation of processes which cannot be studied by any other method.

REFERENCES

1. *R. W. Perkins and J. M. Nielsen. "Cosmic-Ray Produced Radionuclides in the Environment," Health Physics vol. 11, p. 1297. 1965.*

2. *R. W. Perkins, C. W. Thomas, M. W. Hill, and J. M. Nielsen. "Chlorine-38 and Sulfur-38 Produced by Cosmic Radiation," Nature, vol. 205, p. 790. 1965.*

3. *N. A. Wogman, D. E. Robertson, and R. W. Perkins. "A Large Detector Anticoincidence Shielded Multidimensional Gamma-Ray Spectrometer," to be published in Nuclear Instruments and Methods.*

4. *G. Rudstam. "Systematics of Spallation Yields," Z. Naturforschg, vol. 21a, p. 1027. 1966.*

A PORTABLE BOOM-TYPE AIR SAMPLER

J. D. Ludwick*

A completely portable air sampler mast was constructed with vertical sampling capabilities ranging from 0.25 to 12 meters. This mast was installed on a mobile, power-equipped vehicle that allowed air sampling while the vehicle was in motion. The emission plumes from a plant exhaust stack and from reactor effluent water basins were sampled.

INTRODUCTION

One of the most difficult problems associated with predicting atmospheric downwind exposure levels from various sources is that of defining the vertical distribution of the emitted material at a long distance.

Sampling of occasional releases from a plant is complicated by the fact that they are unplanned or, at best, scheduled for a specific date rather than being coordinated with convenient meteorology. Thus, the proper position for downwind sampling can be determined only after the release has started.

In addition to a capability in long distance sampling, there was also need for a mobile sampling arrangement of sufficient height to traverse the entirety of small emission plumes. These types of plumes occur, for example, at reactor cooling basins. Measurements made with such sampling equipment allow one to calculate the total material released to the atmosphere from the source.

A portable sampling arrangement was then needed with special characteristics to best take advantage of the particular sampling situation. Many of the problems associated with measurement of the vertical distribution of a tracer material lie in determining the concentration close to the ground level. Extreme variations may occur in such a location due to the depletion of the tracer due to contact and impact with the vegetation and ground.

To determine this effect, the sampling arrangement required close spacing of sample positions below 2 m. Practical considerations limited the upper size of the apparatus but a minimum height of 10 m was necessary to provide definitive results from both sampling situations.

* *Radiological Chemistry, Radiological Sciences Section*

EXPERIMENTAL

Construction of the sampling boom was based upon its use with a power wagon vehicle housing an electrically-operated extension ladder. It was desired to use as large a diameter material as practicable for the main boom section to allow large collectors and thus to maximize the collection volume and provide greater sensitivity. For this purpose, a 4 in. aluminum water irrigation pipe was used as the main boom material. Standard 4 in. irrigation saddles were attached at the desired sample locations with Neoprene gaskets surrounding pre-drilled holes in the boom. Each saddle was fitted with a one-hole rubber stopper as a fitting to the actual air sampler. A small iron chain about 12 in. above each saddle was attached to the outer end of the sampler housing to lend added support.

The main upper portion of the boom was directly attached to the extended ladder of the truck. After the boom was attached, the ladder could be lowered or raised as desired for long distance transport. With the ladder in the upright position, the lower end of the boom was coupled by means of a "T" connection into a high volume air pump located on the bed of the power wagon. The remaining arm of the "T" connection was coupled to a lower sampler section. Both the upper and lower sections and their respective samplers are illustrated in Figures 1 and 2. Another method of connecting the lower section involved physical support from the "T" so that the entire sampler in a fixed array became completely portable.

The samplers were constructed using a front aluminum housing and a rear plastic cartridge. A 4 in. diam membrane-type filter was held in the aluminum housing and the rear cartridge contained a similar section (0.001 in. thick) of silver-plated thin copper-turnings followed by a 2 in. thick activated-charcoal collector.

A high-volume air pump rated at 100 ft^3/min was used to operate the samplers. Power for the pump was obtained from a 30 kW gasoline-powered generator located on a trailer bed. The vertical locations of the air samplers were at 0.25, 0.50, 1.0, 2.0, 4.0, 6.0, 8.0 and 12 m heights. The air flow through each sampling head was calibrated and found to be approximately 11 ft^3/min. The flow rate was essentially constant at the various sampling positions.

^{131}I Sampling

The sampling boom was utilized to sample radioiodine emitted from a plant exhaust stack during a period of unusuall high release level. Both visual observation of the plume (using the associated NO_2 fumes) and meteorological data were used to position the sampling boom. Samples were taken 4 to 8 miles from the source over periods of several hours. Occasional repositioning of the boom was necessary as meteorological changes occurred. Samples at the source were taken from a small gas loop at the base of the stack to identify the physical and chemical form of the ^{131}I activity at that point.

Neg 0662671-5

FIGURE 1. The Portable Boom-Type Air Sampler (Upper section)

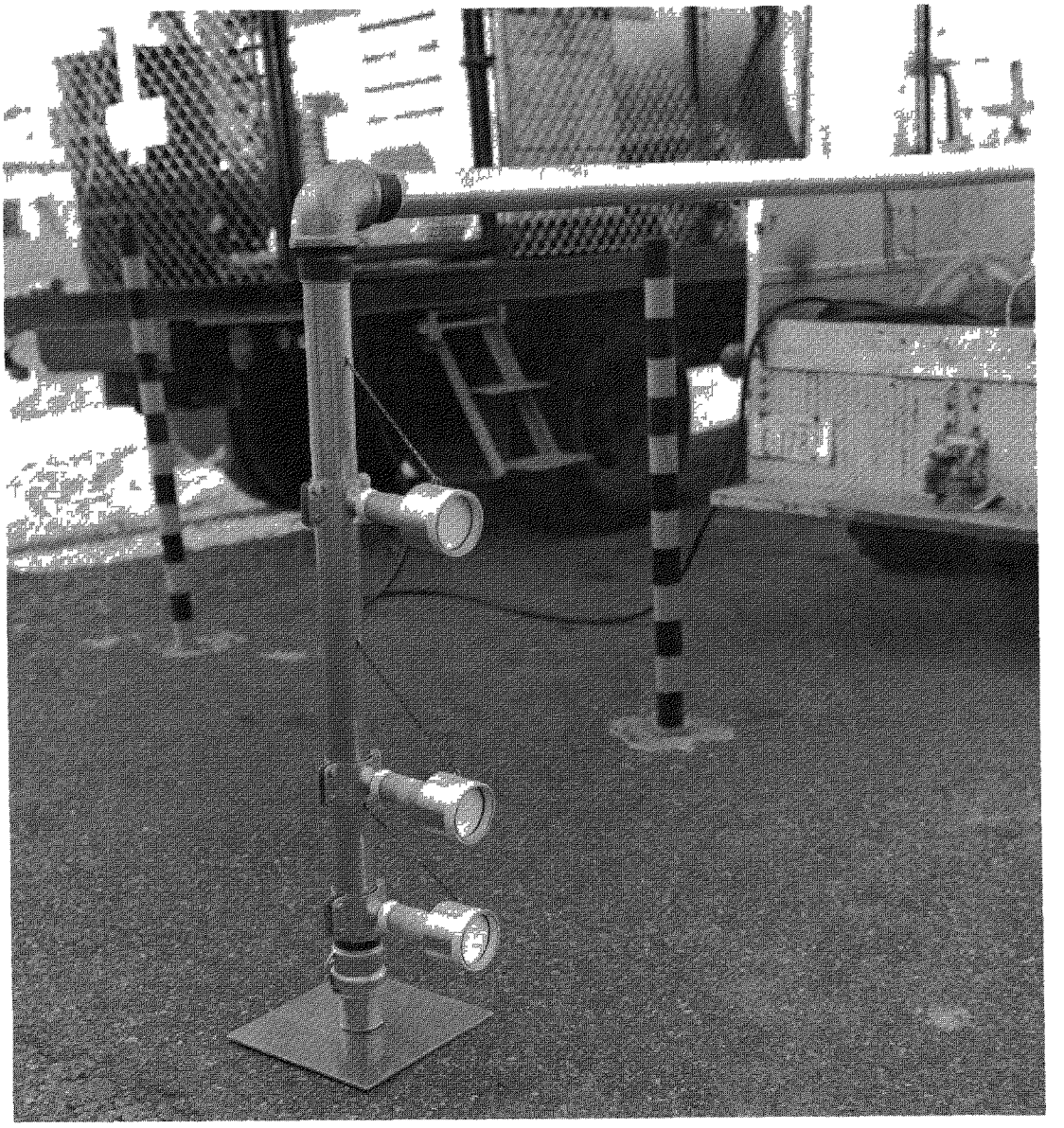

Neg 00662671-4

FIGURE 2. The Portable Boom-Type Air Sampler (Lower section)

Reactor Basin Gas Sampling

The sampling boom was also utilized for traversing the visible exhaust cloud released at a reactor effluent basin. The boom, while operating, was driven through the emission cloud thus defining both the vertical and horizontal radioisotope distributions. The time in the plume was determined by stopwatch.

Sampling of the basins could be accomplished only where close access to their edges was convenient. The warm

plume rises rapidly and the upper edge was generally beyond the uppermost sampler when within 50 meters of the basin and with winds of under 15 knots. Sufficient windspeed was, therefore, necessary before sampling so that the top of a plume would not be significantly higher than the uppermost sampler. Figure 3 illustrates the portable sampler traversing the final edge of a plume from a reactor effluent basin.

DISCUSSION

Samples from the stack indicated that the iodine was almost entirely gaseous and not particulate. A large percentage (72%) was in the reactive form

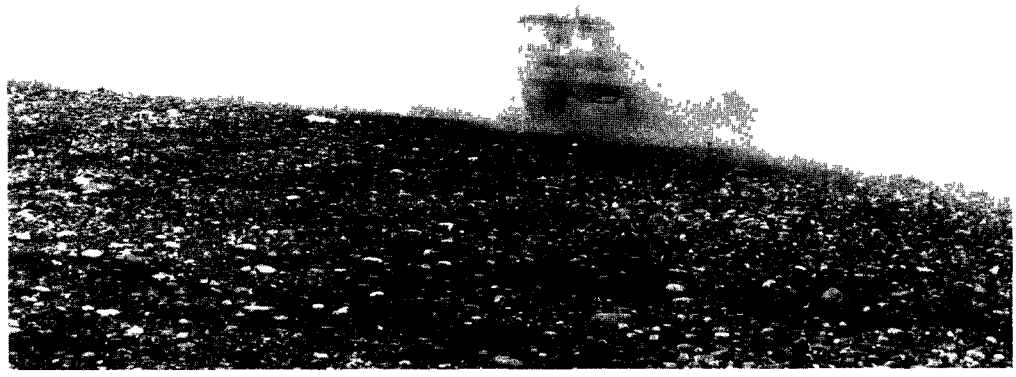

Neg 0670484-8

FIGURE 3. Sampling a Reactor Effluent Basin Plume

as determined by the amount found on the silver section. Results from the assay of three samples taken from the stack gas are summarized in Table I. It is interesting to note the high fraction (25%) of unreactive ^{131}I directly at the source. Table II illustrates the characteristics of the tracer downwind compared to those at the source; also given is the vertical distribution as measured by the boom samplers. Similar behavior had been observed[1] in previous controlled iodine releases, as downwind travel takes place. That is, the gaseous free iodine is quite reactive and readily attaches itself to airborne particulates; the active iodine also combines with atmospheric components to form unreactive gases. Additionally, the iodine may form particulate iodine crystals. The net result of these processes is a steady reduction in the content of reactive iodine with time. Reduction of the reactive species is increased by a decrease in the vertical stability of the air mass.

The vertical iodine distribution found in air samples is also of interest. At about 5 miles from the source, a marked decrease from 4 m to ground level was noted and this can be attributed to lower level depletion of the tracer; however, the reduced activity above 4 m indicates the lack of vertical diffusion of the source plume. One would conclude that considerable vertical diffusion must have taken place and significant radioiodine activity should be present to a considerable elevation. Further work in this regard is necessary, and all is in readiness for future long range sampling of any advantage source.

REFERENCE

1. *J. D. Ludwick. "The Measurement of ^{131}I Transport In Atmospheric Diffusion Experiments," Pacific Northwest Laboratory Annual Report for 1965 in the Physical Sciences, Volume 2: Radiological Sciences, pp. 127-133, BNWL-235 2. Pacific Northwest Laboratory, Richland, Washington, 1966.*

TABLE II. Vertical Distribution of ^{131}I 5 Miles Downwind from Source

(Average percent present: Particulate, 14.5; Reactive, 30.0; Unreactive, 55.5.)

Height, m	Relative ^{131}I Activity
0.25	150
0.5	180
1.0	190
2.0	230
4.0	400
6.0	120
8.0	200
10.0	110

TABLE I. Characteristic of the ^{131}I at the Source

	Relative ^{131}I Activity			Percent Present
	A	B	C	
Filter(Particulate material)	18	31	65	3.5
Silver Bed (Reactive iodine)	213	492	1737	71.5
Charcoal Filter (Unreactive iodine)	35		446	25.0
Charcoal Bed (Unreactive iodine)	42	190	149	25.0

DISTRIBUTION, CHARACTERISTICS, AND BIOTIC AVAILABILITY OF FALLOUT, OPERATION PLUMBBOB*

K. H. Larson**

During the period 1947 to 1963 the Environmental Radiation Division of the Laboratory of Nuclear Medicine and Radiation Biology, School of Medicine, U.C.L.A. was involved in progressively intensified programs designed to answer one principal question, viz., "How much man-made readioactivity distributed in the environment can be tolerated safely by man and his economy?" Within this broad context, the general objectives of Civil Effects Test Organization Program 37 included:

a. The delineation of fallout patterns and their characteristics with respect to particle size and time-of-arrival of fallout from seven tower mounted and four balloon mounted detonations. Comparison of the effects of the yield of the device, the type of device support, and the height of burst on the resultant fallout debris deposited within the fallout pattern to distances at which fallout occurred by H + 12 to H + 16 hr.
b. A detailed-study of the chemical, physical, and radiological characteristics of fallout debris relative to its particle size and occurrence within the fallout pattern.
c. The determination of the biotic availability, rate of accumulation, and retention of radionuclides from fallout debris for various native and domestic plants and animals, as well as the persistence and redistribution of residual contamination in the total environment.

FALLOUT: ITS DISTRIBUTION AND CHARACTERISTICS

Fallout from test devices detonated at Nevada Test Site (NTS) is governed by many complex variables such as: (a) the energy yield of the detonation, (b) the wind structure during the distribution of fallout material, (c) the support used for the detonation of devices, (d) the nature of the surface at ground zero, (e) the degree that the fireball intersects the ground surface, and (f) the mass of inert material surrounding the device. Data presenting the resultant deposition and characteristics of fallout from various detonations studied by the AEP/UCLA laboratory are summarized in the following statements.

1. Characteristics of Fallout Patterns

The coordination of aerial survey measurements of fallout patterns with

---

* *This article is essentially identical to the Summary, Chapt. 9 of the Report of the same title, being WT-1488, July 26, 1966 by K. H. Larson, J. W. Neel, H. A. Hawthrone, H. M. Mork, R. H. Rowland, L. Baurmash, R. G. Lindberg, J. H. Olafson, and B. W. Kowalesky, pp. 210-215.*

** *Present address, Department of Environmental and Radiological Sciences, Pacific Northwest Laboratory, Richland, Washington where the final report referred to above was edited and published.*

ground survey parties using conventional meter measurements greatly increased the detail and accuracy of fallout pattern delineation, as well as increasing the distances to which fallout patterns were defined in the environs of NTS. Dose rates and time-of-arrival of fallout resulting from Shots Boltzmann, Wilson, Priscilla, Hood, Diablo, Shasta, Smoky, Galileo, Newton and Whitney were measured and presented in terms of isodose rate and time-of-arrival on fallout contour maps.

With the adaptation of the aerial survey equipment and techniques developed by the U. S. Geological Survey, fallout radiation intensities could be measured within an area of approximately 10,000 square miles and the readings plotted on maps in about 12 hr by using one aircraft. With appropriate correction and calibration factors, aerial measurements agreed within ± 10% of dose rate measurements made 3 ft above ground by conventional survey meters. During this Test Series, fallout patterns were routinely measured to distances of 200 to 300 miles from ground zero; however, the fallout pattern from Shot Smoky was documented as far as 700 miles from ground zero in 5 flight-days and the radiation levels were readily detectable at that distance.

The detailed documentation of fallout patterns afforded the opportunity to confirm the existence of hot spots in most fallout patterns. Hot spots were first identified and defined in 1948 by the Alamogordo Section of AEP/UCLA when the fallout pattern of Shot Trinity (1945), New Mexico had been outlined in detail.

In the authors' opinion, terrain features, such as mountain ridges, create a significant turbulence in the falling radioactive debris as the cloud moves over the ridge causing increased deposition of fallout to occur on the leeward side. Suggestions of this phenomenon were found in the patterns of Shots Boltzmann, Priscilla, Hood, Diablo, and Smoky. Although rainouts have been reported to be responsible for hot spots whithin 300 miles of NTS, the documented hot spots referred to in this report occurred when no precipitation occurred during fallout.

While the occurrence of hot spots has been associated with prominent terrain features in many cases, a coordinated detailed analysis of the meteorological observations and fallout distribution is required to fully explain the mechanism of their formation and possibly to permit the prediction of their occurrence.

2. Particle Size Distribution in Fallout Patterns

Maximum percentage contributions of various particle sizes occurred at different locations on fallout pattern arcs. Some locations of maximum dose rate across a pattern resulted from moderate percentages of a variety of particle sizes rather than a high percentage of a single size range. Lateral extremities of arcs were characterized by high percentages of less than 44 μ material.

Fallout material less than 44 μ in diameter occurred at close-in arcs as well as at distant arcs while the 44 to 88 μ fraction of fallout material was minimal at close-in distances.

The majority of fallout activity from the balloon mounted Shot Priscilla consisted of particles less than 44 μ in diameter as close to ground zero as 18 miles; larger particles predominated at such distances in fallout material from tower mounted shots.

Within the fallout area determined by the limits of 1 mile from ground zero to distances at which fallout occurred at H + 12 hr and the 1 mR/hr isointensity contour at H + 12 hr approximately 70% of the fallout activity was associated with particle sizes greater than 44 μ in diameter from tower mounted shots while the balloon mounted Shot Priscilla had only 30% of the activity associated with this size range of larger than 44 μ.

Within the limits of H + 1 to H + 12 hr fallout time, Shot Smoky deposited 52 times more total beta radioactivity and 14 times more radioactivity in the less than 44 μ fraction than Shot Priscilla. Both shots had similar yields and identical detonation height.

3. Radioactive Decay of Fallout Debris

Fallout debris from a specific detonation gave similar beta decay curves regardless of particle size or time of fallout. Beta decay curves of most detonations approximated the $T^{-1.2}$ decay relationship over a period of H + 12 to H + 6000 hr. However, slopes of the order of $T^{-1.4}$ occurred from H + 6000 to H + 10,000 hr.

Decay curves of the gamma emission rate were different from those of beta decay for fallout debris from a specific detonation. Gamma decay curves of fallout debris from different detonations were generally similar but more variable than the corresponding beta decay curves.

Plumbbob beta and gamma decay curves, derived from measurements of fallout samples from seven detonations, are presented in relation to the $T^{-1.2}$ decay curve and a theoretical mixed fission product (^{235}U) decay curve.

Estimates of dosage from gamma radiation in fallout areas have generally been calculated on the basis of the $T^{-1.2}$ relationship. However, dose rate decline with time according to the Plumbbob gamma decay (PGD) curve presented in this report yields calculated doses which are 1.8 to 2 times greater than those calculated by the $T^{-1.2}$ relationship to approximately D + 400 days.

4. Gamma Energy Spectrum of Fallout Debris

Samples of different particle size fractions and/or fallout time from each of five detonations were analyzed periodically to H + 3000 hr. Differences in the energy spectra were not detectable among samples of different particle size from a specific detonation; however, differences were detectable among several detonations. Mean energy spectra of fallout material from three detonations indicated that values increased from 0.53 MeV at H + 100 hr to 0.70 MeV at H + 600 hr and ranged from 0.74 to 0.87 MeV at H + 3000 hr. In contrast, the mean energy of the fallout debris from Shot Hood was approximately twice that of the other detonations at H + 100 hr but

decreased to similar values of the other detonations after H + 1200 hr.

The general variation in energy spectrum with time suggests that considerable error can be introduced in the calculations of gamma megacuries from dose rate depending on type of detonation and time of measurement. On the basis of data presented, gamma megacuries per square mile values calculated according to the relationship of 4 R/hr at 3 ft above the ground surface that was used before 1962, would have been 75% too high for a detonation similar to Shot Hood and 25% too low for detonations like Shots Diablo and Shasta.

5. Radiochemical Properties of Fallout Debris

Fallout particles less than 44 μ in diameter had greater percentages of $^{89,90}Sr$ and $^{103,106}Ru$ at D + 30 days than did the larger sized particles. The percentage of $^{89,90}Sr$ and $^{103,106}Ru$ in balloon mounted detonation fallout debris was from two to four times higher than it was in corresponding particle sizes from tower mounted detonations. The reverse was observed for ^{95}Zr. The percentage of ^{140}Ba, ^{141}Ce, and ^{91}Y varied to a lesser degree between fallout from tower and balloon mounted detonations. Strontium-90 averaged 2.7 percent of the total radiostrontium at D + 30 days in fallout originating from detonations mounted on towers.

Similar percentage values for specific radionuclides among the same size fractions of the different tower shots permit the determination of mean percentage values descriptive of tower shots in general. The comparison of mean tower shot percentages to those of Shot Priscilla, a balloon mounted device, indicates that for corresponding size fractions Priscilla radionuclide percentages were approximately 30% higher for ^{140}Ba, 11 to 38% higher for ^{141}Ce + ^{144}Ce-Pr, 300 to 400% higher for $^{103,106}Ru$, 250% higher for ^{89}Sr, 20 to 50% higher for ^{91}Y, and 50% lower for ^{95}Zr.

6. Solubility of Fallout Debris

Solubility of fallout debris is one of the most important properties to consider with respect to the "internal emitter" problem in biological systems. The solubility of radioactive fallout debris in water and in 0.1N hydrochloric acid (HCl) have been used arbitrarily as indices of biological availability.

The radioactivity in fallout debris from tower mounted detonations was determined to be from 1 to 2% soluble in water. Fallout debris from balloon supported detonations was more soluble in both water and 0.1N HCl than debris produced by tower mounted detonations. The solubility of fallout debris from tower supported detonations increased with decreasing particle size; however, in the case of balloon supported detonations, the smaller size particles were somewhat less soluble than larger particles as shown in Table I.

TABLE I. Solubility of Fallout Debris from Tower and Balloon Supported Shots

Support	Particle Size Range, Microns	Solubility, % of Beta Activity Water	0.1N HCl
Tower	>44	<1	5
	<44	<2	14 to 36
Balloon	>44	31	>90
	<44	14	>60

7. Comparison of Fallout Debris from Balloon and from Tower Shots

A comparison was made of fallout debris from a balloon mounted shot (Priscilla) with that from a tower mounted shot (Smoky). These shots were of the same yield and had the same detonation height of 700 ft. The comparison indicated that the amounts of water soluble ^{140}Ba and $^{89,90}Sr$ deposited in the less than 44 μ particle size fraction were similar despite relatively large differences in the total amounts of radioactivity deposited in this particle size fraction.

The widespread distribution of the less than 44 μ particle size fraction from all types of devices detonated at NTS indicates that this particle size fraction is probably the most significant with respect to total area contaminated. Assuming that the soluble fractions of the fallout debris samples studied contain the same ratio of radioelements as that present in the original fallout debris, the application of this ratio to the percent of the soluble activity yields the percent of the various radioelements present in the 0.1N HCl and water-soluble extracts. Based on such calculations, the relative amounts of the several radioelements in the soluble fractions of equal quantities of less than 44 μ fallout debris from tower and balloon supported shots of similar yield and height of detonation are presented in the original document.

The deposition of less than 44 μ fallout debris from the tower mounted detonation considerably exceeded that from the balloon mounted at different fallout times from 1 to 15 hr.

The application of soluble radioelement percentages to the measured and the integrated radioactivities of the less than 44 μ particle size fractions from the two shots, Priscilla and Smoky, gives an estimate of the relative amounts of the various radioelements deposited at different fallout times. While the amounts of total and acid-soluble ^{140}Ba and $^{89,90}Sr$ deposited by less than 44 μ fallout debris from the tower mounted shot were higher over the 1 to 15 hr fallout period, the amounts of water-soluble ^{140}Ba and $^{89,90}Sr$ were similar.

8. Deposition of Radiostrontium in the Environs of Nevada Test Site

Approximately 0.13% of the total amount of ^{89}Sr produced by Shot Priscilla (700 ft) whose fireball very nearly intersected the ground surface, was deposited within the fallout time-of-arrival of H + 12 hr. On the other hand only 0.004 and 0.008 % of the total ^{89}Sr produced was deposited within H + 12 hr fallout time by two balloon mounted shots (1500 ft) whose

fireballs did not intersect the ground. Within H + 12 hr fallout time, tower mounted shots deposited from 0.5 to 2% of the ^{89}Sr produced and from 1.6 to 7.2% of the total ^{90}Sr produced.* Calculations were based on the results of analyses of fallout debris samples for ^{89}Sr and ^{90}Sr and integrated fallout radiation intensities converted to curies by ratios of microcuries per square foot and milliroentgens per hour. The analysis of balloon detonation fallout debris for ^{90}Sr was not performed.

The tower shot percentage deposition of ^{89}Sr was less than that of ^{90}Sr out to distances corresponding to H + 12hr fallout arrival time. This is attributed to relatively low percentages of ^{89}Sr in larger fallout particle size fractions which generally represent the majority of the fallout radioactivity in areas close to ground zero. This fractionation of ^{89}Sr and ^{90}Sr with respect to particle size may be predicted on the basis of the different half-lives of their noble gas precursors, ^{89}Kr and ^{90}Kr, respectively, and the rate of particle formation.

BIOLOGICAL AVAILABILITY OF FALLOUT DEBRIS IN FALLOUT PATTERNS FROM NEVADA TEST SITE

1. Distribution and Redistribution of Fallout Debris in Soils

Surface deposited fallout debris tends to become mechanically trapped in nonagricultural soil. Natural disturbance by wind action causes minor amounts of the total fallout debris, deposited in various native areas studied, to be redistributed within the fallout pattern from the point of original deposition. The amount is dependent on vegetative cover of the area. Fallout particles 44 to 88 μ in diameter contributed an average of 9.7% of the total redistributed radioactive fallout debris following the Priscilla (balloon) detonation as compared to 21% following the Smoky (tower) detonation. Particles less than 44 μ in diameter contributed an average of 85.8% of the beta radioactivity deposited from the Priscilla detonation as compared to 68.3% from the Smoky detonation.

2. ^{90}Sr Distribution in Soils of the Environs of NTS

The ^{90}Sr levels of the surface (0 to 1 in.) soil samples collected in Nevada and Utah in August, 1958, ranged from 32 to 142 mCi/mi^2 in virgin areas near midlines of documented fallout patterns and from 7.5 to 22.7 mCi/mi^2 in agricultural areas which did not necessarily coincide with fallout midlines.

The ^{90}Sr contamination level in 0 to 1 in. surfaces of cultivated soil samples was lower than levels in virgin area samples probably because of both the reduced contamination by fallout debris due to the distance from maximum deposition along the fallout pattern and the subsequent cultivation of the soil. The observed ^{90}Sr levels in agricultural area samples were similar

* *The theoretical potential ^{89}Sr and ^{90}Sr fallout is based on the production of 1 g or 27,700 Ci of ^{89}Sr and 1.14 g or 146 Ci of ^{90}Sr per kiloton yield.*

to those reported for other agricultural areas of the country.

The assumption that NTS activities represent the major source of ^{90}Sr contamination in the virgin area locations is supported by ^{90}Sr percentages of total beta activity. The calculated theoretical percentages of ^{90}Sr for various Testing Series tended to be approached by the observed percentages.

Soil from various sampling sites was subjected to a comparative study of ^{90}Sr contamination. The amount of ^{90}Sr was measured by total solubilization following alkali fusion and leaching with 6N HCl. The results clearly indicate that in the Nevada-Utah area the location of a sampling site in the fallout pattern and the total solubilization of soil samples are necessary to evaluate more accurately the area contamination.

The amounts of ^{90}Sr leached by 6N HCl varied from 13 to 72% of the total ^{90}Sr present. There was little agreement between available data on dose rates or distance from ground zero to that of total ^{90}Sr in the soil.

There were significant differences in distribution of fallout material in soil collected from individual farms within patterns. These differences were closely related to the variety and density of crop whether the radioactivity was measured in terms of gamma dose rate of the location, beta activity per unit area, or as millicuries $^{90}Sr/mi^2$.

3. Fallout Contamination of Forage Plants

It was again confirmed that the principal source of radioactive contamination on native plants was from fallout particles less than 44 μ in diameter, i.e., vegetation within fallout patterns out to 300 mi from NTS was a "selective" particulate collector. The number of fallout particles retained by the foliage depended upon surface characteristics of the foliage, such as hairs, glands, and other mechanical traps of the plant. As much as 21.6% of the radioactive contamination retained by plant foliage during the period from D + 3 to D + 20 days was soluble in 0.1N HCl.

Following both Shots Priscilla and Smoky, the fallout debris contamination of native plant material persisted through the 18 day period. The only measurable change was that due to radioactive decay.

Beyond 200 miles from ground zero, agricultural crops retained less than 15% of the fallout from Shot Smoky.

A very small fraction of the total contamination of the soil by fallout debris from tower mounted detonations was accumulated through the root systems of native forage plants (within 300 miles of NTS).

4. Radionuclide Accumulation by Native Rodents

During the Teapot Series (1955), the concentration of radioiodine in

the thyroids of rabbits and other native rodents was found to be a function of distance from ground zero. The maximum concentrations that were measured at approximately 60 mi from ground zero were from two to seven times higher than those measured at 20 or at 160 miles.

During this series, between 82 and 87% of the total radioactivity found in the thyroid tissue of the native rodents at H + 72 hr was radioiodine. Of this amount, 17 to 20% was ^{133}I and 65 to 67% was ^{133}I. The maximum accumulation occurred at approximately D + 14 days; samples taken at D + 20 days contained only ^{131}I.

Of the several radionuclides (^{89}, ^{90}Sr, ^{91}Y, ^{141}Ce + ^{144}Ce-Pr, $^{136,137}Cs$, and ^{140}Ba) accumulated in rabbit bone, 16 to 45% was accounted for as ^{140}Ba and ^{89}Sr. In Boltzmann samples, both ^{140}Ba and $^{89,90}Sr$ reached maximum concentrations in bone at 78 to 79 miles from ground zero (fallout time-of-arrival: H + 3.7 hr). For Priscilla samples, ^{140}Ba and $^{89,90}Sr$ maximum values occurred at 129 miles from ground zero (fallout time-of-arrival: H + 7.1 hr). In Smoky samples, these radionuclides decreased in concentration in bone with distance from around zero. However, the concentrations of ^{140}Ba and $^{89,90}Sr$ were nearly the same in bone samples from Priscilla and Smoky jackrabbits collected from areas that had a fallout time-of-arrival later than H + 3 hr.

The rate of decay of radioactivity in skin, G.I. tract and contents, and muscle tissue samples collected in the field at the beginning of any particular study and the decline of the radioactive decay of fallout debris. Liver tissue radioactivity levels deviated markedly from the rate of radioactive decay of fallout debris. These relationships were not apparent for bone, which reflected the build-up and retention of specific isotopes.

The radioelement content of jackrabbit bone tissue was studied as a function of time of collection after fallout had occurred. ^{140}Ba, ^{89}Sr, and ^{91}Y concentrations increased with time after fallout to D + 20 days. These radionuclides also were predominant contributors to the beta activity present in the bone. The presence of relatively high levels of ^{91}Y was of interest; this radionuclide is the daughter of the short lived ^{91}Sr.

Effects of chronic exposure of native animals in fallout patterns upon the radiostrontium content in bone tissue have been investigated. Twelve months after the Upshot-Knothole Series (1955), the accumulated $^{89,90}Sr$ was found to be a function of distance from the point of detonation. Maximum concentrations in rabbit bones occurred at 130 miles from ground zero (estimated fallout time of arrival: H + 3.5 hr) within previously delineated fallout patterns.

In rabbits collected along Plumbbob fallout patterns approximately 12 months postseries, bone ^{90}Sr concentrations correlated poorly with soil ^{90}Sr levels. In areas where surface soil ^{90}Sr levels ranged from 13.8 to 142 mCi $^{90}Sr/mi^2$, the ^{90}Sr bone contents ranged from 10 to 22 pCi ^{90}Sr/g Ca with some of the lowest bone contents coinciding with high levels of soil contamination.

In an area included in the Smoky persistence studies (Station VI) jackrabbit bone levels of ^{90}Sr were about the same in 1958 as in 1957. There was

an increase reflected in 1959, followed by a decrease to 1957-58 levels in 1960, and an abrupt drop in 1961, i.e. from 25 to 10 pCi ^{90}Sr/g Ca. This occurred despite the apparent constant level of ^{90}Sr soil environment (about 130 mCi/mi^2).

Data suggest that the higher levels of ^{90}Sr in the indigenous animals are associated with animals that were living in the early sequence of contamination, i.e. during and immediately after fallout, rather than with animals that were born later and merely lived in the contaminated environment.

5. ^{90}Sr in Milk Produced in the Environs of NTS

Milk samples collected from Nevada and Utah farms before, during, and immediately after this test series generally reflected an increase in ^{90}Sr immediately following deposition from the Plumbbob detonations. A reduction in ^{90}Sr in milk occurred with increased time after contamination. The ^{90}Sr in milk was a function of the cows' uptake of ^{90}Sr but the relationship was not linear with dietary ^{90}Sr, or stable calcium and strontium. Data suggest that increases in ^{90}Sr levels of milk produced on such farms could be minimized by immediate reduction of pasture grass consumption following contamination. The substitution for a period of several months of fields that were outside the fallout pattern would reduce the ^{90}Sr in milk to as little as one-third the levels otherwise present.

DISTRIBUTION

No. of Copies	
1	AEC Chicago Patent Group R. K. Sharp
9	AEC Richland Operations Office L. C. Brayly J. P. Derouin N. W. Fraser C. L. Robinson Technical Information LIbrary(2) M. W. Tiernan D. G. Williams C. N. Zangar
1	AEC, RDT Site Representative - PNL P. G. Holsted
1	AIF Task Force MPR Associates, Inc. 815 Connecticut Ave. NW Washington D. C. 20006
1	Air Force Cambridge Research Laboratory Bellford, Massachusetts D. A. Haugen
1	Argonne National Laboratory J. Loeding
2	Atlantic Richfield Hanford Company D. J. Brown R. E. Tomlinson
1	Atomic Energy of Canada Limited Chalk River, Ontario C. A. Mawson
2	Atomic Energy Establishment Trombay Bombay 73, India P. N. Krishnamoorthy K. T. Thomas
2	Atomic Energy Research Establishment Harwell, Berks, England R. H. Burns E. Glueckauf

No. of Copies	
1	Australian AEC Post Office Coogee New South Wales, Australia A. W. R. Wilson
1	Brookhaven National Laboratory L. P. Hatch
1	Center for Nuclear Studies P. O. Box 6, Fontenay-aux-Roses (Seine) France A. de Calmes
2	Center for Nuclear Studies P. O. Box 2, Saclay Gif-sur-Yvette (S & O), France F. Duhamel A. Menoux
2	Commonwealth Scientific and Industrial Research Organization Aspendal, Victoria, Australia B. B. Hicks
270	Division of Technical Information Extension
4	Douglas United Nuclear T. W. Ambrose P. C. Jerman M. C. Leverett M. Lewis
2	duPont Company Aiken, South Carolina W. B. Scott
1	duPont Company Wilmington, Deleware V. R. Thayer

No. of Copies	
1	ENEA (OECD) Health and Safety Office 38, Blvd. Suchet, Paris XVI, France E. Wallauschek
2	Eurochemic Library Mol, Belgium
1	General Electric Company Advanced Technology Laboratories 1 River Road Schenectady 5, New York J. W. Healy
1	Geological Survey of the United Kingdom Water Division Stevenson Buchan, Chief Geologist
2	Geological Survey of the United States Washington 25, D.C. M. King Hubbert C. V. Theis
1	George Washington University Washington, D.C. C. R. Naeser
1	Geotechnical Corporation Box 28277, Dallas 28, Texas W. B. Heroy
1	Gesellschaft Kernforschung mbH Karlsrhue 5 West Germany H. Krause
2	Hanford Environmental Health Foundation G. H. Crook P. A. Fuqua
1	Health and Safety Laboratory New York City John Harley

No. of Copies	
2	International Atomic Energy Agency Vienna 1, Kaerntnerring 11, Austria H. Seligman J. Servant
1	Johns Hopkins University Baltimore, Maryland W. A. Patrick
2	Lawerence Radiation Laboratory Livermore, California G. H. Higgins J. B. Knox
2	National Institute of Radiological Sciences 250, Kurosuna-Cho, Chiba-shi, Japan M. Saiki M. Suzuki
2	N.V. Belchim 200 Boeretang Mol, Belgium Leo H. Baetsle Paul Dejonghe
2	Oak Ridge National Laboratory K. Z. Morgan E. G. Struxness
1	University of Arizona Tucson, Arizona Department of Geology E. S. Simpson
1	University of California Berkeley, California Department of Civil Engineering W. J. Kaufman
1	University of Illinois Department of Agronomy M. B. Russell

No. of Copies

1 University of North Carolina
Chapel Hill, N. C.
Department of Chemistry
H. C. Thomas

1 University of Wisconsin
Department of Chemistry
H. Gladys Swope

15 U.S. Atomic Energy Commission
Washington, D.C.
Division of Biology and Medicine
N. F. Barr
H. D. Bruner
W. W. Burr
J. J. Davis
C. W. Edington
J. Z. Holland
J. S. Kirby-Smith
A. W. Klement
S. A. Lough
J. R. Totter
J. N. Wolfe

Division of Naval Reactors
R. S. Brodski

Division of Production
W. L. Lennemann

Division of Reactor Development and Technology
W. G. Belter

Division of Space Nuclear Systems
J. A. Powers

1 U.S. Atomic Energy Commission
Savannah River Operations Office
K. K. Brown

1 U. S. Public Health Service
Division of Health Mobilization
Washington, D.C.
J. J. Lang, Research Branch

1 World Health Organization
Geneva, Switzerland
R. L. Dodson

1 World Meteorological Organization
Geneva, Switzerland

201 Battelle Northwest
F. W. Albaugh
G. J. Alkire
W. J. Bair
J. H. Bender
C. A. Bennett
R. J. Brouns
R. E. Brown
W. J. Clarke
M. R. Compton(3)
G. M. Dalen
R. F. Dickerson
R. L. Dillon(2)
W. L. Dotson
C. E. Elderkin
R. F. Foster
J. J. Fuquay(75)
W. A. Haney(5)
K. M. Harmon
J. F. Honstead
F. P. Hungate
R. T. Jaske
R. L. Junkins
D. R. Kalkwarf
A. R. Keene
H. A. Kornberg
C. R. Lagergren
H. V. Larson
K. H. Larson
R. E. Nakatani
C. E. Newton,Jr.
J. M. Nielsen
R. F. Palmer
H. M. Parker
R. S. Paul(5)
D. W. Pearce
R. W. Perkins
E. H. Phinney
W. C. Roesch
P. T. Santilli
G. A. Sawyer
L. C. Schwendiman
W. G. Spear
C. L. Simpson(50)
R. J. Sorenson
A. J. Stevens
M. F. Sullivan
R. C. Thompson
C. R. Tipton,Jr.
C. J. Touhill(5)
E. E. Voiland
W. E. Wilson
D. C. Worlton
Biology Library(2)
Technical Information Files(5)
Technical Publications(2)